# BIOCHEMICAL AND STRUCTURAL STUDIES OF 4-HYDROXYPHENYLACETATE DECARBOXYLASE AND ITS ACTIVATING ENZYME

D i s s e r t a t i o n

zur Erlangung des akademischen Grades

d o k t o r r e r u m n a t u r a l i u m

(Dr. rer. nat)

im Fach Biologie

eingereicht an der

Mathematisch-Naturwissenschaftlichen Fakultät I

der Humboldt-Universität zu Berlin

Von

Brinda Selvaraj

Präsident der Humboldt-Universität zu Berlin

Prof. Dr. Jan-Hendrik Olbertz

Dekan der Mathematisch-Naturwissenschaftlichen Fakultät I

Prof. Dr. Stefan Hecht

Gutacher/innen: 1. Prof. Holger Dobbek

2. Prof. Wolfgang Buckel

3. Prof. Athina Zouni

Tag der Abgabe: 10.12.2013

Tag der mündlichen Prüfung: 25.06.2014

**பல வேடிக்கை மனிதரைப் போலே**
**நான்வீழ்வேன் என்றே நினைத்தாயோ?**
**--- மஹாகவி சுப்ரமணிய பாரதி**

**Did you think,**
**that i too would give up and fall,**
**like some risible fools?**
**--- Mahakavi Subramaniya Bharathi**

Diese Arbeit wurde von April 2010 bis Dezember 2013 an der Humboldt Universität zu Berlin angefertigt. Teile der im zeitlichen Rahmen dieser Dissertation erzielten Ergebnisse sind in folgenden Publikationen veröffentlicht:

This study was performed from April 2010 to December 2013 at the Humboldt University of Berlin. Parts of this work have been or will be published under the following titles

**Brinda Selvaraj**, Antonio J. Pierik, Eckhard Bill, Berta M. Martins
4-Hydroxyphenylacetate decarboxylase activating enzyme catalyses a classical *S*-adenosylmethionine reductive cleavage reaction
*J Biol Inorg Chem* (2013) 18:633-643

**Brinda Selvaraj**, Antonio J. Pierik, Eckhard Bill, Berta M. Martins
The futile auxiliary clusters of 4-Hydroxyphenylacetate decarboxylase activating enzyme in *S*-adenosylmethionine reductive cleavage reaction
*J Biol Inorg Chem* (2014) *In press*

**Brinda Selvaraj**, Antonio J. Pierik, Lisa Schilder, Berta M. Martins
Structural and kinetic studies of 4-hydroxyphenylacetate decarboxylase in complex obligewith substrates and inhibitors support a Kolbe-type decarboxylation for *p*-cresol formation
(In preparation)

# Acknowledgements

I start my acknowledgements by thanking **Dr. Berta M Martins** for introducing me to this topic and walking the lane throughout with me.

Speical thanks to **Prof. Holger Dobbek** for nurturing and fine-tuning my scientific views.

I acknowledge **Prof. Antonio J Pierik** and **Dr. Eckhard Bill** for measuring the EPR and Mössbauer spectra respectively and also for making impressive figures.

I am deeply indebted to **Prof. T. N. Guru Row** for kindling my early interests in crystallography.

I express my gratitude to **Jae-Hun** and **Martin** for all the fruitful discussions, knowledge transfer and encouraging ideas. I am very grateful to **Tobias** for helping me in measuring and interpreting the *stopped-flow* results.

I convey my sincere thanks to **Tzong-Yuan** for rendering his timely help during my starting days in lab, **Sebastian** for showing me the Bavarian hospitality, **Sandra** for all the coffee conversations and delicious cakes and **Jochen** (messy fessy) for all the great fun and the terrific time in lab. I also convey my thanks to sweet juniors **Christina, Yulia, Lilith** and all former members from the group of Prof. Dobbek.

I thank **Silke** and Thatha`s family (**Dietrich**) who have been my extended kith and kin in Berlin.

I would like to thank and treasure the good times I spent with **Vandana, Gopal, Prabha, Surya, Kumar, Ananth** and all my friends in Berlin. Thanks for making my stay in Berlin, a pleasant one. I thank **Amola, SPT, Patla, Rams** and all my friends for being in my life and making it an inexplicably wonderful journey.

I owe all my accomplishments and extend my gratitude to my **Appa, Amma** and **Paapa,** for all that I am now is because of them.

# Table of contents

**Table of contents** ..... **1**

**Abbreviations** ..... **5**

**Zusammenfassung** ..... **7**

**Summary** ..... **9**

**Introduction** ..... **11**

1. Anaerobic degradation of aromatic compounds ..... 11

2. Radical enzymes ..... 11

2.1. Coenzyme $B_{12}$-dependent enzymes ..... 12

2.2. Radical SAM enzymes ..... 13

2.2.1 Radical SAM enzymes with auxiliary Fe/S cluster(s) ..... 17

2.3. Glycyl radical enzymes (GREs) ..... 18

4-Hydroxyphenylacetate decarboxylase (4Hpad) ..... 21

Crystal structure of 4Hpad ..... 22

4-Hydroxyphenylacetate decarboxylase activating enzyme (4Hpad-AE) ..... 26

**Goals** ..... **27**

**Materials and methods** ..... **29**

1. Chemicals and kits ..... 29

2. Anaerobic work ..... 29

3. Bacterial strains ..... 30

4. Media and antibiotics ..... 30

5. Molecular biology ..... 31

5.1. Cloning of 4Hpad-AE ..... 31

5.2. Cloning of Δ66-AE ....31
5.3. Cloning of AE-9M ....32
5.4. Mutagenesis of 4Hpad....32
6. Protein expression ....33
6.1. Expression of 4Hpad-AE and its variants ....33
6.2. Expression of 4Hpad and its variants....34
7. Protein purification....34
7.1. Purification of 4Hpad-AE and its variants ....34
7.2. Purification of 4Hpad and its variants....35
7.3. Protein concentration....35
8. Reconstitution of Fe/S clusters in 4Hpad-AE and its variants ....36
8.1. UV-vis spectroscopy ....36
8.2. Colorimetric determination of non-heme iron ....37
8.3. EPR spectroscopy....37
8.4. Mössbauer spectroscopy ....37
9. Enzymatic assays....38
9.1. Activity assay for reductive cleavage of SAM by 4Hpad-AE and Δ66-AE ....38
9.1.1. Reverse-phase HPLC separation....39
9.1.2. ESI-MS....39
9.1.3. TLC ....39
9.2. 4Hpad-coupled activity assay for reductive cleavage of SAM by 4Hpad-AE and Δ66-AE....40
9.3. Correlation between 5'-deoxyadenosine and glycyl radical formation ....40
9.4. Activity assay for *p*-cresol production by 4Hpad....41

10. Isothermal titration calorimetry (ITC)....41
11. Stopped-flow spectrometry....42
12. Michaelis-Menten kinetics....42
13. Crystallographic methods....42
13.1. Crystallization of 4Hpad and its variants....42
13.2. Crystallization trails of 4Hpad-AE and its variants....43
13.3. Data collection, structure determination and refinement....44
14. Complex formation between 4Hpad and 4Hpad-AE*....44
**Results and discussion....44**
1. Molecular biology....44
1.1. Cloning of 4Hpad-AE....44
1.3. Primer designing for AE-9M....48
1.4. 4Hpad mutants....49
2. Protein expression and purification....49
2.1. Expression and purification of 4Hpad-AE and its variants....49
2.2. Expression and purification of 4Hpad and its variants....51
3. Characterization of Fe/S clusters of 4Hpad-AE and its variants....52
3.1. Spectroscopic analysis of 4Hpad-AE....52
3.1.1. UV-vis & colorimetric analysis....52
3.1.2. EPR spectroscopic analysis....54
3.2. Spectroscopic analysis of 4Hpad-AE*....55
3.2.1. UV-vis & colorimetric analysis....55
3.2.2. EPR and Mössbauer analysis....57
3.3. Spectroscopic analysis of Δ66-AE....59

3.3.1. UV-vis & colorimetric analysis ..... 59
3.3.2. EPR and Mössbauer analysis ..... 60
4. Enzymatic assays ..... 62
4.1. Reductive cleavage of SAM (Uncoupled assay) ..... 62
4.1.1. 5'-deoxyadenosine detection ..... 62
4.1.2. Methionine detection ..... 64
4.2. Reductive cleavage of SAM in the presence of 4Hpad (Coupled assay) ..... 66
4.3. Correlation between 5'-deoxyadenosine and glycyl radical formation ..... 67
4.4. *p*-Cresol production by 4Hpad ..... 70
5. Kinetics ..... 72
5.1. Michaelis-Menten kinetics ..... 72
5.2. Binding affinity of 4Hpad-AE to SAM ..... 73
5.3. Reduction kinetics ..... 75
6. Complex formation between 4Hpad and 4Hpad-AE ..... 77
7. Crystallization ..... 77
7.1. Co-crystallization of 4Hpad ..... 77
7.2. Crystal structure of 4Hpad variants ..... 81
**Outlook ..... 83**
**References ..... 85**
**Appendix ..... 95**
1. Appendix tables ..... 95
2. Appendix figures ..... 97
3. SDS-PAGE ..... 98
**Selbständigkeitserklärung ..... 100**

# Abbreviations

| | |
|---|---|
| GRE | Glycyl radical enzyme |
| AE | Activating enzyme |
| Fe/S-GRE | Fe/S cluster containing glycyl radical enzyme |
| GRE-AE | Glycyl radical activating enzyme |
| RS cluster | SAM binding $[4Fe\text{-}4S]^{2+/1+}$ cluster |
| ISC | Iron sulfur cluster |
| 4Hpad | 4-Hydroxyphenylacetate decarboxylase |
| HE2Q | 4Hpad double mutant at H536Q and E637Q |
| 4Hpad-AE | 4-Hydroxyphenylacetate decarboxylase activating enzyme |
| 4Hpad-AE* | As-isolated 4-hydroxyphenylacetate decarboxylase activating enzyme on *in vitro* biological Fe/S reconstitution (6.0 ± 0.5 mol Fe per mol protein) |
| 4Hpad-AE** | Reconstituted 4Hpad-AE treated with ISC proteins (12.0 ± 0.3 mol Fe per mol protein) |
| Δ66-AE | As-isolated 4-hydroxyphenylacetate decarboxylase activating enzyme variant missing the cysteine rich insert, on *in vitro* biological Fe/S reconstitution (3.5 ± 0.2 mol Fe per mol protein) |
| AE-9M | As-isolated 4-hydroxyphenylacetate decarboxylase activating enzyme variant designed by surface entropy reduction method (3.5 ± 0.5 mol Fe per mol protein). |
| WT-AE | Wild type activating enzyme |
| Pfl-AE | Pyruvate formate-lyase activating enzyme |
| Nrd-AE | Class-III ribonucleotide reductase activating enzyme |
| Gdh-AE | Glycerol dehydratase activating enzyme |
| BssD-AE | Benzylsuccinate synthase activating enzyme |
| EPR | Electron paramagnetic resonance |
| ITC | Isothermal titration calorimetry |
| RP-HPLC | Reversed phase high-performance liquid chromatography |
| TLC | Thin layer chromatography |
| ESI-MS | Electro spray ionization mass spectrometry |
| UV-vis | Ultraviolet-visible |

| | |
|---|---|
| 4-HPA | 4-Hydroxyphenylacetate |
| 3, 4-DHPA | 3, 4-Dihydroxyphenylacetate |
| 4-HPAA | 4-Hydroxyphenylacetamide |
| 4-APA | 4-Aminophenylacetate |
| SAM | S-adenosyl-L-methionine |
| SAH | S-adenosyl-L-homocysteine |
| 5'-AdoH | 5'-deoxyadenosine |
| 5'-Ado< | 5'-deoxyadenosyl radical |
| Ado | Adenosine |
| MTA | 5'-deoxy 5'-(methylthio)adenosine |
| DT | Sodium dithionite |
| DTT | Dithiothreitol |
| DTB | D-Desthiobiotin |
| IPTG | Isopropyl-β-D-thiogalactopyranoside |
| ATH | Anhydrotetracyclin |
| ATP | Adenosine triphosphate |
| AMP | Adenosine monophosphate |
| PEG | Polyethylene glycol |
| HEPES | 4-(2-hydroxyethyl)-1-piperazineethanesulfonic acid |
| OD | Optical density |
| w/v | Weight per volume |
| $k_{cat}$ | Catalytic rate constant |
| $k_{obs}$ | Observed rate constant |
| $K_d$ | Dissociation constant |
| $K_m$ | Michaelis constant |

# Zusammenfassung

Die Spaltung chemisch inerter CH-Bindungen von aromatischen und aliphatischen Verbindungen in der Abwesenheit von Sauerstoff ist aufgrund einer hohen Aktivierungsenergie ein energetisch ungünstiger Prozess. Um diese schwierige Aufgabe zu erfüllen, nutzt die Natur Radikalspezies als Katalysatoren. Glycinradikal Enzyme (GREs) verwenden dazu ein stabiles proteingebundenes Glycinradikal, welches durch Abstraktion eines Wasserstoffatoms entsteht. Strikt anaerobe Bakterien wie *Clostridium difficile* und *C. scatologenes* verwenden GRE, um die chemisch ungünstige Decarboxylierung von 4-Hydroxyphenylacetat zu *p*-Cresol zu katalysieren. Das Enzymsystem besteht aus einer Decarboxylase und dem zugehörigen Aktivierungsenzym. Die 4-Hydroxyphenylacetat-Decarboxylase (4Hpad) besitzt zusätzlich zum Protein-basierten Glycinradikal eine weitere Untereinheit mit bis zu zwei [4Fe-4S] Clustern und repräsentiert hierdurch eine neue Klasse von Fe/S-Cluster-haltigen GREs, die aromatische Verbindungen umsetzen. Das Aktivierungsenzym (4Hpad-AE) weicht vom Standardtypus ab, indem es zusätzlich zum S-Adenosylmethionin(SAM)-bindenden [4Fe-4S]-Cluster (RS-Cluster) mindestens einen weiteren [4Fe-4S]-Cluster bindet.

- In dieser Studie wurden heterologe Expressions- und Reinigungsprotokolle für 4Hpad und 4Hpad-AE entwickelt. Kristallstrukturen von 4Hpad cokristallisiert mit den Substraten (4-Hydroxyphenylacetat, 3,4-Dihydroxyphenylacetat) und dem Inhibitor (4-Hydroxyphenylacetamid) zeigten geringe strukturelle Änderungen im aktiven Zentrum des Proteins, wodurch die zuvor berichteten Strukturen (PDB: 2Y8N und 2YAJ) bestätigt wurden. Mutagenese der 4Hpad-Reste (E505, H536, E637), welche in der Kolbe-Typ Decarboxylierung beteiligt sein sollten, zeigte eine Beeinträchtigung der Produktion von *p*-Cresol aus 4-Hydroxyphenylacetat. Die Struktur der Doppelmutante, in welcher die beiden Reste H536 und E637, die an der Substratbindung beteiligt sind, ausgetauscht wurden, zeigten keine Substratbindung. Dies ist ein zusätzlicher Hinweis, dass diese Reste essenziell zur Bindung des Substrats in einer geeigneten Position zur Kolbe-Typ Decarboxylierung zur *p*-Cresol-Bildung durch 4Hpad sind.
- Die Radikalbildung am 4Hpad-AE wurde durch die Überprüfung einer klassischen reduktiven Spaltung von SAM zu den Reaktionsprodukten 5'-Deoxyadenosin und Methionin bestätigt. Diese Beobachtung zerstreut den Vorschlag, wonach Glycin-radikal

Aktivierungsenzyme die zusätzliche Cluster enthalten, eine alternative SAM-Spaltungsreaktion katalysieren, wie zuvor für das Aktivierungsenzym der Glycerol-Dehydratase gezeigt wurde. EPR- und Mössbauer-Spektroskopische Analysen zeigten, dass 4Hpad-AE mindestens einen zusätzlichen [4Fe-4S] Cluster neben dem einzelnen RS-Cluster enthält.

- Die katalytische Notwendigkeit eines zusätzlichen Clusters wurde durch eine Mutationsanalyse untersucht, wobei eine verkürzte Version des Enzyms (Δ66-AE) ohne die zusätzliche Cystein-reiche Insertion konstruiert wurde. Δ66-AE ist stabil, beinhaltet einen vollkommen aktiven [4Fe-4S] RS-Cluster und kann die Decarboxylase aktivieren. Ähnliche SAM-Spaltungsraten von Δ66-AE (0.13 bis 0.19 $min^{-1}$) und 4Hpad-AE (0.04 bis 0.19 $min^{-1}$) zeigen, dass die Reaktivität des RS-Clusters durch die Abwesenheit des zusätzlichen Clusters unbeeinträchtigt ist. Dadurch kann die Möglichkeit, dass der zusätzliche Cluster als Elektronentransferleitung zum RS-Cluster für eine effektive SAM-Spaltung benötigt wird, ausgeschlossen werden. Die zusätzlichen Cluster sind vermutlich bei der 4Hpad-Aktivierung von Bedeutung, was durch die geringere Bildung und den schnelleren Zerfall des Glycin-Radikals bei der Aktivierung durch Δ66-AE ($t_{1/2} \approx 5$ min), verglichen mit Wildtyp-AE ($t_{1/2} > 30$ min), belegt wird.
- Der Radikaltransfer zwischen 4Hpad-AE oder Δ66-AE und der Decarboxylase wurde durch Korrelation der zeitabhängigen Bildung von 5'-Deoxyadenosin durch 4Hpad-AE und die Glycin-Radikalbildung durch Hpad untersucht. Wie zu erwarten kam es zu keiner Komplexbildung zwischen 4Hpad-AE und AE, da das Glycin-Radikal nach jedem Umsatzzyklus recycelt werden kann; ein dauerhafter Komplex zwischen GREs und ihren zugehörigen Aktivierungsenzymen ist nicht nötig.

Durch Kombination von biochemischen und kristallographischen Methoden zur Untersuchung des 4-Hydroxyphenylacetat-Decarboxylase-Systems hoffe ich zum Verständnis beizutragen, wie Enzyme Radikale zur Umsetzung von Kohlenwasserstoffverbindungen unter anoxischen Bedingungen verwenden.

# Summary

The inert C-H bond cleavage in aromatic and aliphatic compounds in the absence of dioxygen is a chemically challenging process due to high activation energy. However nature uses radical species as catalyst for doing this job. Glycyl radical enzymes (GREs) employ a stable protein-bound glycyl radical generated by a hydrogen atom abstraction. Strict anaerobic bacteria, *Clostridium difficile* and *C. scatologenes* employ a GRE to catalyze the chemically unfavorable decarboxylation of 4-hydroxyphenylacetate to *p*-cresol. The enzyme system comprises of a decarboxylase and its cognate activating enzyme. The 4-hydroxyphenylacetate decarboxylase (4Hpad) has an extra subunit harboring up to two [4Fe-4S] clusters in addition to the protein-based glycyl radical, and represents a new class of Fe/S cluster containing GREs acting on aromatic compounds. Its activating enzyme (4Hpad-AE) also deviates from the standard type by binding at least one [4Fe-4S] cluster in addition to the *S*-adenosylmethionine (SAM) binding [4Fe-4S] cluster (RS cluster).

- In this study, heterologous expression and purification protocols for both 4Hpad and 4Hpad-AE were developed. Crystal structures of 4Hpad co-crystallized with substrates (4-hydroxyphenylacetate, 3,4-dihydroxyphenylacetate) and inhibitor (4-hydroxyphenylacetamide) showed subtle structural change in the active site pocket of the protein, which confirmed the previously reported structure (PDB: 2Y8N and 2YAJ). Mutagenesis of 4Hpad residues (E505, H536, E637) that are supposed to be involved in the Kolbe-type decarboxylation showed impaired production of *p*-cresol from 4-hydroxyphenylacetate. The structure of double mutant where the two residues H536 and E637 that helps in anchoring the substrate were mutated together, failed to show substrate binding. This is added evidence that the residues are essential to bind the substrate in a position suitable for the Kolbe-type decarboxylation for *p*-cresol formation by 4Hpad.
- The radical initiation at the 4Hpad-AE was confirmed by verifying the classical reductive cleavage of SAM, the reaction products being 5′-deoxyadenosine and methionine. This observation casts doubt on the suggestion that the glycyl radical activating enzymes containing auxiliary clusters catalyze the alternative SAM cleavage reaction observed for glycerol dehydratase activating enzyme. EPR and Mössbauer spectroscopic analysis revealed that 4Hpad-AE contains at least one auxiliary [4Fe-4S] cluster besides the

unique RS cluster.

- The catalytic need for the additional clusters was evaluated by mutational analysis in which a truncated version of the protein lacking the additional cysteine rich insert (Δ66-AE) was constructed. Δ66-AE is stable; harbors a fully active [4Fe-4S] RS cluster, and can activate the decarboxylase. Similar cleavage rates for SAM displayed by Δ66-AE (0.13 to 0.19 $min^{-1}$) and 4Hpad-AE (0.04 to 0.19 $min^{-1}$) indicate the reactivity of the RS cluster is unaffected by the absence of the additional clusters. Thus the possibility that the additional clusters act as a conduit for electron transfer to the RS cluster for effective SAM cleavage is ruled out. The auxiliary clusters are presumably relevant for 4Hpad activation, which is accounted by the less and fast decaying glycyl radical in 4Hpad when activated by Δ66-AE ($t_{1/2} \approx 5$ min) compared to wild type AE ($t_{1/2} > 30$ min).
- The radical transfer between 4Hpad-AE or Δ66-AE and decarboxylase was studied by correlating the time-dependent formation of 5´-deoxyadenosine formed by 4Hpad-AE and the glycyl radical formation by 4Hpad. The non-detected complex formation between the 4Hpad and AE is predicted since the glycyl radical can be recycled after each turnover; a lasting complex between the GREs and dedicated activating enzymes is not required.

By combining biochemical and crystallographic methods to study the 4-hydroxyphenylacetate decarboxylase system, I hope to contribute a better understanding of how enzymes use radicals to achieve anoxic biocatalysis of hydrocarbon compounds.

# Introduction

## 1. Anaerobic degradation of aromatic compounds

Microbial degradation of hydrocarbons was considered to be an absolute oxygen-dependent process for many years but recently it is proved that the discovery of aromatic and aliphatic hydrocarbon catabolism in the complete absence of molecular oxygen is possible (Heider & Fuchs, 1997). Since then, the number of hydrocarbon compounds catabolized anaerobically by microorganisms has been steadily increasing, which includes toluene, ethylbenzene, xylene, cymene, cresol, phenylacetate, ethyl benzene, methyl benzene and so on (Heider *et al.*, 1998). Cleavage or syntheses of carbon-carbon and carbon-hydrogen bonds are energy-demanding processes. Aerobic aromatic metabolism is catalyzed by oxygenases through hydroxylating or cleaving the aromatic ring structures using molecular oxygens (Boll & Fuchs, 2005) while in the absence of oxygen, the sufficient energy required for these processes could be solved by employing stable, protein-based radicals (Sawers, 1998).

## 2. Radical enzymes

Nature has evolved low-energy pathways wherever possible and only employs "chemically difficult" higher-energy pathways via radicals when there is no alternative (Buckel & Golding, 2006). Radical-mediated catalysis is found especially in enzymes from anaerobic microorganisms since radicals are highly reactive towards dioxygen (Buckel & Golding, 1998). Recent years show great increase in the number of radical enzymes and significant achievements in understanding the structure and function of these enzymes. Most of the radical mediated enzyme catalysis commences by generating a radical which then activates the substrate by abstracting of a hydrogen atom to give a substrate-derived radical. The substrate-derived radical undergoes chemical reaction generating a product-derived radical that gets converted into product by abstracting the hydrogen atom from the enzyme regenerating the initial radical (Buckel & Golding, 2006; Buckel, 2009). The radicals are localized on cofactors as in adenosylcobalamin generated by homolytic fission of the Co-C bond or in *S*-adenosyl-L-methionine (SAM) generated by cleaving the sulfur-carbon bond or one electron oxidation on an amino acid (Gly,

Cys, or Tyr) (Buckel & Golding, 1998; Stubbe & van der Donk, 1998; Frey, 2001). Depending on where and how the radical generation starts there are three classes of radical enzymes, namely coenzyme $B_{12}$-dependent, radical SAM dependent and glycyl radical enzymes.

## 2.1. Coenzyme $B_{12}$-dependent enzymes

Adenosylcobalamin (AdoCbI) or Coenzyme $B_{12}$ is a complex organometallic cofactor that serves as a radical initiator in the catalytic cycles of the adenosylcobalamin-dependent enzymes (Frey *et al.*, 2006). AdoCbI-dependent enzymes are not especially oxygen sensitive in contrast to the anaerobic radical SAM enzymes (Marsh *et al.*, 2010). AdoCbI generates 5'-deoxyadenosyl radical by homolytic fission of its Co-C bond (Marsh *et al.*, 2010, Figure 1).

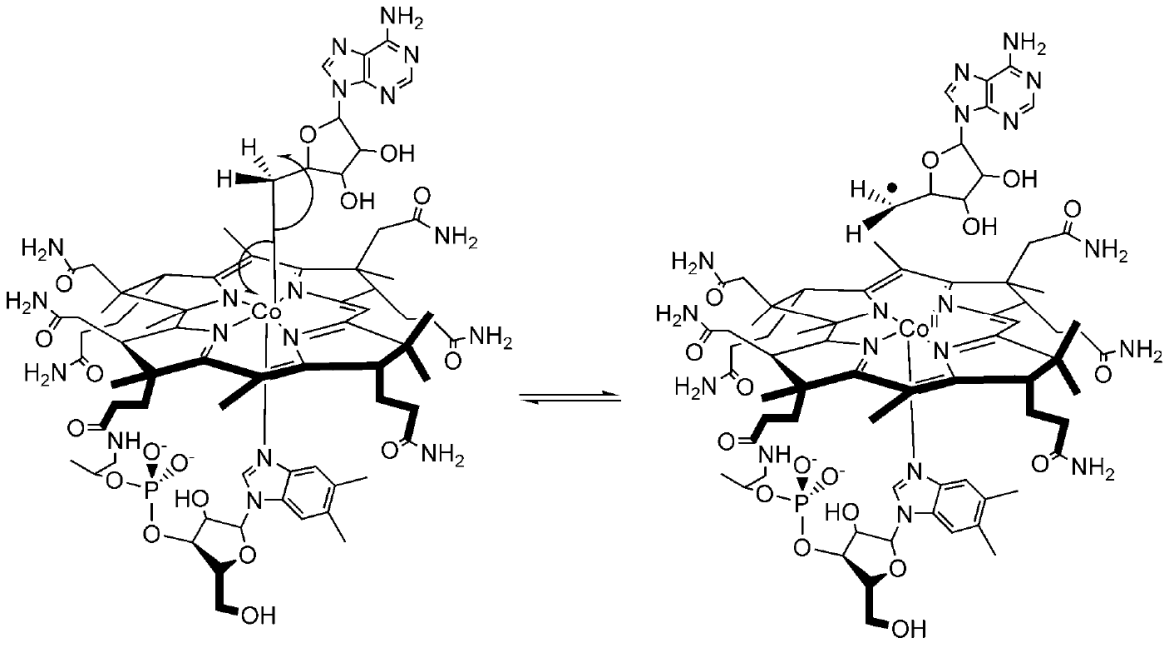

**Figure 1. Radical generation by homolysis of the Co-C bond of adenosylcobalamine** (Figure adapted from Marsh *et al.*, 2010)

The generated radical abstracts a hydrogen atom from the substrate forming a substrate-derived radical, which rearranges to the product-related radical. Eventually one of the hydrogen atoms of the transiently formed 5'-deoxyadenosine is transferred to the product-related radical resulting in

the formation of the product along with the regeneration of 5'-deoxyadenosyl radical (Banerjee, 2003; Sandala *et al.*, 2010, Scheme 1).

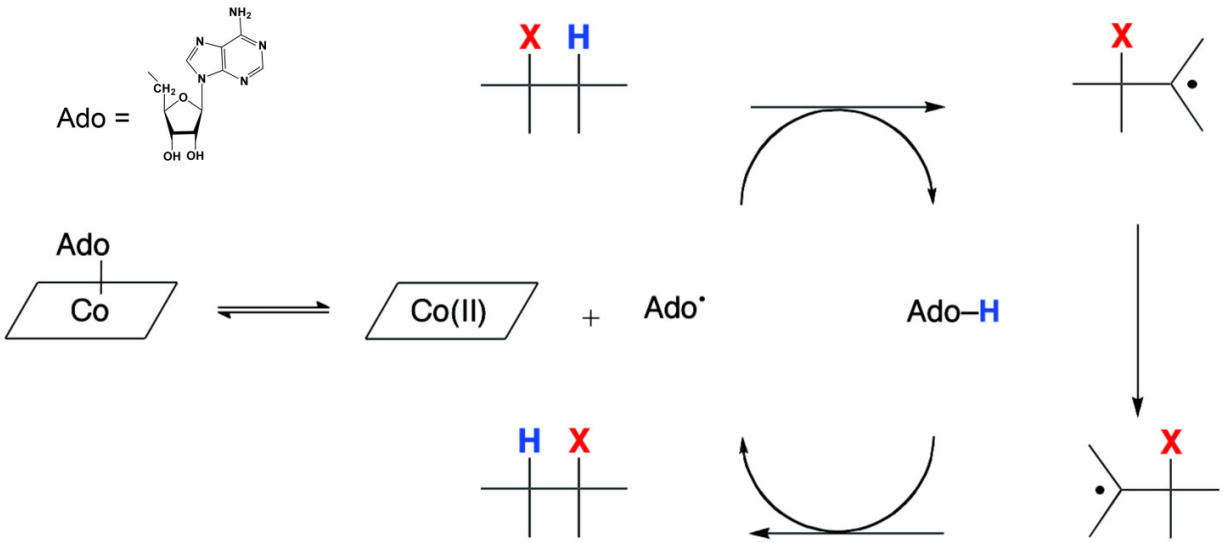


**Scheme 1. Minimal mechanism for the 1, 2-rearrangements catalyzed by AdocbI radical enzymes.** X in the scheme may be OH, $NH_2$ or a carbon-containing fragment (Marsh *et al.*, 2010; Sandala *et al.*, 2010)

## 2.2. Radical SAM enzymes

Bioinformatics genome analyses detected almost 3000 members of the SAM radical enzyme family (Pfam PF04055). Enzymes in the SAM radical superfamily catalyze a wide range of reactions including cofactor biosynthesis, DNA repair, modification of RNA, enzyme activation and synthesis of antibiotics (Sofia *et al.*, 2001). Despite their diverse catalyzing chemistry, Radical SAM (RS) enzymes utilize a common mechanism that involves an unconventional [4Fe-4S] cluster (RS cluster) coordinated by three rather than four cysteines present in a CxxxCxxC motif. The unique fourth iron of the cluster is coordinated by SAM (Layer *et al.*, 2004; Shisler & Broderick, 2012; Frey *et al.*, 2006) (Figure 2). The unique RS cluster is extremely oxygen labile and thus the enzymes only remain active under strict anoxic conditions (Marsh *et al.*, 2004).

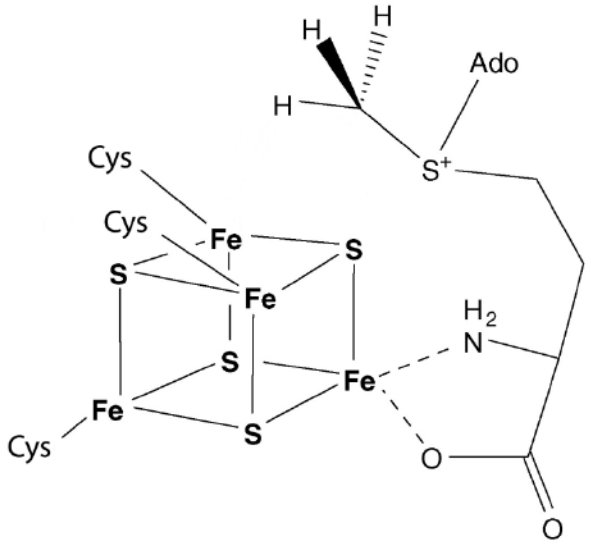


**Figure 2. SAM bound to the unique RS cluster** (Adapted from Walsby *et al.*, 2005)

RS enzymes require a strong one-electron reducing agent such as ferredoxins or flavodoxins to reduce the [4Fe-4S] cluster from the resting +2 to the active +1 state. The cluster in its reduced state $[4Fe\text{-}4S]^{+}$ transfers an electron to the sulfonium atom of SAM to promote homolytic cleavage of the S-5'C bond of SAM, producing methionine and the highly active 5'-deoxyadenosyl radical intermediate (Fontecave *et al.*, 2001; Nicolet *et al.*, 2009). The 5'-deoxyadenosyl radical abstracts a hydrogen atom from the substrate (SH) to produce a substrate radical (S< ) and 5'-deoxyadenosine (Figure 3). If the source of this hydrogen atom is an organic substrate resulting in the formation of corresponding substrate radical, then the radical enzymes are true enzymes as in lysine 2,3-aminomutase (LAM), biotin synthase (BioB), spore photoproduct lyase (SPP lyase), oxygen-independent coproporphyrinogen III oxidase (HemN), lipoate synthase (LipA) and tRNA-methyltransferase (MiaB). If the substrate is a protein that forms a catalytic glycyl radical, then the radical enzymes are termed as activases as in 4-hydroxyphenylacetate decarboxlyase activating enzyme (4Hpad-AE), anaerobic ribonucleotide reductase activating enzyme (aRNR-AE), pyruvate formate-lyase activating enzyme (PFL-AE), benzylsuccinate synthase activating enzyme (BssD-AE), and $B_{12}$-independent glycerol dehydratase activating enzyme (DhaB2) (Layer *et al.*, 2004 and references within).

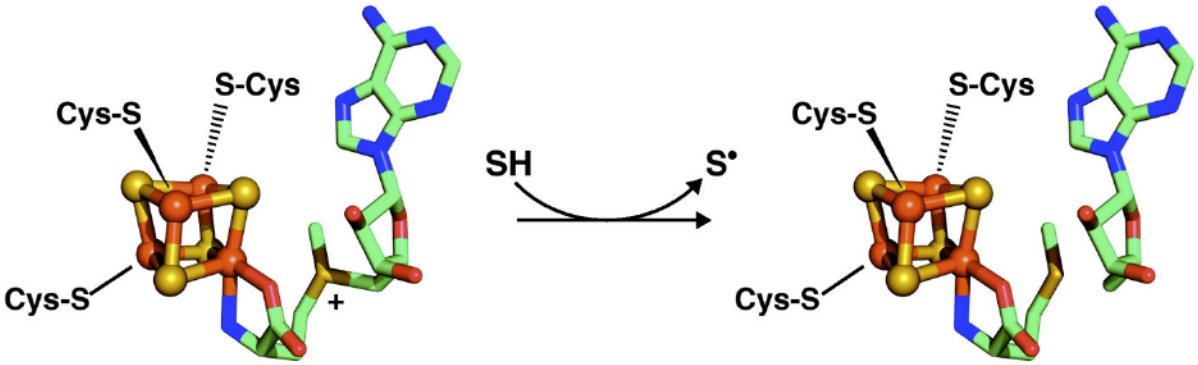


**Figure 3. RS enzymes catalyze the reductive cleavage of SAM.** SAM coordinated to the unique iron site of the [4Fe-4S] cluster (left). An electron is transferred to SAM from the reduced [4Fe-4S] cluster resulting in homolytic cleavage to methionine and 5'-deoxyadenosyl radical that activates the substrate (SH) by abstracting a hydrogen atom to produce a substrate radical (S<), methionine and 5'-deoxyadenosine (right). (Adapted from Shisler & Broderick, 2012)

Some enzymes like lysine-2, 3-aminomutase (LAM) and spore photoproduct-lyase (Figure 4) use SAM as a true cofactor in which the 5'-deoxyadenosyl radical is reversibly formed from SAM. Here SAM behaves similar to the AdoCbI (Frey, 2001; Fontecave, 2006; Friedel *et al.*, 2006; Marsh *et al.*, 2010). But in other enzymes like biotin synthase, lipoate synthase and a group of activating enzymes that generate glycyl radicals on its cognate partner enzymes (Figure 4) use SAM as a co-substrate where the resulting 5'-deoxyadenosyl radical is formed irreversibly from SAM and functions as a powerful oxidizing agent forming 5'-deoxyadenosine and methionine at each turn over (Ugulava *et al.*, 2001; Cicchillo & Booker, 2005; Marsh *et al.*, 2010). Thus the 5'-deoxyadeonsyl radical formed from SAM serves two biochemical functions, as a reactive catalyst and as a powerful one-electron oxidant. The reactions are summarized in figure 4.

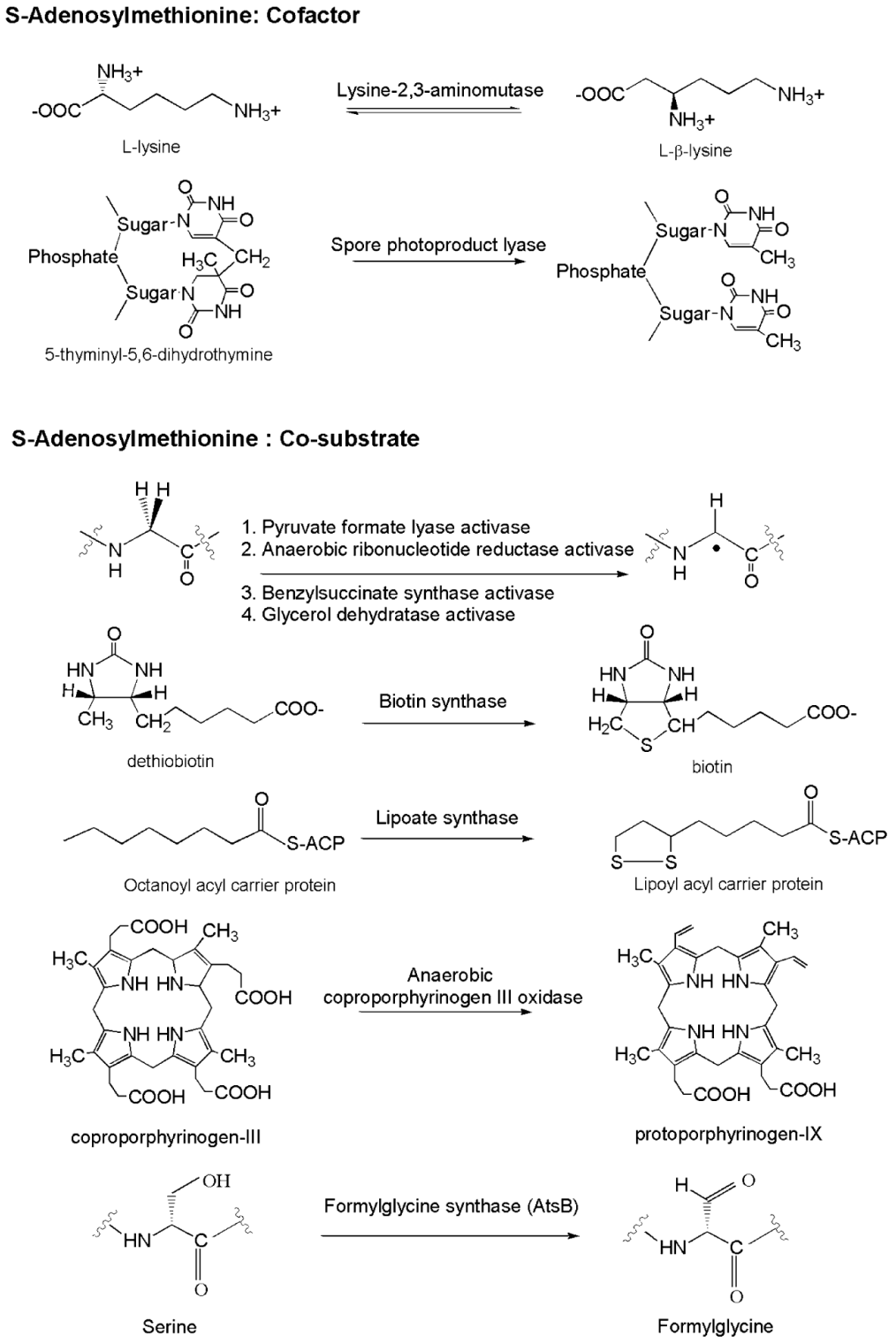


**Figure 4. Reactions catalyzed by SAM radical enzymes.** SAM acts as a cofactor in some enzymes and in some enzymes SAM serves as a co-substrate (Figure is taken from Marsh *et al.*, 2004).

## 2.2.1 Radical SAM enzymes with auxiliary Fe/S cluster(s)

A subset of radical SAM enzymes contain one or more Fe/S clusters which are termed as auxiliary clusters in addition to the unique RS cluster. Biotin synthase (BioB) is the first enzyme in the RS superfamily identified to contain an auxiliary Fe/S cluster (Ugulava *et al.*, 2001) followed by the characterization of many more enzymes that have the additional cysteine-rich motifs that could coordinate at least one auxiliary [4Fe-4S] cluster. In each case this auxiliary cluster(s) has been found to be essential for catalysis and the additional cysteine-rich motif is always found C-terminal to the RS motif (Scheme 2, Lanz & Booker, 2012).


**Scheme 2. Diagrammatic representation of N-terminal amino acids of radical SAM enzymes with auxiliary Fe/S clusters**. The RS cluster binding motif is shown by a green box with the three cysteines as bars. The red box represents the additional cys-rich motif with conserved cysteines marked as bars.

Though these auxiliary clusters are wide spread among the radical SAM superfamily their role is still under debate (Booker *et al.*, 2007). A role in electron transfer between the physiological electron donor and the RS cluster has been postulated for auxiliary clusters (Lanz & Booker, 2012). They also probably have a stabilizing effect on the protein structure, which may influence the kinetics of the RS cluster reduction (Shisler & Broderick, 2012; Lanz & Booker, 2012 and references within). In some better-studied enzymes, the auxiliary clusters serve as the source of sulfur insertion that is catalyzed by the RS cluster (Booker, 2009).

Enzymes such as BtrN and anSMEs, which belong to the dehydrogenase subfamily of SAM radical enzymes house auxiliary [4Fe-4S] clusters in addition to the RS cluster. BtrN binds one additional cluster proximal to the active site (Fig 5A) whereas anSMEs binds two, one near the active site and another near the protein surface (Fig 5B). X-ray structures of these enzymes show that these auxiliary cluster(s) are used for direct substrate ligation to catalyze dehydrogenation. The structural data also suggest that these auxiliary cluster(s) are placed in such a way that they create a conduit for electrons to travel from the buried substrate to the protein surface (Figure 5, Goldman *et al.*, 2013a; Goldman *et al.*, 2013b).

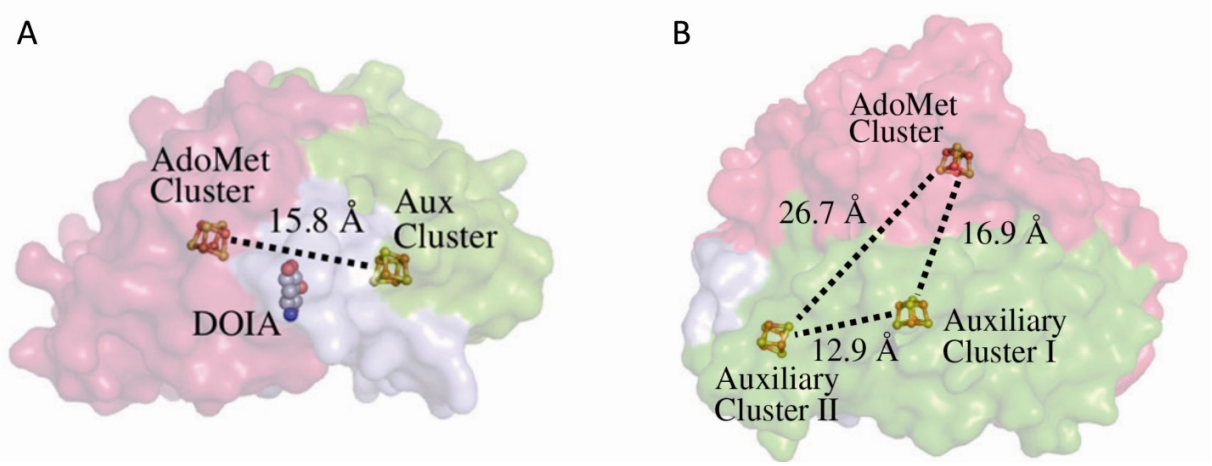


**Figure 5. X-ray structure of BtrN & anSMEcpe.** A) Structure of BtrN. B) Structure of anSMEcpe. The Adomet domain is colored in magenta, auxiliary cluster domain in green and linker region in grey. The [4Fe-4S] clusters are shown by ball and stick representation with Fe in orange and S in yellow. Distance between each cluster is given in Angstrom. The substrate of BtrN, DOIA (2-deoxy-scyllo-inosamine) colored in grey binds between the clusters. (Figure is taken from Goldman *et al.*, 2013a; Goldman *et al.*, 2013b).

The auxiliary clusters are also found in the group of enzymes which post translationally activates the glycyl radical enzymes. They are termed as glycyl radical activating enzymes (GRE-AEs) (Eklund & Fontecave, 1999; Fontecave, 1998). Except Pyruvate formate-lyase activating enzyme (Pfl-AE, Knappe *et al.*, 1984) and anaerobic ribonucleotide reductase activating enzyme (aRNR-AE, Fontecave, 1998), which are the early members of this family all other GRE-AEs harbor two additional cysteine containing motifs that are thought to bind Fe/S clusters.

## 2.3. Glycyl radical enzymes (GREs)

Many strict and facultative anaerobic bacteria, archaea and eukarya use glycyl radical enzymes (GREs) as biocatalysts to catalyze chemically difficult reactions (Buckel & Golding, 1998; Frey, 2001; Selmer *et al.*, 2005). GREs are synthesized as inactive proenzymes that are activated by its cognate activating enzymes (AE) (Eklund & Fontecave, 1999). Recently increasing number of new enzymes that contain glycyl radicals in their active sites have been characterized. The GREs are involved in various metabolic pathways like pyruvate degradation, ribonucleotide reduction, toluene metabolism, fermentative production of *p*-cresol, glycerol dehydration (Selmer *et al.*,

2005 and references within) and generation of trimethylamine from choline (Craciun & Balskus, 2012) all of which occurs in the absence of dioxygen (Figure 6).

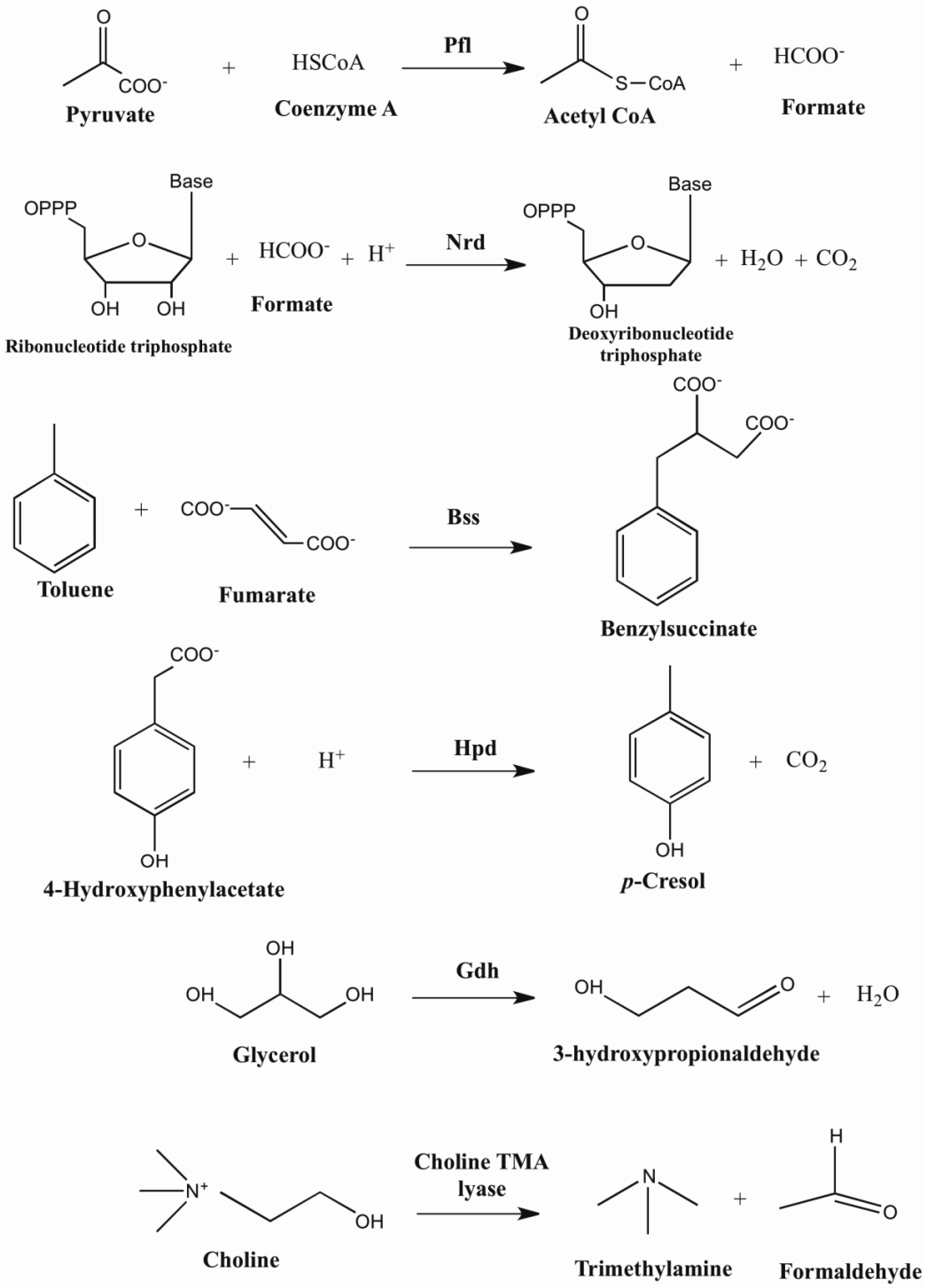


**Figure 6. Reactions catalyzed by GREs**

GREs are activated by the stereo specific abstraction of the C-2 *pro-S* hydrogen atom from a strictly conserved glycyl residue in the RVXG motif located at the C-terminal domain of the protein, by the 5'-deoxyadenosyl radical; generating a stable protein-bound glycyl radical (Frey *et al.*, 1994, Unkrig *et al.*, 1989). The glycyl radical is stabilized by delocalization of a free electron over the adjacent peptide backbone, which is called *captodative effect* (Viehe *et al.*, 1985) and can exhibit a half-life on the order of hours under anaerobic conditions. In the presence of oxygen, the radical becomes unstable and the enzyme is inactivated by the cleavage of the polypeptide chain at the glycine residue (Wagner *et al.*, 1992). Hence these enzymes can occur only in anaerobically competent microorganisms. During catalysis, the radical transfers to a specific cysteine residue located in close neighborhood of the glycyl radical site to yield a thiyl radical that removes a hydrogen atom from the substrate (Scheme 3, Selmer *et al.*, 2005, Becker *et al.*, 1999). Pyruvate formate lyase (Pfl) deviates from this mechanism, where the radical transfer is relayed on the thiol of another conserved cysteine that forms a covalent bond with the substrate activating it to a radical intermediate (Unkrig *et al.*, 1989).

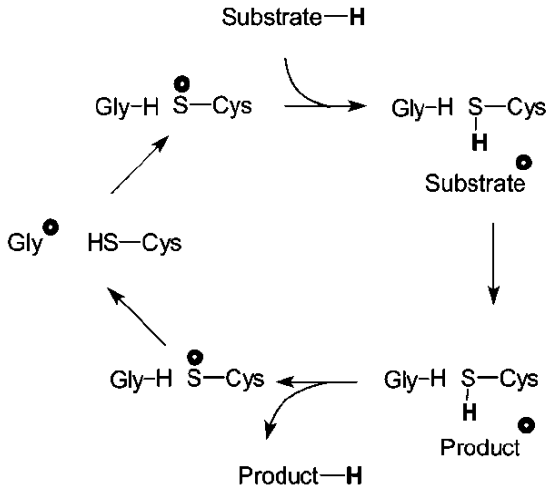


**Scheme 3. General mechanism of GREs** (Adapted from Selmer *et al.*, 2005). Detailed in text above.

Recently characterized GREs acting on aromatic compounds share more complex structures containing extra subunits that harbor Fe/S clusters. Their cognate AEs contain extra Fe/S clusters in addition to the unique RS cluster (Frey *et al.*, 2008, Eklund & Fontecave, 1999). Examples of these GREs are benzylsuccinate synthase from *Thauera* species involved in toluene degradation (Leuthner *et al.*, 1998, Li *et al.*, 2009) and 4-hydroxyphenylacetate decarboxylase from

*Clostridium* species that catalyzes the production of *p*-cresol in the last step of tyrosine fermentation (Barker, 1981, Selmer *et al.*, 2005).

# 4-Hydroxyphenylacetate decarboxylase (4Hpad)

*Clostridium scatologenes* and the human pathogen *C. difficile* ferment tyrosine to *p*-cresol (D'Ari & Barker, 1985). Most members of the *Clostridium* family degrade organic molecules and play a vital role in food spoilage (Barker, 1981). Decarboxylation of 4-hydroxyphenylacetate is the last step of the fermentation pathway and it is catalyzed by 4-hydroxyphenylacetate decarboxylase (4Hpad, E.C. 4.1.83) (Selmer & Andrei, 2001). The decarboxylation product of 4-hydroxyphenylacetate, *p*-cresol is a virulence factor of the human pathogen *C. difficile*, and its secretion may provide competitive advantage for the pathogen by suppressing the endogenous gastrointestinal microflora, favoring the development of gastrointestinal infections (Figure 7, Meijers & Evenepoel, 2011, Borriello & Wilcox, 1998, Smith & Macfarlane, 1997).

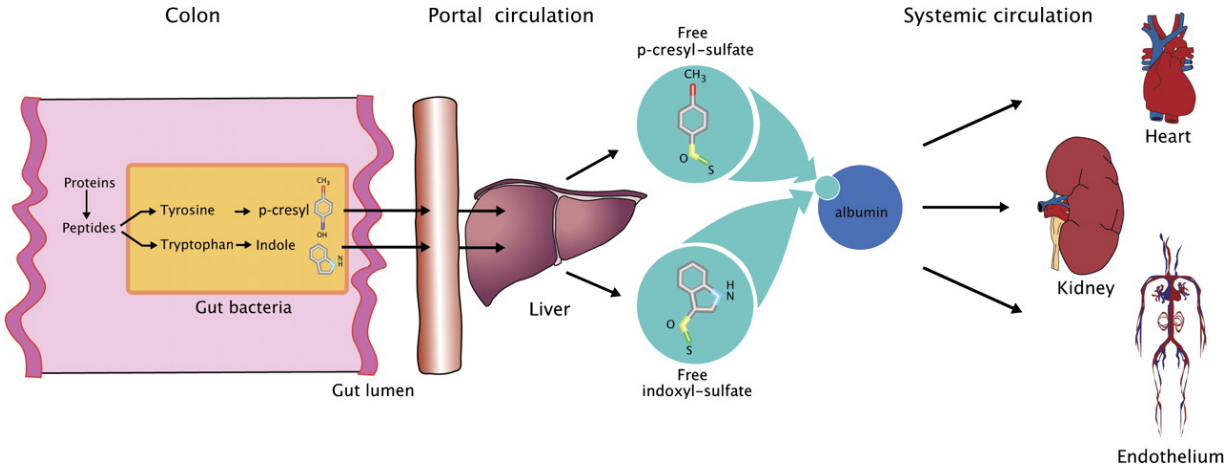


**Figure 7**. **Fermentation of tyrosine by *C. difficile*.** Amino acids such as tyrosine and tryptophan are fermented into *p*-cresol and indole, respectively. The products are absorbed in the liver and further metabolized to *p*-cresyl sulfate and *p*-indoxyl sulfate and transported to the kidney (Figure is taken from Meijers & Evenepoel, 2011).

4Hpad, first identified in *Clostridium difficile* (D'Ari & Barker, 1985) and recently in *C. scatologenes* (Selmer & Andrei, 2001) is a Fe/S cluster containing GRE (Fe/S-GRE). The enzyme is a functional heterotetramer $(\beta\gamma)_4$ composed of a 100 kDa catalytic active β-subunit

harboring the glycyl/thiyl radical dyad and a 10 kDa small γ-subunit that binds two [4Fe-4S] clusters. The γ-subunit is proposed to be involved in the regulation of the decarboxylase oligomeric state and activity (Andrei *et al.*, 2004; Martins *et al.*, 2011). 4Hpad is catalytically inactive until it is post-translationally activated by its cognate activating enzyme (4Hpad-AE). Upon substrate binding the radical is transferred from the glycine, Gly873 to the active site cysteine, Cys503 generating the thiyl radical that attacks the substrate (Selmer & Andrei, 2001). The cognate AE is a 35 kDa monomer belonging to the radical SAM family and contains up to two [4Fe-4S] clusters in addition to the characteristic RS cluster (Figure 8, Yu *et al.*, 2006).


**Figure 8. Arrangement of genes coding for 4Hpad system in *Clostridium* species.** Green and red are the β and γ-subunit of decarboxylase, respectively; blue is the activating enzyme (α-subunit).

4Hpad can also convert 3,4-dihydroxyphenylacetate into *p*-methylcatechol, 4-hydroxylmandelate into *p*-hydroxybenzyl alcohol and 4-hydroxyphenylacetamide acts as a competitive inhibitor (Selmer & Andrei, 2001). The crystal structure of 4Hpad from *C. scatologenes* has been solved in both substrate-free and substrate-bound states, the latter being obtained by crystal soaking (Martins *et al.*, 2011).

## Crystal structure of 4Hpad

The crystal structure of 4Hpad (1.8 Å resolution) reveals the presence of a cloverleaf shaped tetramer of heterodimers $(\beta\gamma)_4$ with D2 symmetry (Martins *et al.*, 2011). Each heterodimer comprises of a catalytic β-subunit sheltering the radical dyad and a γ-subunit with two [4Fe-4S] clusters. The shortest distance between each cluster and the active site is around 40 Å (Figure 9).

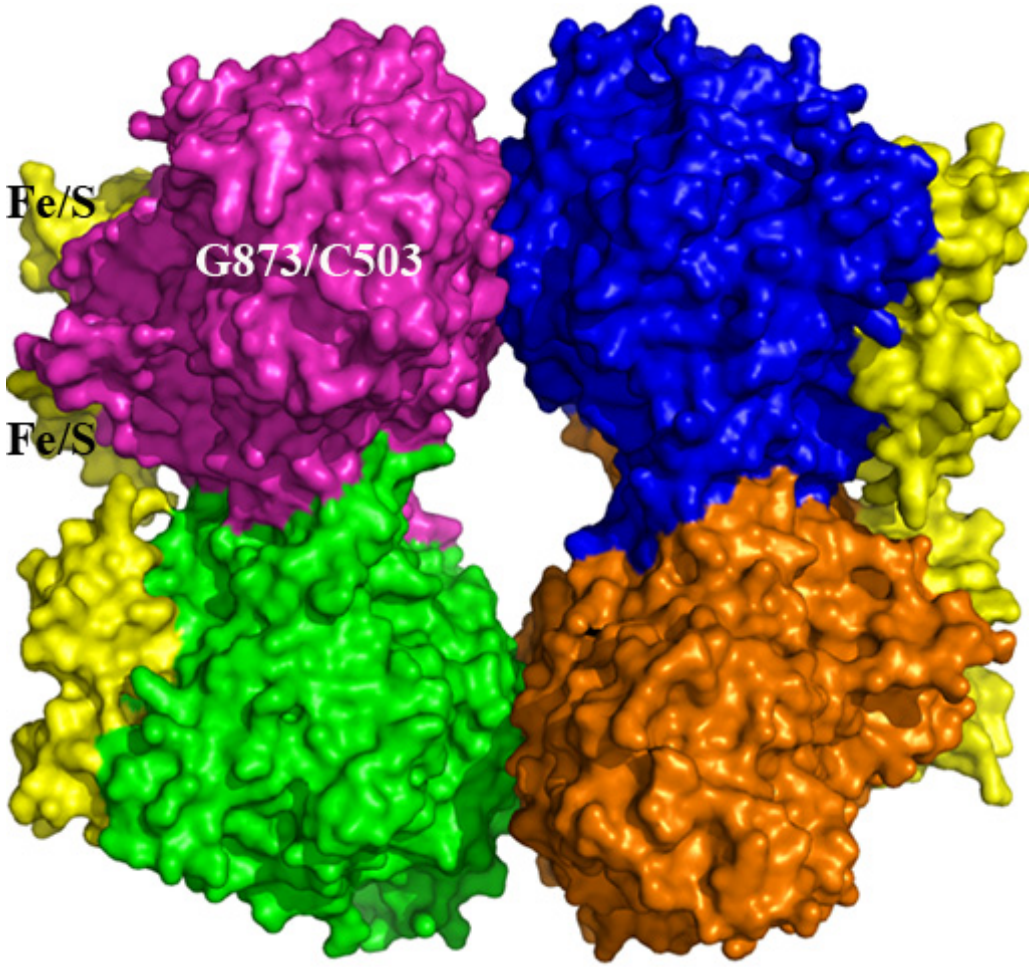


**Figure 9. Quaternary structure of 4Hpad.** Tetramer with four β subunits colored in pink, green, blue and orange and γ subunit in yellow. The Fe/S clusters embedded in the γ subunit are 20 Å apart from each other and 40 Å apart from the active G873/C503 radical dyad.

The active site pocket of 4Hpad is occupied by six water molecules coordinated by hydrogen bonds in the substrate-free state. In the substrate-bound state the location of five waters are displaced by the atoms of 4-HPA (Figure 10). 4-HPA is neatly bound in the active site through a network of hydrogen-bonding interactions by its functional groups, the carboxyl group with Ser344, Gly345, Cys503 and Glu505, and the hydroxyl group with His536 and Glu637. The Cys503 and Gly873 radical dyad is not a part of the active site pocket and separated from each other by 4.7 Å.

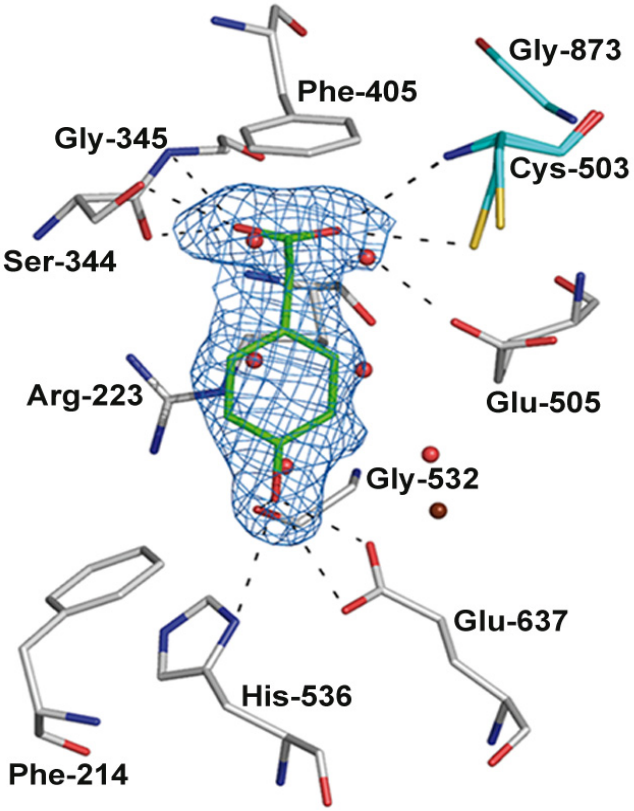


**Figure 10. Active site pocket of 4Hpad.** Protein residues are colored in gray for carbon, red for oxygen, blue for nitrogen and yellow for sulfur. The active radical dyad Cys503/Gly873 is indicated with carbons in cyan. Hydrogen bonding distances are displayed as dash lines and solvent molecules are shown as red spheres and brown sphere for the remaining water molecule that is not replaced by the substrate. The observed dual conformation of Cys503 is shown. The substrate 4-HPA is colored green for carbon and red for oxygen (Adapted from Martins *et al.*, 2011).

It was suggested in a previous study (Selmer & Andrei, 2001) that 4-HPA binds in the active site with its hydroxyl group close to the radical located at the Cys503. This binding mode suggested that the reaction starts by the abstraction of phenolic hydrogen from the substrate by Cys503 generating a *p*-phenoxy-acetate radical anion followed by decarboxylation. In contrary, the substrate-bound structure of 4-HPA (Figure 10) shows a different binding mode of the substrate. The carboxyl group is located in the close vicinity of Cys503 and the hydroxyl group is hydrogen bonded to Glu637 enabling a Kolbe-type decarboxylation (Scheme 4) (Martins *et al.*, 2011).

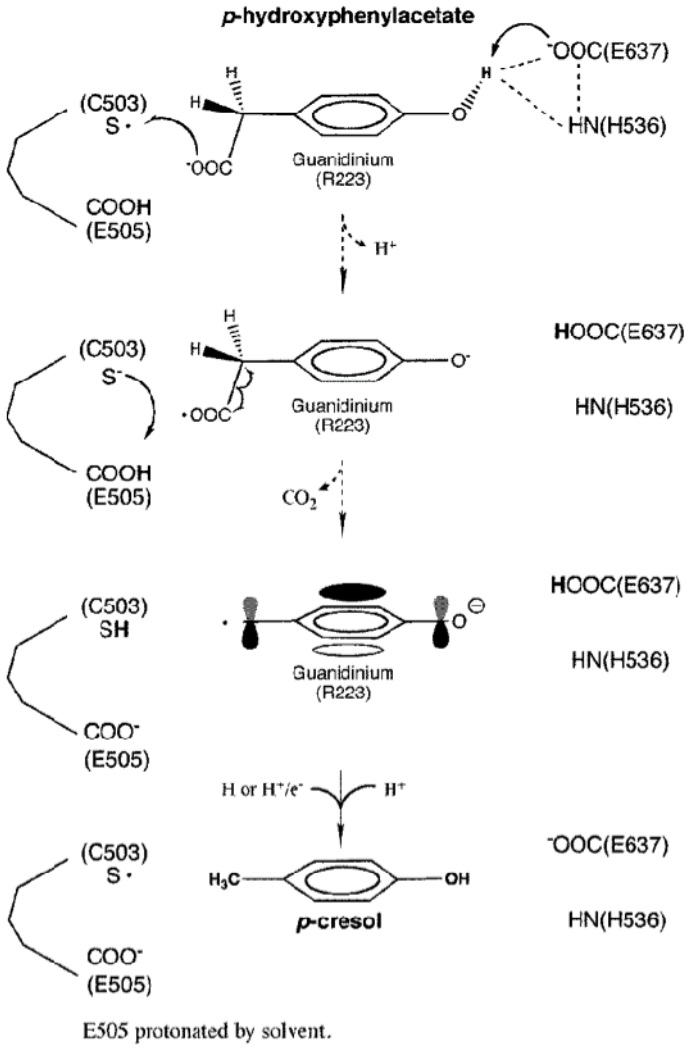


**Scheme 4. Putative catalytic mechanism of 4Hpad.** Detailed in text below.

Kolbe-type decarboxylation is defined as the one-electron oxidation of carboxylate ions ($COO^-$). A) The substrate, 4-HPA could be activated by the abstraction of proton by Glu637 and abstraction of electron by Cys503 radical forming a phenoxy-acetate radical anion. B) The carboxylic group probably gets detached to release $CO_2$, forming a *p*-benzoquinone methide radical anion that is stabilized by resonance. The decarboxylation step could be coupled with a proton transfer from Glu637 back to the substrate radical moiety forming a *p*-hydroxybenzyl radical. Simultaneously the thiolate of Cys503 is supposed to abstract a proton from Glu505 followed by the hydrogen atom transfer from the Cys503 to the *p*-hydroxybenzyl radical to form *p*-cresol. Thus the thiyl radical gets regenerated for the next catalytic cycle and the Glu505 could be protonated by the solvent (Scheme 4, Martins *et al.*, 2011; Feliks *et al.*, 2013).

# 4-Hydroxyphenylacetate decarboxylase activating enzyme (4Hpad-AE)

The glycyl radical activating enzymes (GRE-AEs) for pyruvate formate-lyase (Pfl-AE, Knappe *et al.*, 1984) and class-III ribonucleotide reductase (Nrd-AE, Gambarelli *et al.*, 2005) were the first to be isolated and have been extensively characterized. Both are monomers of 28 kDa and share the conserved SAM-binding cluster (RS cluster) $CX_3CX_2C$ motif near the N-terminus of the protein devoid of the additional Fe/S cluster. In contrast, all other identified GRE-AEs including 4-hydroxyphenylacetate decarboxylase activating-enzyme (4Hpad-AE) display two clostridial $CX_{2\text{-}5}CX_{2\text{-}4}CX_3C$ motifs within a 50 to 60 amino acid insert downstream of the RS cluster motif, suggesting these GRE-AEs might bind one or two auxiliary $[4Fe\text{-}4S]^{2+/1+}$ clusters (Lanz & Booker, 2012 and references within). 4Hpad-AE is a 35 kDa monomer and responsible for activating its partner decarboxylase, 4Hpad. In the presence of a strong one-electron reducing agent such as ferredoxin or flavadoxin, 4Hpad-AE convert SAM bound at the RS cluster into methionine and 5'-deoxyadenosyl radical that abstracts a hydrogen atom from the conserved glycine residue from its partner enzyme, thus activating it (Scheme 5).

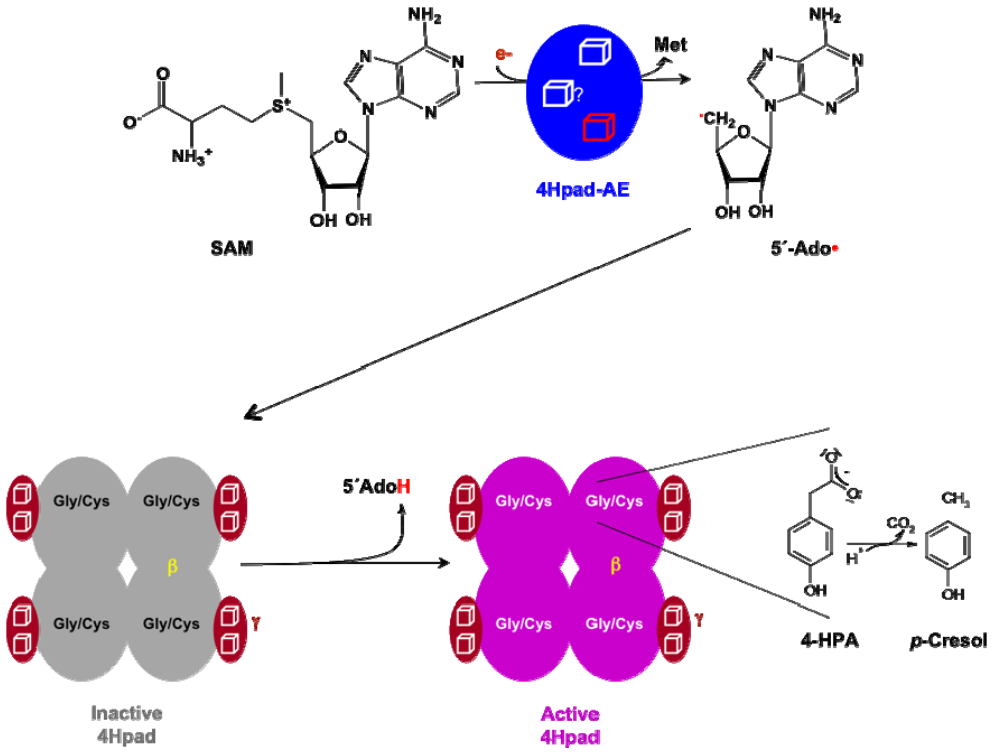


**Scheme 5. Decarboxylation of 4-HPA by 4Hpad system.** Detailed in text above.

Recently, an alternative homolytic cleavage mechanism for SAM has been reported for a GRE-AE, $B_{12}$-independent glycerol dehydratase activating enzyme (Gdh-AE, Figure 6). The alternative SAM cleavage generates a putative 3-amino-3-carboxypropyl radical and 5'-deoxy 5'-(methylthio), instead of a 5'-deoxyadenosyl radical and methionine. It was also suggested that the other homologous glycyl radical activating enzymes (GRE-AEs) containing the auxiliary cysteine-rich motifs might share this cleavage mechanism (Demick & Lanzilotta, 2011). However, the functions of the two putative auxiliary clusters are currently unknown (Lanz & Booker, 2012).

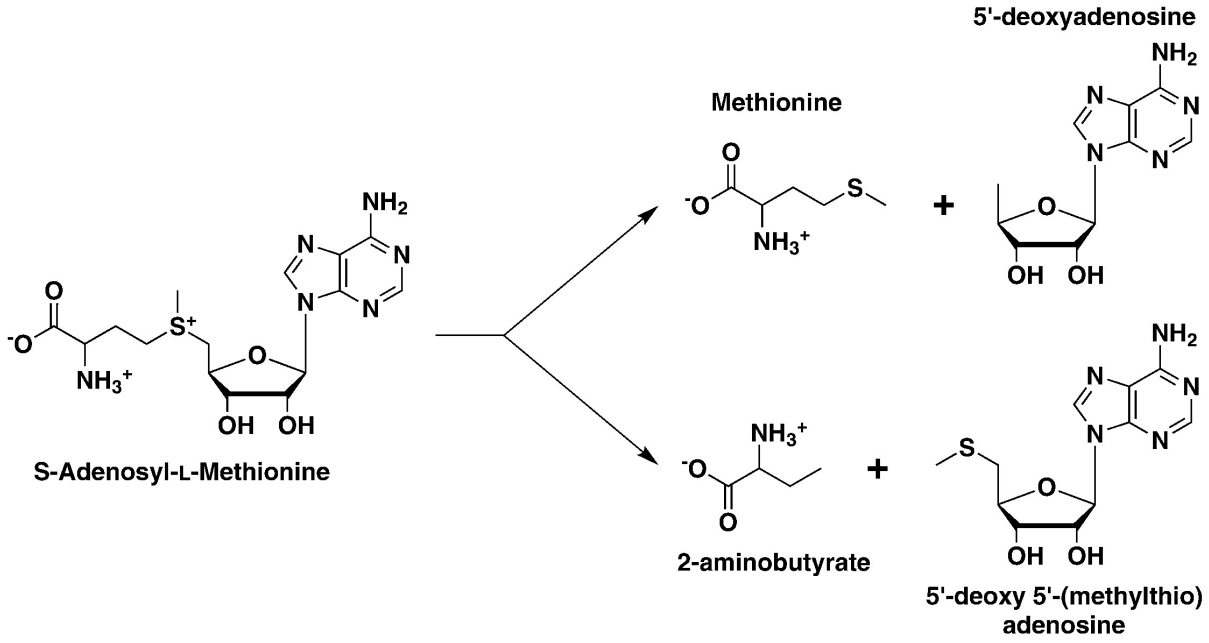


**Figure 6**. **Possible pathways for SAM cleavage** (Adapted from Lanz & Booker, 2012).

# Goals

The overall goal of this work was to obtain a complete mechanistic picture of the catalytic cycle of 4-hydroxyphenylacetate decarboxylase system. The functional interplay between the decarboxylase (4Hpad) and its cognate activating enzyme (4Hpad-AE) was investigated by studying both the enzymes kinetically and structurally. The main goal was split into three sub-goals.

## 1. To determine the mechanism of substrate activation by 4Hpad

- Heterologous expression and purification of 4Hpad in *E. coli* was improved thereby enhancing the yield and solubility of the protein.
- 4Hpad was co-crystallised with substrates and its analogues to visualize the structural changes in the active site pocket of the protein in the presence of various substrates and analogues.
- Residues of 4Hpad that are supposed to be involved in the Kolbe-type decarboxylation (E505, E637, H536) were mutated and characterized biochemically and structurally.

## 2. To diagnose the mechanism of radical formation at 4Hpad-AE

- Heterologous expression system for 4Hpad-AE in *E. coli* was constructed and a suitable purification protocol was developed.
- Classical reductive cleavage of SAM into 5′-deoxyadenosine and methionine by 4Hpad-AE was verified thereby ruling out the alternate SAM reductive cleavage mechanism suggested for GRE-AEs with auxiliary clusters.
- Spectroscopic analysis of the Fe/S clusters in 4Hpad-AE was performed to figure out the composition and state of each cluster.
- The role of the putative auxiliary Fe/S clusters present in 4Hpad-AE was investigated in an attempt to find out their biological relevance in 4Hpad/4Hpad-AE complex.
- Trials to determine the crystal structure of 4Hpad-AE were performed

## 3. To inspect the complex formation and radical transfer between 4Hpad & 4Hpad-AE

- Experiments to identify the conditions promoting the complex formation between 4Hpad and 4Hpad-AE were conducted.
- 5’-deoxyadenosine production by 4Hpad-AE and glycyl radical formation by 4Hpad was correlated to verify the efficiency of 4Hpad-AE in activating 4Hpad.

# Materials and methods

## 1. Chemicals and kits

Enzymes used in the molecular biology were purchased from Fermentas, New England Biosciences or Finnzymes (Thermo Fischer). Kits for PCR purification, Gel extraction and Plasmid purification were obtained from Fermentas or Qiagen. Chromatography columns and materials were purchased from GE healthcare (Nickel Sepharose Fast Flow, Mono Q 5/50 GL, Superdex-200 5/150 GL, HILOAD 16/60 SUPERDEX 200 PG) and IBA GmbH (Strep-Tactin® MacroPrep). Protein concentrators were purchased from Merck Millipore or Vivascience GmbH. $N_2$ and $N_2/H_2$ (95% / 5%) gases were obtained from Air Liquide (Berlin, Germany). Electrophoresis materials were supplied from Carl Roth and SDS-PAGE protein markers were from Fermentes. $^{57}Fe$ was purchased from Chemotrade (Düsseldorf, Germany). SAM and Sodium dithionite (DT) were purchased from Sigma and stock solutions were made in stock buffer (100 mM Tris/HCl pH 8.0, 150 mM sodium chloride, 5 mM magnesium chloride, 5 mM ammonium sulfate). Their concentrations were determined using molar extinction coefficient of 15,400 $M^{-1}$ $cm^{-1}$ at 260 nm and 6900 $M^{-1}$ $cm^{-1}$ at 315 nm, respectively. All other chemicals were purchased from Sigma, AppliChem, Fermentas, Fluka, Merck and Carl Roth and were of at least analytical grade. Silica 60 TLC plates (SIL G-25) were supplied by Macerey-Nagel (Germany), HPLC auto sampler vials were purchased from Chromacol (UK) and the protein vials with butyl septa were from Carl Roth. EPR tubes and Mössbauer cups were kindly provided by Dr. Antonio Pierik (Philipps-Universität Marburg, Germany) and Dr. Eckhard Bill (MPI für Chemische Energie Konversion Mülheim, Germany), respectively. All pET series and pASKIBA17plus expression vectors used in this work were from Novagen and IBA, respectively. The plasmid for TEV protease was constructed by Dr. Martin Bommer (Strukturbiologie/Biochemie, HU) as described in (Cabrita *et al.*, 2007). The expression plasmid pASK-BC for 4Hpad was kindly given by Prof. Dr. Thorsten Selmer (Fachhochschule Aachen, Germany).

## 2. Anaerobic work

Anoxic solutions were prepared in glass bottles with butyl rubber septa by at least four cycles of evacuation and flushing with $N_2$ gas at a vacuum-gas line. Unless otherwise stated, all protein

purifications and manipulations including crystallization trials were performed under oxygen-free atmosphere inside a glove box operated at an atmosphere of 95% $N_2$ / 5% $H_2$ (Model B, Coy laboratory Products, Inc., Michigan, USA). Materials were equilibrated in the anaerobic glove box 24 hour prior to the start of the experiments except protein, DT and SAM, which were readily introduced. SAM once dissolved in buffer was stored at -20 °C for two to three weeks and used for several measurements whereas DT was prepared fresh for each measurement. Isothermal titration calorimetry and *Stopped-flow* kinetics were performed inside an MBraun LABstar glovebox operated under a nitrogen atmosphere with $O_2$ < 0.5 ppm (MBraun Inertgas-systeme, Germany).

# 3. Bacterial strains

**Table 3.1**. *Escherichia coli* strains used in this study

| Strain | Genotype | Source |
|---|---|---|
| DH5α | $F^-$ Φ80*lac*ZΔM15 Δ(*lac*ZYA-*arg*F) U169 *rec*A1 *end*A1 *hsd*R17 ($rK^-$, $mK^+$) *pho*A *sup*E44 $\lambda^-$ *thi*-1 *gyr*A96 *rel*A1 | Invitrogen™ |
| BL21(DE3) | $F^-$ *ompT hsdSB(*$rB^-$ *mB*$^-$*) gal dcm* (DE3) | Novagen |
| Rosetta™(DE3) | $F^-$ *ompT hsdSB(*$rB^-$ *mB*$^-$*) gal dcm* (DE3) pRARE6 ($Cam^R$) | Novagen |
| Rosetta(DE3)pLysS | $F^-$ *ompT hsdSB(*$rB^-$ *mB*$^-$*) gal dcm* (DE3) pLysSRARE6 ($Cam^R$) | Novagen |

# 4. Media and antibiotics

**Table 4.1.** Media used in this study

| Media | Ingredients |
|---|---|
| LB (Luria-Bertini) | 10 g/L trypton, 5 g/L yeast, 10 g/L NaCl |
| LBG (Luria-Bertini with glucose) | 10 g/L trypton, 5 g/L yeast, 10 g/L NaCl, 2 g/L glucose |
| TB (Terrific Broth) | 12 g/L trypton, 24 g/L yeast, 4 ml/L 97% glycerol, 100 ml/L phosphate buffer* |
| mTB (modified Terrific Broth) | 12 g/L trypton, 24 g/L yeast, 8 ml/L 97% glycerol, 100 ml/L phosphate buffer* |

*Mixture of 0.17 M $KH_2PO_4$ and 0.72 M $K_2HPO_4$ in water, autoclaved separately; the media were adjusted to pH 7.0.

**Table 4.2**. Antibiotics used in this study

| Name | Stock concentration | Working concentration |
|---|---|---|
| Carbenicillin (Cb) | 50 mg/ml in $H_2O$ | 50 µg/ml |
| Chloramphenicol (Cam) | 34 mg/ml in Ethanol | 34 µg/ml |
| Kanamycin (Km) | 50 mg/ml in $H_2O$ | 50 µg/ml |

# 5. Molecular biology

## 5.1. Cloning of 4Hpad-AE

The open reading frame coding for 4Hpad-AE from *Clostridium scatologenes* (accession number ABB05048; monomer of 36 kDa) and from *Clostridium difficile* (accession number CAD65891; monomer of 36 kDa) were codon-optimized for recombinant heterologous expression in *E. coli* by GenScript (USA) using the codon adaptation index (CAI) method (Sharp & Li, 1987) and Eurofins MWG Operon (Germany), respectively. In both cases, the synthetic genes were inserted at the *Nde*I and *Xho*I restriction sites of the MCS (multiple cloning site) of pET28a(+) to generate a TEV (Tobacco Etch Virus) protease cleavable N-terminal $His_6$-tagged construct. The resulting plasmids were named as pET28a-Csd_AE and pET28a-Hpd_AE. The plasmids were transformed in chemically competent *E. coli* DH5α strain with Km as antibiotic using standard protocols (Sambrook & Fritsch, 1989), isolated using a plasmid purification kit and the nucleotide sequences were verified by DNA sequencing (Eurofins MWG Operon, Germany).

## 5.2. Cloning of Δ66-AE

Δ66-AE was cloned by PCR using the expression plasmid pET28a-Csd_AE as template with primers mentioned in Table 5.1. Gene amplification by PCR was performed using the standard mixture by the given PCR protocol (appendix table A1). The resulting PCR product was phosphorylated in the presence of polynucleotide kinase and ATP prior to ligation to pET28a(+) producing the expression plasmid pET28a-Δ66-AE. Ligation, determination of DNA concentration, preparation of competent cells and transformation in DH5α strain were performed as described in (Sambrook & Fritsch, 1989). The plasmid was isolated using a plasmid

purification kit and the nucleotide sequence was verified by DNA sequencing (Eurofins MWG Operon, Germany).

## 5.3. Cloning of AE-9M

AE-9M was cloned by the *polymerase incomplete primer extension method* (PIPE cloning) as described by (Klock *et al.*, 2008); (Klock & Lesley, 2009) and modified by Dr. M. Bommer (in-house source) using the four set of primers mentioned in Table 5.1. *Pfu* DNA polymerase amplified the pET28a-Csd_AE plasmid with the primers carrying the mutations (PCR conditions mentioned in appendix table A2). The PCR reaction was stopped slightly before the elongation time finished and the product was verified by 2% (w/v) agarose gel. The amplified product was then ligated to a pET-28a(+) vector with *pipe* cloning competent overhangs by simply incubating in ice for 5 min and straightly transformed in chemically competent *E. coli* DH5α strain with Km as antibiotic. The plasmid was isolated using a plasmid purification kit and all the mutations were confirmed by DNA sequencing (Eurofins MWG Operon, Germany).

**Table 5.1.** Primers and Plasmids used in the mutagenesis of 4Hpad-AE

| Name | Nucleotide sequence (5'-3') |
|---|---|
| pET28a-Δ66-AE | Fw: AAAGAATATACCGTTGATGAACTGATGACGATCC<br>Rv: GCCGCCATGGGTGGTCCAAGATTCCGGGTTGGCACACC |
| pET28a-AE-9M | Patch1_Fw: CCGGAATCTTGGACCGCGGCAGCTCATATCATGGTGGCAG<br>Patch1_Rv: CTGCCACCATGATATGAGCTGCCGCGGTCCAAGATTCCGG<br>Patch2_Fw: CAGTTGGGATACCTGCGCTGCATGTGCAACGTTTGATTGCGTGAAC<br>Patch2_Rv: GTTCACGCAATCAAACGTTGCACATGCAGCGCAGGTATCCCAACTG<br>Patch3_Fw: CCAAATGGAATCAGCTGGGTGCTGCATATGCGTACAGCAAATACGGCG<br>Patch3_Rv: CGCCGTATTTGCTGTACGCATATGCAGCACCCAGCTGATTCCATTTGG<br>PIPE_Fw: CTTGTATTTCCAGGGCCATATGAAAGAAAAAGGCCTG<br>PIPE_Rv: CGACGGAGCTCGAATTCGGATCCTTAAAACGGGGTATTATCACCGATG |

All the primers were synthesized by Eurofins MWG Operon, Germany.

## 5.4. Mutagenesis of 4Hpad

QuickChange site-directed mutagenesis method from stratagene was used to construct the site-directed 4Hpad mutants. PCR was performed with the two corresponding mutation primers

(Table 5.2) and the conditions are given in the appendix table A3. The PCR product was verified by 1% Agarose gel followed by *DpnI* (2 U/µl) digestion at 37 °C for 60 min. The plasmid was then purified by PCR purification kit and transformed in *E. coli* DH5α strain with Cb as antibiotic. Point mutations were confirmed by DNA sequencing (Eurofins MWG Operon, Germany).

**Table 5.2.** Primers and Plasmids used in the cloning and mutagenesis of 4Hpad

| Name | Nucleotide sequence (5'-3') | Source[a] |
|---|---|---|
| pASK-E505Q | Fw: GGAGGATGTCTACAATCTGCACCTGGATGTTTC<br>Rv: GAAACATCCAGGTGCAGATTGTAGACATCCTCC | Diploma work Lisa S, 2009 |
| pASK-E637Q | Fw: CCTACATGTGGTACAGGTGTTCAGTTTATTGGTATGCCT<br>Rv: AGGCATACCAATAAACTGAACACCTGTACCACATGTAGG | |
| pASK-H536Q | Fw: GGAGCAAGATATAATTCATGTATTAATTTTCAATCCTGTGGAACTATTAC<br>Rv: GTAATAGTTCCACAGGATTGAAAATTAATACATGAATTATATCTTGCTCC | |
| pASK-HE2Q | E637Q<br>Fw: CCTACATGTGGTACAGGTGTTCAGTTTATTGGTATGCCT<br>Rv: AGGCATACCAATAAACTGAACACCTGTACCACATGTAGG<br>H536Q<br>Fw: GGAGCAAGATATAATTCATGTATTAATTTTCAATCCTGTGGAACTATTAC<br>Rv: GTAATAGTTCCACAGGATTGAAAATTAATACATGAATTATATCTTGCTCC | pASK-E637Q & pASK-H536Q were used |

[a]Unless otherwise stated, plasmids were constructed during the course of this study. All the primers were supplied by Eurofins MWG Operon, Germany.

# 6. Protein expression

## 6.1. Expression of 4Hpad-AE and its variants

The plasmid pET28a-Csd_AE or pET28a-Hpd_AE was transformed into *E. coli* BL21(DE3) and single colonies were grown overnight at 37 °C in 50 ml LB medium supplemented with Km as antibiotic. Overnight cultures (ON) were inoculated to 2 L mTB medium in 5L Erlenmeyer flasks (1:100) and the cultures were grown aerobically at 37 °C by shaking. When the OD at 595 nm reached 0.6-0.8, Mohr's salt and sodium sulfide (0.1 mM each) were supplemented into the media prior to induction with 0.2 mM isopropyl-β-D-thiogalactopyranoside (IPTG). The cultures were further agitated at 25 °C for 6-8 hours and harvested at 7,000 rpm for 20 minutes at 8 °C

(Beckman-Coulter centrifuge). Expressions of Δ66-AE and AE-9M variants were performed similarly.

## 6.2. Expression of 4Hpad and its variants

Cells harboring the expression plasmid pASK-BC were transformed in *E. coli* Rosetta$^{TM}$(DE3). Single colony was used to inoculate a ON culture grown aerobically at 37 °C in 200 ml LBG medium containing Cb/Cam with shaking. The ON culture was used to inoculate 4 L LBG medium with Cb/Cam in 5 L glass bottles (1:20) with butyl rubber septum. Initially the culture was grown aerobically at 37 °C by bubbling air and enriched with 0.5 mM Mohr's salt and sodium sulfide. When the $OD_{595\ nm}$ reached 0.6-0.8, air bubbling was arrested and the culture was supplemented with 2% Ethanol, 50 mM $KNO_3$ followed by the induction with anhydrotetracyclin (ATH, 0.2 ng/ml). Cells were further cultivated at 25 °C anaerobically by $N_2$ gas flushing and harvested after 20 h under $N_2$ gas flushing followed by centrifugation at 7,000 rpm for 20 minutes at 8 °C. Cell pellet was frozen in liquid $N_2$ and stored at -20 °C until needed. Expressions of all the variants of 4Hpad were performed identically as described for the wild-type protein. Detailed information on tested factors and optimal growth conditions are given in the appendix table A4.

# 7. Protein purification

## 7.1. Purification of 4Hpad-AE and its variants

Fresh or frozen cells were resuspended in buffer A (50 mM Tris-HCl pH 7.5, 150 mM NaCl, 5 mM β-mercaptoethanol) supplemented with 20 mM imidazole, DNAse and lysozyme (10 µg $ml^{-1}$ each). Cells were broken in an ice-cooled glass rosette by ultrasounds (4x 50% pulse for 5 minutes with 5 minutes interval; Sonoplus HD 2200) and cell debris was removed by ultracentrifugation at 35,000 rpm for 1 h at 18 °C (Beckman-Coulter centrifuge). The supernatant was passed through a nickel-SHP affinity column (5 ml volume) pre-equilibrated with buffer A containing 20 mM imidazole, followed by washing the column with the same buffer. His-tagged 4Hpad-AE was eluted with buffer A containing 250 mM imidazole. Protein containing fractions were pooled, concentrated (10 kDa cutoff), shock-frozen in glass vials with butyl rubber septa and stored in liquid nitrogen. For $His_6$-tag cleavage, pooled fractions were concentrated and

desalted on a PD-10 column equilibrated in buffer A and incubated overnight with $His_6$-tagged TEV protease in a 1:100 protein ratio at 8-10 °C. The tag-free proteins were recovered in the flow-through of a nickel-NTA affinity column (5 ml volume), concentrated (10 kDa cutoff), shock frozen in glass vials and stored in liquid nitrogen.

In an attempt to enhance the reconstitution of Fe/S clusters in 4Hpad-AE (*in vitro* cluster assembly), cells harboring the expression vectors were incubated and lysed along with cell lysates containing over expressed ISC operon proteins (Nakamura *et al.*, 1999) in buffer A supplemented with magnesium chloride, cysteine and ATP (5 mM each), 0.2 mM Mohr's salt, DNAse and lysozyme (10 μg $ml^{-1}$ each). Purification and $His_6$-tag cleavage were similar as above and the protein purified by *in vitro* cluster assembly will be henceforth called as 4Hpad-AE*. Purifications of Δ66-AE and AE-9M were performed identically as the wild type 4Hpad-AE.

## 7.2. Purification of 4Hpad and its variants

Fresh or frozen cells were resuspended in 100 ml buffer B (100 mM Tris/HCl pH 8.0, 500 mM sodium chloride, 5 mM magnesium chloride, 5 mM ammonium sulfate, 5 mM DTT) supplemented with cysteine and ATP (5 mM each), 0.2 mM Mohr's salt, DNAse and lysozyme (10 μg $ml^{-1}$ each) and a pinch of Avidin. Cells were broken in an ice-cooled glass rosette by ultrasounds (4x 50% pulse for 5 minutes with 5 minutes interval; Sonoplus HD 2200) and cell debris was removed by ultracentrifugation at 35,000 rpm for 1 h at 18 °C (Beckman-Coulter centrifuge). The supernatant was passed through a Streptactin® MacroPrep affinity column (10 ml volume) pre-equilibrated with buffer B followed by washing the column with three column volumes of the same buffer until the absorption at 280 nm reached zero. Strep-tagged 4Hpad was eluted with buffer B containing 2.5 mM Desthiobiotin. Protein containing fractions were pooled, concentrated (10 kDa cutoff), shock-frozen in glass vials with butyl rubber septa and stored in liquid nitrogen. Purification of all the variants of 4Hpad was performed similar to the wild-type protein.

## 7.3. Protein concentration

Protein concentrations were determined by measuring the absorbance at 280 nm after denaturing in 6 M guanidine hydrochloride containing 0.1% trifluoroacetic acid (Gill & Hippel, 1989). The

molar extinction coefficients (Table 7.1) for all the proteins were calculated from the amino acid sequences using the ProtParam tool (http://web.expasy.org/protparam/).

**Table 7.1.** Molar absorption coefficients of all the enzymes and its variants used in this study

| Enzyme | Extinction coefficient at 280 nm ($M^{-1}$ $cm^{-1}$) |
|---|---|
| His-tagged 4Hpad-AE | 59360 |
| Tag free 4Hpad-AE | 57870 |
| His-tagged Δ66-AE | 48360 |
| Tag free Δ66-AE | 46870 |
| Tag free AE-9M | 57870 |
| Strep-tagged 4Hpad | 150060 |
| Strep-tagged E505Q | 150059 |
| Strep-tagged E637Q | 150059 |
| Strep-tagged H536Q | 150051 |
| Strep-tagged HE2Q | 150050 |

# 8. Reconstitution of Fe/S clusters in 4Hpad-AE and its variants

Iron-sulfur clusters in 4Hpad-AE, 4Hpad-AE* and Δ66-AE were reconstituted similarly using a modified protocol described by (Li *et al.*, 2009) and (Ugulava *et al.*, 2001). 4Hpad-AE (25 µM in buffer A) was treated with 5 mM β-mercaptoethanol for 1 h and incubated with a 10-fold molar excess of ferric ammonium citrate followed by the addition of lithium sulfide slowly. The reconstitution mixture was incubated for 2 h at 15 °C with occasional stirring. Excess of iron and sulfur were removed on a PD-10 column equilibrated with buffer A and eluted proteins were concentrated, aliquoted and stored in liquid nitrogen as described above. Detailed information on various tested reconstitution conditions and their results are tabulated in the appendix table A5. Incorporation of Fe/S clusters in 4Hpad-AE, 4Hpad-AE* and Δ66-AE were verified by methods such as UV-vis, EPR and Mössbauer spectroscopy.

## 8.1. UV-vis spectroscopy

UV-visible spectra were recorded using an Agilent 8453 diode array spectrophotometer. Non-

heme iron content was determined with UV-visible spectroscopy at 400 nm using a molar extinction coefficient of 4 $mM^{-1}$ $cm^{-1}$ for 1 mol Fe per mol protein (Sweeney & Rabinowitz, 1980).

## 8.2. Colorimetric determination of non-heme iron

Non-heme iron content of the Fe/S clusters in 4Hpad-AE, 4Hpad-AE* and Δ66-AE were also determined with a ferene-derived colorimetric assay as described in (Fish, 1988).

## 8.3. EPR spectroscopy

EPR spectroscopy was carried out at the Core facility for protein spectroscopy, Institute of Cytobiology and Cytopathlogy, Philipps University Marburg, Germany by Antonio J Pierik. The measurements were performed at 10 K with a Bruker ESP-300E spectrometer equipped with an ER-4116 dual mode cavity and an Oxford Instruments ESR-900 helium-flow cryostat with ITC4 temperature controller. Spin integration was carried out under non-saturating conditions using 10 mM $CuSO_4$ in 2 M $NaClO_4$/10 mM HCl as standard. The samples measured were as follows

- As-isolated 4Hpad-AE, 4Hpad-AE* and Δ66-AE: 80 µM protein in buffer C (100 mM Tris/HCl pH 8.0, 150 mM sodium chloride, 5 mM magnesium chloride, 5 mM ammonium sulfate, 5 mM β-mercaptoethanol)
- Reduced 4Hpad-AE, 4Hpad-AE* and Δ66-AE: 80 µM protein reduced by five-fold molar excess of DT for 5 min in buffer C
- Reduced 4Hpad-AE, 4Hpad-AE* and Δ66-AE samples plus SAM: 80 µM protein were treated with 2 mM SAM after 5 min of reduction with DT in buffer C

Samples were shock-frozen in ethanol/liquid nitrogen inside an anaerobic glove box.

## 8.4. Mössbauer spectroscopy

Mössbauer spectra were recorded at the Max Planck Institute for Chemical Energy Conversion, Mülheim, Germany by Eckhard Bill. The spectra were recorded on a spectrometer with alternating constant acceleration of the γ-source. The minimum experimental line width was 0.24 mm/s (full width at half-height). The sample temperature was maintained constant in an Oxford

Instruments Variox or in an Oxford Instruments Mössbauer-Spectromag cryostat. The latter is a superconducting split-pair magnet system for applied fields up to 7 T, where the temperature of the sample can be varied in the range 1.5 K to 250 K. Zero-field spectra were fitted using quadrupole doublets, and applied field measurements were simulated with the Zeeman Hamiltonian for $S = 1/2$ and the usual nuclear Hamiltonian for nuclear Zeeman and electric hyperfine interactions (Glaser, 2011). In both cases Voigt profiles have been invoked for the line shapes, corresponding to Gaussian distributions of Lorentzian lines, calculated using the complex error function with the rational approximation of (Hui *et al.*, 1978) and (Schreier, 2011). The Lorentzian contributions were fixed to the natural line width of $^{57}$Fe spectra (0.2 mm/s).

To enrich 4Hpad-AE with the Mössbauer isotope, 33.5 mg from $^{57}$Fe metal were dissolved in 1 ml of 8 M HCl at room temperature for 12 h. The volume was adjusted to 5 ml with double deionized water and 0.68 mmol of trisodium citrate dihydrate were added. The solution was neutralized with ammonia to a pH of 5 to 6 to form ammonium ferric citrate. Addition of this stock solution to 2 l of mTB medium (pH 7-8) resulted in a $^{57}$Fe concentration of 300 µM (final concentration circa 355 µM). $^{57}$Fe enriched 4Hpad-AE was purified in the presence of auxiliary proteins from the ISC assembly machinery as described above for 4Hpad-AE* (In vitro cluster assembly). The samples measured were as follows

- As-isolated 4Hpad-AE*: 0.4 mM 4Hpad-AE* in buffer C
- SAM treated 4Hpad-AE*: 0.3 mM 4Hpad-AE* treated with 2 mM SAM in buffer C

Samples were shock-frozen in liquid nitrogen inside an anaerobic glove box.

Similar experiments were carried out for Δ66-AE.

# 9. Enzymatic assays

## 9.1. Activity assay for reductive cleavage of SAM by 4Hpad-AE and Δ66-AE

All the enzymatic assays were determined in buffer C. 12 µM of 4Hpad-AE or Δ66-AE was incubated with a 30 fold molar excess of DT for 5 minutes in one ml cuvette. The reduction was verified by UV-visible spectroscopy (observing decrease at 420 nm absorption), after which 2 mM SAM was added. Typical reaction volumes were 500 µl and the assay was carried out at

30 °C. 50 µl samples were withdrawn at fixed time intervals up to 2 hours and the reaction was stopped by adding 50 µl 10% trifluoroacetic acid containing 30 µM adenosine as internal standard. The SAM cleavage products were analyzed by the following methods.

### 9.1.1. Reverse-phase HPLC separation

The 100 µl product samples thus obtained at fixed time intervals after treating with SAM were centrifuged at 14,000 x g for 30 minutes to remove precipitated protein. 50 µl of supernatant were injected into a Jasco HPLC system containing a 100 C18 5 µm Kromasil (250 x 4.6 mm) column, UV-2075 Plus and automatic sampler 2055 Plus (Jasco Inc., Germany). Detection wavelength was set at 259 nm and flow rate at 1 ml $min^{-1}$. Eluents A and B consisted of 2% acetonitrile in triethylamine pH 7.5 and 80% acetonitrile in triethylamine pH 7.5, respectively. After injection, the mobile phase was kept at 100% eluent A for 2 minutes before eluent B was increased to 20% for 18 minutes. The concentrations of SAM and 5'-deoxyadenosine were calculated via integration of the peak areas and comparison to a linear calibration curve from a series of standards at known concentrations or by using a detector response factor via the internal standard method. Detected HPLC elution fractions were compared with those of standard SAM, adenosine (Ado), 5'-deoxyadenosine (5'-AdoH), 2'-deoxyadenosine (2'-AdoH), 5'-deoxy 5'(methylthio)adenosine (MTA) and S-adenosylhomocysteine (SAH).

### 9.1.2. ESI-MS

HPLC elution peaks corresponding to 5'-AdoH and SAM were dried under vacuum, dissolved in 50% acetonitrile and analyzed by ESI-MS in a ThermoFinnigan LCQ DECAXP mass spectrometer at the Mathematisch-Naturwissenschaftliche Fakultät I, Humboldt University Berlin, Germany by Angelika Woyda. The flow rate was 8 µl $min^{-1}$ and 100 spectra were collected at 0.8 half width resolution in positive mode.

### 9.1.3. TLC

TLC using phenylisothiocyanate (PITC) derivatization after protein precipitation (Dimova, 2003) detected production of methionine. PITC-reagent was freshly prepared by mixing PITC with

water, ethanol and triethylamine (1:1:7:1). 100 µl from the supernatant of the assay mixture after centrifugation was mixed with 400 µl of PITC-reagent and incubated at room temperature for 15 minutes. After solvent removal by freeze-drying, the residue was dissolved in PITC-reagent and a small amount was spotted on a Silica Gel 60 plate. After development with an ethanol/water (3:1) mobile phase, PITC-derivatives were visualized by spraying 0.2% ninhydrin in acetone.

## 9.2. 4Hpad-coupled activity assay for reductive cleavage of SAM by 4Hpad-AE and Δ66-AE

12 µM 4Hpad-AE in buffer C was reduced with a 15-fold molar excess of DT for 5 min (reduction was verified by UV-visible spectroscopy) after which, 12 µM 4Hpad in buffer C was added in the reaction solution. The reaction was started with 2 mM SAM. Typical reaction volumes were 500 µl and the assays were carried out at 30 °C. 50 µl samples were withdrawn at fixed time intervals up to 30 min and treated as mentioned in 9.1.

## 9.3. Correlation between 5'-deoxyadenosine and glycyl radical formation

4Hpad-AE* or Δ66-AE (80 µM in 2.5 ml final volume) was reduced with a 15 fold molar excess of sodium dithionite (reduction was verified by UV-visible spectroscopy) at 30 °C. After 5 minutes 4Hpad (20 µM in buffer B) was added to the mixture and the reaction was initiated by adding 2 mM SAM. 50 µl of samples were withdrawn at fixed time intervals up to 30 min and the reaction was stopped with 50 µl 10% trifluoroacetic acid containing 30 µM adenosine as internal standard. The precipitated protein was removed by centrifugation for 30 min at 14,000 g and 5'-deoxyadenosine (quenched 5'-deoxyadenosyl radical form) production was detected by HPLC as described in 9.1.1. In parallel, 300 µl samples were withdrawn at the same time intervals for glycyl radical detection by EPR (see above, 8.3). For detection and quantification of glycyl radical formation, a liquid nitrogen finger Dewar was used.

## 9.4. Activity assay for *p*-cresol production by 4Hpad

12 µM of 4Hpad in buffer C was added to reduced and SAM treated 12 µM 4Hpad-AE (prepared as for reductive cleavage of SAM) in a total volume of 100 µl. 25 mM of 4Hydroxyphenylacetate in buffer C was added and the reaction mixture was incubated for 1 h a 30 °C. At fixed time intervals 100 µl samples were withdrawn, the reaction was stopped by adding 50 µl 10% perchloric acid and neutralized with 50 µl 10% potassium bicarbonate (with 3 mM phenol as internal standard). The precipitated protein was removed by centrifugation and filtering through a 0.45 µM membrane filter. 50 µl of supernatant were injected into a Jasco HPLC system running with an isocratic eluent containing 0.1% trifluoroacetic acid in 30% acetonitrile/water at a flow rate of 1 ml $min^{-1}$ and the detection wavelength was set at 275 nm. Product (*p*-cresol) formation was analyzed and quantified using calibration curves for respective standards or internal standard peak ratio. Specific activity and turnover were calculated using the molecular mass for a 4Hpad monomer, 110 kDa. Similar activity assays were conducted for 4Hpad activated with 4Hpad-AE* and Δ66-AE.

# 10. Isothermal titration calorimetry (ITC)

The binding affinity of oxidized 4Hpad-AE* or Δ66-AE for SAM was determined with a VP-ITC system (MicroCal) inside a glove box (LABstar, MBraun Inertgas-Systeme, Germany) operated under a nitrogen atmosphere with less than 0.5 ppm $O_2$. All samples were degassed under vacuum for 15 min prior to the experimental runs. The sample cell was loaded with 50 µM 4Hpad-AE* in buffer C and the syringe was filled with 2 mM SAM in the same buffer. This experiment consisted of 85 consecutive injections of 4 µl SAM over 8 s with a 5 min time interval between the injections. A stirring speed of 307 rpm was utilized to ensure thorough mixing. All measurements were carried out at 30 °C. Raw data were corrected for heats of dilution and further analyzed by nonlinear fitting using the software provided by the manufacturer (MicroCal Origin 7.0 software). The thermodynamic analysis and the binding stoichiometry (N) were calculated by one-site fit model. The same setup was used to determine the binding affinity of AMP (4 mM in injection syringe). Competitive binding of SAM (2 mM in injection syringe) was measured in the presence of 4 mM AMP in both reaction cell and injection syringe.

# 11. Stopped-flow spectrometry

Rapid mixing reactions were performed under anoxic conditions ([$O_2$] < 0.5 ppm, LABstar glove box) using a BioLogic SFM 400 stopped-flow system with a 1 cm observation path length cuvette coupled to either a diode array detector or a photomultiplier. The reaction temperature (30 °C) was controlled with a Haake SC100-A10 thermostat. Reduction kinetics of 8 µM 4Hpad-AE* or Δ66-AE in buffer C with different concentrations of dithionite (30 to 500 µM in same buffer) were performed by monitoring the absorbance changes at 418 nm. The observed rate constants ($k_{obs}$) were derived from a double exponential fit using the BioKine (BioLogic) software.

# 12. Michaelis-Menten kinetics

The kinetic constants $K_m$ and $k_{cat}$ were derived from steady-state assays with varying SAM concentrations from 0.15 to 4 mM at a constant enzyme concentration of 15 µM of 4Hpad-AE in buffer C. Initial velocities were determined from plotting product formation (detected as aforementioned) against time. The program Sigma plot (Systat Software) was used for nonlinear regression analysis applying the Michaelis-Menten equation. Experiments were conducted in duplicate and error estimates represent ± SD.

# 13. Crystallographic methods

## 13.1. Crystallization of 4Hpad and its variants

Crystallizations were carried out in a glove box (Model B, Coy laboratory Products, Inc., Michigan, USA). All the crystals reported for 4Hpad and its variants with or without substrate/inhibitor were grown by the sitting drop vapor diffusion method. Crystals were obtained by mixing 1 µl of 23 - 25 mg/ml protein in buffer B with 1 µl of reservoir buffer and equilibrated against 300 µl of reservoir buffer. To obtain crystals with bound substrate/inhibitor, 23 - 25 mg/ml protein was incubated with 10-20 mM 4-HPA in buffer B for 1-2 hours at room temperature. Using sitting drop vapor diffusion method, 1 µl of this solution is mixed with 1 µl of

reservoir buffer and equilibrated against 300 µl of reservoir buffer. The crystals grew within 10-14 days. A reservoir solution containing 15% 2R, 3R-butanediol was used as a cryo-protectant for all the crystals that were shock frozen and stored in liquid nitrogen until they were exposed to X-rays. The conditions in which 4Hpad and its mutants crystallized are given in table 11.1.

**Table 11.1.** Crystallization conditions of 4Hpad and its variants

| Protein | Substrate/Inhibitor | Reservoir condition |
|---|---|---|
| 4Hpad | None | 0.2 M Ammonium acetate<br>0.1 M Na HEPES 7.5<br>25% PEG 3350 |
| 4Hpad | 20 mM 4-HPA (substrate) | 0.1 M $MgCl_2$<br>0.1 M Na HEPES 7.0<br>15% PEG 4000 |
| 4Hpad | 10 mM 3,4-DHPA (substrate) | 0.1 M $MgCl_2$<br>0.1 M Na HEPES 7.0<br>10% PEG 4000 |
| 4Hpad | 20 mM 4-HPAA (Inhibitor) | 0.2 M $MgCl_2$<br>0.1 M Na HEPES 8.0<br>8% PEG 4000 |
| E505Q | 10 mM 4-HPA (substrate) | 0.1 M $MgCl_2$<br>0.1 M Na HEPES 7.0<br>15% PEG 4000 |
| HE2Q<br>(E637Q & H536Q,<br>Double mutant) | 20 mM 4-HPA (substrate) | 0.1 M Na HEPES 7.5<br>18% PEG 4000 |

## 13.2. Crystallization trails of 4Hpad-AE and its variants

4Hpad-AE and its variants were tried crystallizing with and without ligands (SAM, 5'-AdoH, Methionine, SAH, 4Hpad) using many commercially available screens: JCSG-*plus* HT-96, Proplex HT-96, Structure screen 1 & 2 HT-96, Morpheus, MIDAS™ HT-96, PACT *premier*™

HT-96, Stura Footprint screen and MacroSol Screen HT-96 (Molecular dimensions) Wizard I/II (Emerald), PEG-PGA, Salt Rx and PEG/Ion HT screen (Hampton Research).

## 13.3. Data collection, structure determination and refinement

All the diffraction experiments were performed at the BESSY synchrotron beam lines 14.1 and 14.2 (Berlin, Germany). Diffraction data were integrated and scaled using XDS (Kabsch, 1993). The structures were solved by Patterson search techniques using PHASER (McCoy *et al.*, 2007) using the crystal structures of 4Hpad (with and without 4-HPA, PDB ID: 2Y8N and 2YAJ respectively) (Martins *et al.*, 2011) as homologous search models. Protein models were built with COOT (Emsley & Cowtan, 2004) and refined with PHENIX (Adams *et al.*, 2010). Figures were prepared with PyMol (Schrödinger, 2010).

## 14. Complex formation between 4Hpad and 4Hpad-AE*

The complex formation between 4Hpad-AE* and 4Hpad was investigated by gel filtration experiments using a Superdex$^{TM}$ 200 prep-grade gel filtration column inside the glove box (Model B, Coy laboratory Products, Inc., Michigan, USA). 40 µM of both proteins in buffer C was incubated for 10-30 min and injected into the column. Complex formation was also tested by incubating 4Hpad-AE* and 4Hpad in the presence of DT, SAM or mixture of both. ITC was also performed to check complex formation. The sample cell was loaded with 10 µM 4Hpad in buffer C and the syringe was filled with 50 µM of 4Hpad-AE* incubated with 2 mM SAM in the same buffer. The procedure was maintained same as in section 10 (ITC). Complex formation was also investigated between Δ66-AE and 4Hpad using similar methods.

# Results and discussion

## 1. Molecular biology

### 1.1. Cloning of 4Hpad-AE

The open reading frame coding for 4Hpad-AE from *C. scatologenes* (accession number ABB05048; monomer of 36 kDa) was codon-optimized for recombinant heterologous expression

in *E. coli* (Figure R1) generating the expression vector pET28a-Csd_AE. Similarly, the open reading frame coding for 4Hpad-AE from *C. difficile* (accession number CAD65891; monomer of 36 kDa) was codon-optimized for usage in *E. coli* (Figure R2) generating the expression vector pET28a-Hpd_AE.

**(NdeI)**
**CATATG**AAAGAAAAAGGCCTGATTTTTGATATCCAGAGCTTCTCTGTGCATGATGGC
CCGGGTTGCCGTACCAGCGTGTTTTTCATTGGTTGTCCGCTGCAGTGCAAATGGTGT
GCCAACCCGGAATCTTGGACCAAGAAAAAACATATCATGGTGGCAGAAAACGTTTGC
AAATGGAAAAATGGCTGCCGCAGCTGTATTAATGCATGTAGTCACGATAGCATCAAA
TTCTCTGAAGATGGTAAACTGAAAATCAGTTGGGATACCTGCGAAAAATGTGAAACG
TTTGATTGCGTGAACATGTGTCCGAACAATGCGCTGAAACAGTGCGTGAAAGAATAT
ACCGTTGATGAACTGATGACGATCCTGAAACGTGATTTTAACAATTGGGGCAGCGAT
GGCGGTGTTACCTTCACGGGCGGTGATCCGCTGATGCATCACGAATTTCTGGTGGA
AGTTCTGAAAAAATGTTACGATAGTCAGATCCATAAAGCGATCGAAACCAGCGGTTAT
GCCAAACAGGAAGTGTTCCTGGAAGTTCTGAAATACATTGATTTTGCGTTCATCGATG
TGAAAAATATGGATCGTGAAAAACACAAACAGGGCACCGGTGTTTATAACGATCTGA
TTCTGAGCAATATCGAAGCCCTGAAAAAATCTAACTGGAATGGCCGTCTGGTGCTGC
GCCAGCCGACGATTGCAGGTTATAACGATTCTGATGAAAATGCGTACAAACTGATCG
AATTCATGAACAAAAACAGTCTGTACGAAATCAACCTGCTGAAATTTCATCGCCTGGG
CGAAACCAAATGGAATCAGCTGGGTAAAGAATATGAATACAGCAAATACGGCGATAT
GACGAACGAAAAAATGGAACACCTGCAGCAGCTGTATCTGGATAACAATATTGCCTG
CTACATCGGTGATAATACCCCGTTTTAA**CTCGAG(XhoI)**

**Figure R1. Sequence of the codon-optimized gene for 4Hpad-AE from *C. scatologenes*.** *Nde*I and *Xho*I restriction sites allow direct insertion into the pET28a(+) expression vector.

(NdeI)
**CATATG**TCATCCCAGAAACAGCTCGAAGGCATGATTTTCGATGTGCAGAGCTT
TAGCGTTCATGATGGTCCTGGCTGTCGCACTACGGTGTTCTTGAATGGTTGTC
CACTGTCATGCAAATGGTGTGCCAACCCAGAAAGCTGGACTGTACGTCCGCA
CATGATGTTTAGCGAACTGTCTTGTCAGTATGAGAACGGCTGCACCGTGTGTC
ATGGCAAATGCAAGAATGGTGCGTTGAGCTTCAACCTGGACAACAAACCGGTT
ATTGACTGGAACATCTGCAAAGACTGCGAAAGCTTTGAATGCGTCAATAGTTG
CTACTATAACGCCTTTAAACTGTGCGCAAAACCGTATACGGTGGATGAACTTG
TTCAGGTCATCAAGCGTGACTCGAATAATTGGCGCAGTAATGGCGGTGTAACC
TTTAGTGGTGGAGAACCGTTACTGCAACACGAGTTCCTGCACGAAGTCCTCCT
CAAATGTCATGAGGTTAACGTACATACCGCAATCGAGACAAGTGCTTGTGTGT
CAAATGAAGTGTTTAACAAAATCTTCAACGACATTGATTTTGCGTTTATCGATAT
CAAACACATGGATCGGGAAAAGCACAAAGAACAAACCGGCGTGTACAATGAT
CTGATTCTGGAGAACATTTCGAACCTGGCTAATTCGGACTGGAATGGACGCCT
GGTGTTACGTGTCCCCGTCATTTCTGGGTTTAACGATTCCGACGAAAACATTA
GCGACATTATTTCCTTCATGCACAAGAACAACCTGGTGGAAATCAATCTGTTG
CCGTTTCATCGCCTTGGTGAGTCTAAATGGACCCAATTAGGGAAAGAGTACGA
ATATTCGGATAAAGGCGATGTTGATGAAGGGCATCTGGAAGAACTGCAGGATA
TCTTCCTTGATAATGGTATTGCCTGCTATGTAGGCCAT
GTTACGGCGTTCTAA**CTCGAG(XhoI)**

**Figure R2. Sequence of the codon-optimized gene for 4Hpad-AE from *C. difficile*.** *NdeI* and *XhoI* restriction sites allow direct insertion in pET28a(+) expression vector.

4Hpad-AE expressed and purified from pET28a-Csd_AE was used for all the biochemical and crystallization studies mentioned in this work. 4Hpad-AE, expressed and purified from pET28a-Hpd_AE was only used for crystallization trials.

# 1.2. Cloning strategy for Δ66-AE

Comparing the sequence alignments of the known glycyl radical activating enzymes (GRE-AE), 4Hpad-AE revealed possible binding sites for up to two putative auxiliary Fe/S clusters (Motif II & Motif III, Figure R3) in addition to the well-known SAM binding cubane cluster (RS cluster, Motif I). Interestingly, all conserved cysteines possibly involved in binding these putative clusters are located in a 60 amino acid stretch, which is missing in the activating enzymes of Pfl (Vey *et al.*, 2008) and Nrd (Ollagnier *et al.*, 1997), but found in all other known GRE-AEs out of which only very few are functionally characterized. To elucidate the role of these putative clusters in the reduction of AE and the regulation of the decarboxylase activity, the conserved cysteines in the putative motifs for Fe/S clusters could be mutated either separately or together, eliminating the binding sites of individual putative clusters.

The nine-cysteines rich containing insert in 4Hpad-AE is homologous to the clusters binding region of eight-iron clostridial ferredoxins (Pfam: PF00037) where they provide crossed-coordinating cysteinyl ligands for two [4Fe-4S] clusters: one cluster is coordinated by the first three cysteines from motif II and the last cysteine from motif III, and the second cluster is coordinated by the last cysteine in motif II and the first three cysteines from motif III (Figure R3).

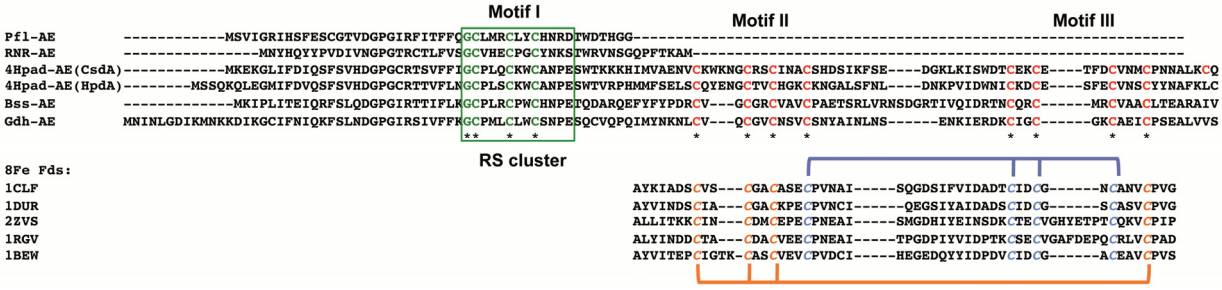


**Figure R3. Alignment of N-terminal amino acids of glycyl radical activating enzymes and eight-iron ferredoxins (8Fe Fds).** The N-terminal amino acid sequences of glycyl radical activating enzymes are aligned along with the cluster-binding region of eight-iron clostridial ferredoxins. The RS cluster binding motif (Motif I) is represented by a green box with the conserved amino acids in green. Cysteines conserved among glycyl radical activating enzymes are red. The two cysteine-rich motifs of glycyl radical activating enzymes (**C**56X$_3$**C**62X$_2$**C**65X$_3$**C**69(*motif II*)-gap-**C**89X$_4$**C**92X$_4$**C**97X$_2$**C**101(*motif III*)-gap-**C**109) are present in eight-iron clostridial ferredoxins where they provide crossed-coordinating cysteinyl ligands for two [4Fe-4S] clusters, showed by color co-ordination.

Site-directed mutagenesis and EPR spectroscopic analysis on 4Hpad-AE (Blaser, 2007) had been applied to study the role of the putative auxiliary clusters after introducing mutations on cysteines to serines in the motif II and III, which eliminate the function of cysteines as a ligands for Fe/S clusters. However, the results were not conclusive as the variants showed decreased solubility and diminished activity. The same behavior was noticed in the previously reported variants of strep-tagged 4Hpad-AE (Yu *et al.*, 2006). The inconclusive results could be due to the ambiguity in the cross linking fashion of cysteines that ligate the insert clusters. To overcome this obstacle, the X-ray structure of Pfl-AE (Vey *et al.*, 2008) was used to design a truncated polypeptide of 4Hpad-AE (Δ66-AE) harboring only the motif I (**C**30X$_3$**C**34X$_2$**C**37) for the RS cluster shown in Figure R4A.

When the cysteine-rich insertion of 4Hpad-AE was mapped on the crystal structure of Pfl-AE (Vey *et al.*, 2008) based on the sequence alignment, it locates within an extended loop at the surface (Figure R4B, yellow colored cartoon). The Δ66-AE variant comprises the N-terminal sequence from WT-AE until Thr44 followed by a linker from Pfl-AE (Thr44-His-Gly-Gly47, yellow color, Figure R4B) connected to the C-terminal part of WT-AE (Lys111 to Phe312). The residues from Lys45 to Val110 are deleted. Hence presumably Δ66-AE with a Pfl-AE like fold could be stable and harbor an active RS cluster.


**Figure R4A. Design of the Δ66-AE construction deduced from the primary structure alignment to Pfl-AE structure.** The N-terminal amino acid sequence of 4Hpad-AE is aligned along with Pfl-AE and Δ66-AE. Color codes are same as in Figure R3 with the linker region in yellow.

B

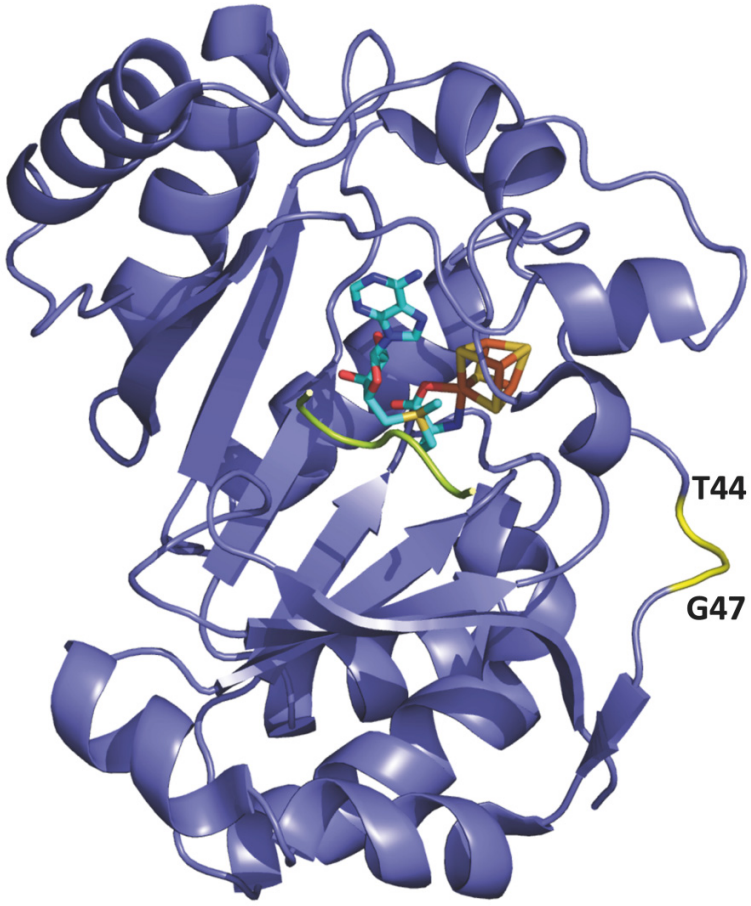


**Figure R4B. Cartoon representation of Pfl-AE crystal structure in complex with SAM and a peptide substrate** (PDB code 3CB8): RS cluster as sticks colored red for iron and yellow for sulfur; SAM as sticks colored cyan for carbon, blue for nitrogen, red for oxygen and yellow for sulfur; peptide substrate as green cord.

## 1.3. Primer designing for AE-9M

In an attempt to crystallize the 4Hpad-AE, surface entropy reduction method was tried. This approach minimizes the loss of entropy of protein by replacing the flexible, solvent-exposed residues by residues with lower conformational entropy making crystallization thermodynamically favorable (Goldschmidt *et al.*, 2007; Cooper *et al.*, 2007). A web server SERp sever (http://www.doe-mbi.ucla.edu/Services/SER) was used to design surface entropy reduced mutations that may facilitate crystallization. This server works based on the algorithm incorporating conformational entropy profile, secondary structure prediction, and sequence

conservation. The sequence of 4Hpad-AE was aligned with PFL-AE and sent to the SER server. The results from the server showed the possibility of mutating nine amino acids that were expected to be on the surface. All these nine residues were mutated to Ala as suggested by the server and the enzyme is named as AE-9M (Figure R5).

**Figure R5. Sequence alignment of 4Hpad-AE (CsdA) with AE-9M.** A) The amino acid sequence of 4Hpad-AE is aligned along with AE-9M. The nine mutated amino acids in AE-9M as suggested by the SERp server are highlighted in red.

The primers had been designed and cloned by Polymerase Incomplete Primer Extension (PIPE) cloning method as described in Materials and methods 5.3. AE-9M was only used for crystallization during this study.

## 1.4. 4Hpad mutants

4Hpad residues predicted to be involved in the Kolbe-type decarboxylation were mutated by site-directed mutagenesis. Glu505, which is supposed to donate a proton to the Cys503 was mutated to glutamine (E505Q). A double mutant (HE2Q) was also constructed where both the two residues H536 and E637 that might help in anchoring the substrate are mutated to glutamate. Two single mutants involving the H536 and E637 residues were also constructed (E637Q and H536Q).

# 2. Protein expression and purification

## 2.1. Expression and purification of 4Hpad-AE and its variants

Various factors like culture media, cultivation temperature, inoculation time and concentration of IPTG were adjusted to get the best expression and purification yield. The best expression levels were obtained using *E. coli* BL21(DE3) cells grown in mTB medium supplemented with Mohr's salt and sodium sulfide at 25 °C for 6 to 8 hours after inducing with 0.2 mM IPTG. Typical yields of purified 4Hpad-AE were 10 mg from one liter of

aerobic culture and showed 4.0 ± 0.5 mol Fe per mol protein for as-isolated and 7.5 ± 0.2 mol Fe per mol protein after *in vitro* chemical reconstitution (Materials and Methods 8).

To improve the amount of intact Fe/S cluster, an *in vitro* biological cluster assembly with ISC auxiliary proteins was tried by incubating cell lysates containing expressed AE with cell lysates of proteins from ISC operon that was expressed separately from the pRKISC plasmid (Nakamura *et al.*, 1999). This as-isolated protein on *in vitro* biological Fe/S reconstitution is hitherto referred as 4Hpad-AE* (Figure R6). Yields were similar to 4Hpad-AE. 4Hpad-AE* was further subjected to chemical reconstitution and the reconstituted enzyme showed 12.0 ± 0.3 mol Fe per mol protein (referred as 4Hpad-AE**) with substantially improved the metal contents of the protein compared to 4Hpad-AE.

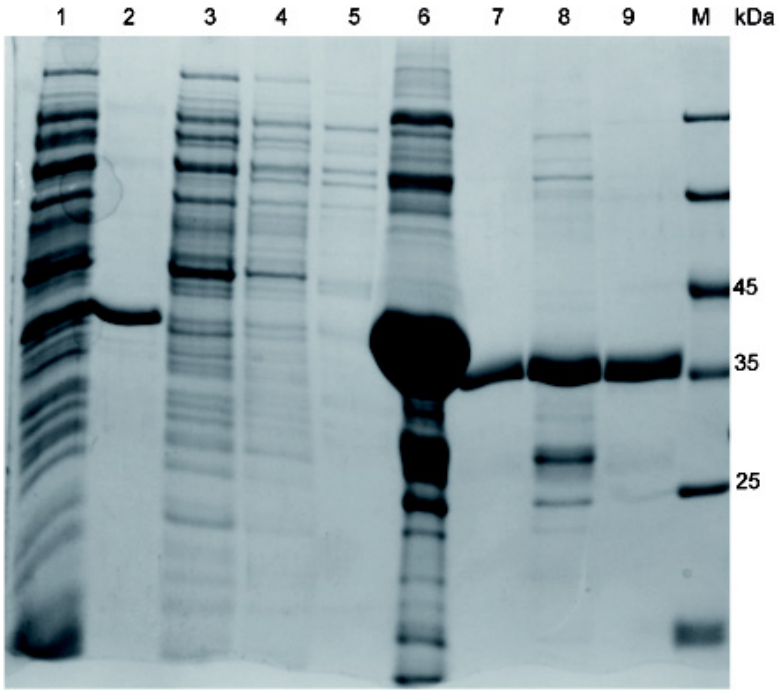


**Figure R6. Purification of 4Hpad-AE* analyzed by Coomassie blue-stained 12% (w/v) SDS-Page.** Lane 1; soluble cell free extract, Lane 2; insoluble pellet after centrifugation, Lane 3; Flow-through from the Ni-SHP column, Lanes 4 & 5; Wash fractions, Lane 6; Pooled fraction of the eluted 4Hpad-AE* (38 kDa), Lanes 7 & 9; Tag free 4Hpad-AE* (36 kDa), Lane 8; Mixture of tag free 4Hpad-AE* and TEV protease (29 kDa), Lane M; Molecular mass protein markers.

The Δ66-AE was expressed and purified as 4Hpad-AE* with yields of ~10 mg per liter culture, which is comparable to the yield of wild type. The corrected molecular weight (29 kDa) and homogeneity of the truncated protein were verified on SDS-PAGE (Figure R7). Iron content of Δ66-AE was 3.5 ± 0.3 mol Fe per mol protein. This rules out the need for any

reconstitution as only one [4Fe-4S] cluster is expected in Δ66-AE. The AE-9M variant was also purified as described for 4Hpad-AE* with a yield of 5 mg per liter culture and iron content of 3.5 ± 0.5 mol Fe per mol protein.

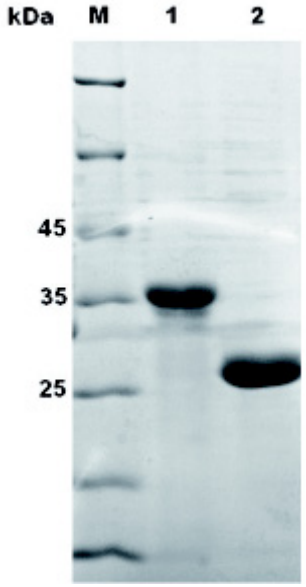


**Figure R7. Coomassie blue-stained 12% (w/v) SDS-PAGE of purified 4Hpad-AE* and Δ66-AE**
Lane M; Molecular mass protein markers, Lane 1; Tag-free 4Hpad-AE* (36 kDa), Lane 2; Tag-free Δ66-AE (29 kDa).

## 2.2. Expression and purification of 4Hpad and its variants

*E. coli* BL21(DE3) cells harboring pASK-BC plasmid were grown in LBG medium initially under aerobic condition by air-flushing at 37 °C and supplemented with Mohr's salt and sodium sulfide. After inducing with AHT, the cultivation was switched to anaerobic system by flushing $N_2$. Cells were harvested after 20 h and the protein was purified, which produced 1 mg of 4Hpad from one liter of culture with 4.0 ± 0.5 mol Fe per mol protein (Figure R8). The solubility of the protein, which was a quite challenging problem, was improved by anaerobic cultivation resulting in an increase in the yield by 40%. All the variants of 4Hpad were purified similar to the wild type protein.

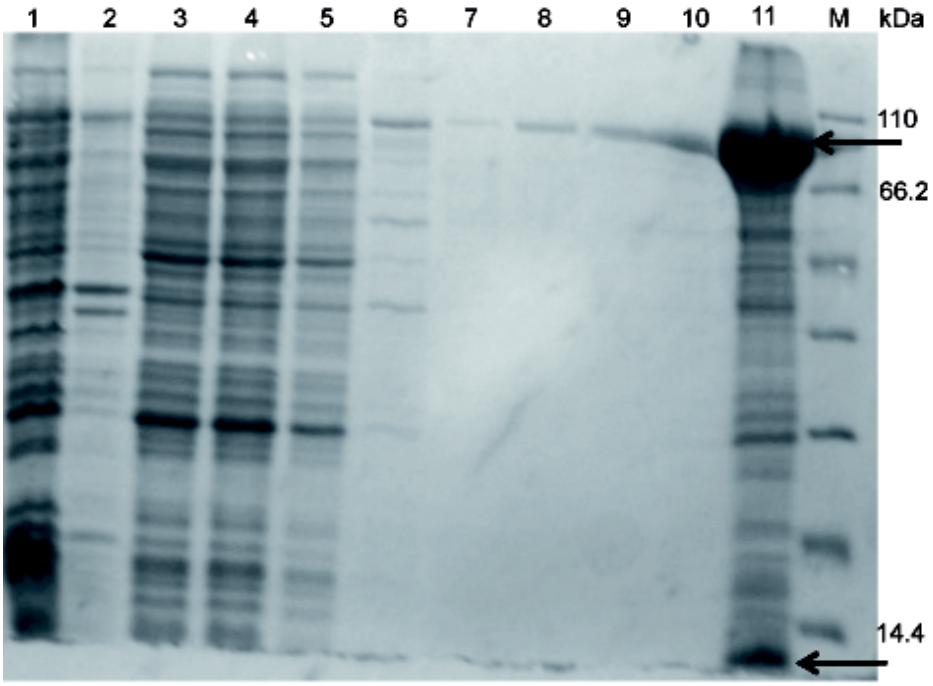


**Figure R8. Purification of 4Hpad analyzed by Coomassie blue-stained 16% (w/v) SDS-PAGE.** Lane 1; soluble cell free extract, Lane 2; insoluble pellet after centrifugation, Lane 3; Flow-through from the Streptactin® MacroPrep column, Lanes 4, 5 & 6; Washed fractions, Lane 7, 8, 9 & 10; Eluate E1, E2, E3 & E4, Lane 11; Pooled eluted fractions of 4Hpad (E1-E4) (100 kDa β subunit and 10 kDa γ subunit, shown by arrows), Lane M; Molecular mass protein markers.

# 3. Characterization of Fe/S clusters of 4Hpad-AE and its variants

Reconstitution of Fe/S clusters in 4Hpad-AE and 4Hpad-AE* were verified by UV-vis, ferene-derived colorimetric assay, EPR and Mössbauer spectroscopy.

## 3.1. Spectroscopic analysis of 4Hpad-AE

### 3.1.1. UV-vis & colorimetric analysis

As-isolated $His_6$-tagged 4Hpad-AE displayed a typical brownish-red color indicating the presence of Fe/S clusters that is confirmed by UV-vis spectra and ferene-derived colorimetric assay.

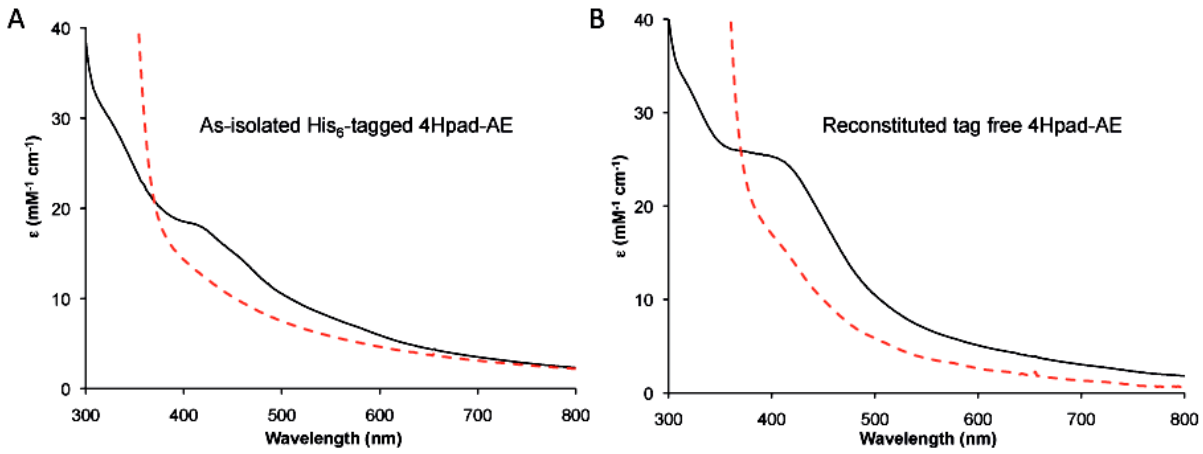


**Figure R9. UV-visible spectra of 4Hpad-AE.** (A) UV-visible spectra of as-isolated $His_6$-4Hpad-AE (24 µM in buffer C; 4.0 ± 0.5 mol Fe per mol protein) before (—) and after (---) reduction with a 30-fold molar excess of sodium dithionite for 5 minutes. (B) UV-visible spectra of chemically reconstituted tag-free 4Hpad-AE (12 µM in buffer C; 7.5 ± 0.2 mol Fe per mol protein) before (—) and after (---) reduction with a 30-fold molar excess of sodium dithionite for 5 minutes. The absorbance at 315 nm results from sodium dithionite.

The absorption spectra of the as-isolated protein showed a shoulder at 420 nm indicating the presence of $[4Fe\text{-}4S]^{2+/1+}$ cluster (Sweeney & Rabinowitz, 1980) (Figure R9A, solid line). Ferene-derived colorimetric assay gave an iron content of 4.0 ± 0.5 mol Fe per mol protein, which could be assumed to one putative cubane cluster in the as-isolated protein. The absorbance at the maximum difference near 400 nm decreased by 30% upon reduction with DT, (Figure R9A, dashed line). Since 50% bleaching in absorbance indicates a complete reduction of $[4Fe\text{-}4S]^{2+/1+}$ clusters (Sweeney & Rabinowitz, 1980) these results suggested incomplete reduction of the putative bound cubane cluster. Chemically reconstituted tag free 4Hpad-AE yielded a dark brown-greenish solution with 7.5 ± 0.2 mol Fe per mol protein (Figure R9B, solid line). The efficiency of reconstitution was not improved by removing the affinity tag but in turn facilitate reduction with DT as seen by an almost 50% bleaching at 400 nm (Figure R9B, dashed line). The iron content calculated from the UV-vis spectra and calorimetric assay are given in the table.

**Table 3.1.1.** Iron content analysis of 4Hpad-AE

| 4Hpad-AE | Mol Fe per mol protein | |
|---|---|---|
| | UV-vis | Colorimetric |
| As-isolated $His_6$-tagged | 2.7 ± 0.3 | 4.0 ± 0.5 |
| Reconstituted $His_6$-tagged[1] | 5.3 ± 0.3 | 7.0 ± 0.7 |
| Non-reconstituted tag free[2] | 3.3 ± 0.2 | 5.0 ± 0.3 |
| Reconstituted tag free[3] | 5.8 ± 0.6 | 7.5 ± 0.2 |

[1]chemically reconstituted sample; [2]as-isolated after removal of $His_6$-tag by TEV protease; [3]chemically reconstituted sample after removal of $His_6$-tag by TEV protease.

## 3.1.2. EPR spectroscopic analysis

EPR (Electron Paramagnetic resonance) spectroscopy is widely used to identify the type and stoichiometry of the Fe/S clusters for the metalloproteins. The typical sharp signal at g=2.02 exhibited by as-isolated 4Hpad-AE (Figure R10A) corresponds to 0.25 $[3Fe\text{-}4S]^{1+}$ cluster per protein. This value decreases to 0.07 $[3Fe\text{-}4S]^{1+}$ cluster per protein in the reconstituted 4Hpad-AE (Figure R10B). This is due to the conversion of [3Fe-4S] to [4Fe-4S] cluster that is also seen in other radical enzymes (Walsby *et al.*, 2005). The possibility of [3Fe-4S] cluster reduction during reconstitution is also taken into account. Upon reduction by DT, reconstituted 4Hpad-AE shows *g* values of 2.04 and 1.94 (Figure R10C) corresponds to the characteristic rhombic EPR signal of $[4Fe\text{-}4S]^{1+}$ clusters (Walsby *et al.*, 2002). While the iron content of the reconstituted 4Hpad-AE shows 7.5 ± 0.2 mol Fe per mol protein that could indicate the presence of two [4Fe-4S] clusters, the EPR spin quantification estimates 0.7 $[4Fe\text{-}4S]^{1+}$ cluster per protein. This suggests that the reduction shown by UV-visible spectroscopy (Figure R9B, dashed line) is partly due to the cluster breakdown rather than complete reduction. It cannot be excluded that a part of the analytically detected iron is not cluster-bound since part of the clusters appears not to be detected by EPR. The presence of SAM does not increase the extent of cluster reduction, even though subtle changes in the EPR line shape can be noted (Figure R10D). These findings are in contrast to the drastic effect reported for PFL-AE (Walsby *et al.*, 2005) and Ndr-AE (Ollagnier *et al.*, 1997) that EPR signal is dramatically perturbed in the presence of SAM, transforming from rhombic to axial signal, but are consistent with the less pronounced changes observed in Gdh-AE (Demick & Lanzilotta, 2011) and strep-tagged 4Hpad-AE (Yu *et al.*, 2006).

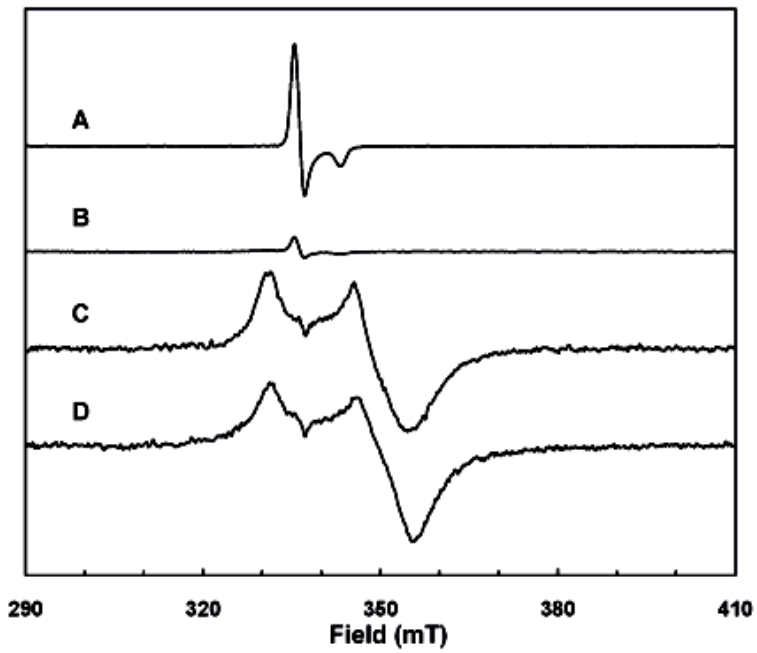


**Figure R10. EPR spectra of 4Hpad-AE.** EPR spectra of (A) as-isolated $His_6$-4Hpad-AE (80 µM in buffer C); (B) reconstituted 4Hpad-AE (80 µM in buffer C); (C) reconstituted 4Hpad-AE reduced with a five-fold molar excess of DT; and (D) as in (C) plus incubation with SAM (2 mM) for 5 minutes. Spectra were recorded at 10 K with 0.8 mW microwave power, 1.25 mT modulation amplitude and a microwave frequency of 9.459 GHz. Figures were prepared by Antonio J Pierik at the Core facility for protein spectroscopy, Institute of Cytobiology and Cytopathlogy, Philipps University Marburg, Germany.

## 3.2. Spectroscopic analysis of 4Hpad-AE*

Since 4Hpad-AE might bind up to two auxiliary [4Fe-4S] clusters as mentioned in (Yu *et al.*, 2006), an attempt to improve Fe/S cluster assembly and stability of 4Hpad-AE has been tried by concomitant purification with an *in vitro* biological cluster assembly. (Please refer to methods and materials for details).

### 3.2.1. UV-vis & colorimetric analysis

The iron content for the as-isolated 4Hpad-AE* samples is slightly higher (6.0 ± 0.5 mol Fe per mol protein) and increased to 12.0 ± 0.3 mol Fe per mol protein upon further chemical Fe/S cluster reconstitution (See Results and discussion 2.1). Reconstituted 4Hpad-AE** has a dark brown-greenish color. The UV-vis spectra shows shoulders at 320 nm and 420 nm (Figure R11A, solid line) and reduction with DT causes a 50% bleaching at 400 nm (Figure

R11B, dashed line). The iron content calculated from the UV-vis spectra and calorimetric assay are given in table 3.2.1.

**Table 3.2.1.** Iron content analysis of 4Hpad-AE*

| 4Hpad-AE* | Mol Fe per mol protein | |
|---|---|---|
| | UV-vis | Colorimetric |
| As-isolated $His_6$-tagged | 3.3 ± 0.2 | 6.0 ± 0.5 |
| Reconstituted $His_6$-tagged[1] | 6.3 ± 0.8 | Not measured |
| Non-reconstituted tag free[2] | 4.0 ± 0.2 | Not measured |
| Reconstituted tag free[3] | 7.9 ± 0.3 | 12.0 ± 0.3 |

[1]chemically reconstituted 4Hpad-AE*; [2]as-isolated 4Hpad-AE* after removal of $His_6$-tag by TEV protease; [3]chemically reconstituted 4Hpad-AE** after removal of $His_6$-tag by TEV protease.

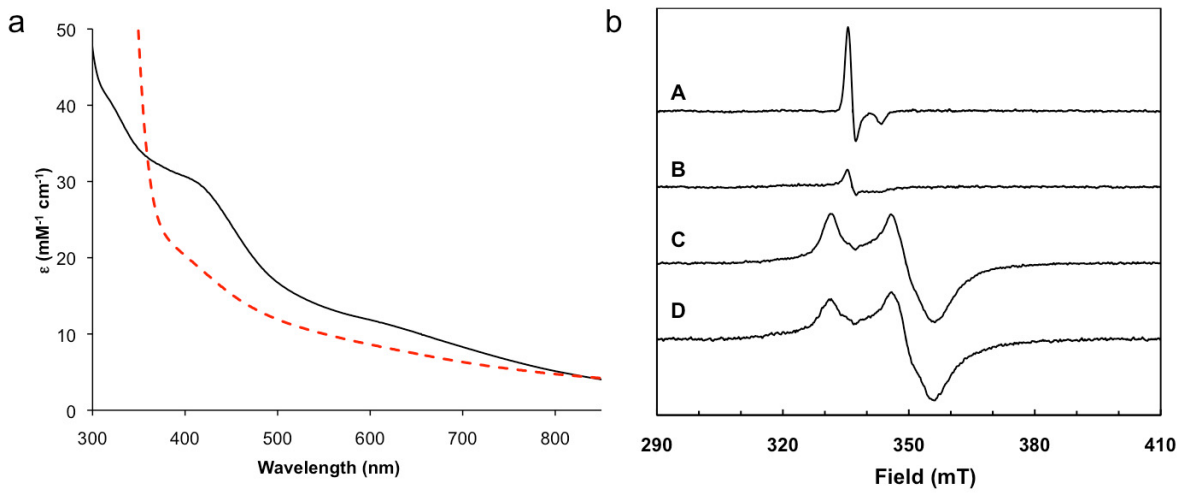


**Figure R11. UV-visible and EPR spectra of 4Hpad-AE*.** (a) UV-visible spectra of reconstituted tag free 4Hpad-AE* (15 µM in buffer C; 12.0 ± 0.3 mol Fe per mol protein) before (—) and after (---) 5 min reduction with a 30-fold molar excess of DT. (b) EPR spectra of as-isolated $His_6$-4Hpad-AE* **(**A) (80 µM in buffer C; 6.0 ± 0.5 mol Fe per mol protein); 4Hpad-AE** **(**B) (80 µM in buffer C; 12.0 ± 0.3 mol Fe per mol protein); (C) 4Hpad-AE** reduced with a five-fold molar excess of DT for 5 minutes; and (D) as in (C) plus incubation with 2 mM SAM for 5 minutes. Spectra were recorded at 10 K with 0.8 mW microwave power, 1.25 mT modulation amplitude and a microwave frequency of 9.459 GHz. EPR figures were prepared by Antonio J Pierik at the Core facility for protein spectroscopy, Institute of Cytobiology and Cytopathlogy, Philipps University Marburg, Germany.

## 3.2.2. EPR and Mössbauer analysis

EPR spectra of the $His_6$-4Hpad-AE* shows a sharp signal at g=2.02, typical of $[3Fe\text{-}4S]^{1+}$ clusters corresponding to 0.08 $[3Fe\text{-}4S]^{1+}$ cluster per protein (Figure R11b, trace A). On chemical reconstitution, 4Hpad-AE** (Figure R11b, trace B) showed g value corresponding to 0.03 $[3Fe\text{-}4S]^{1+}$ cluster per protein. Spin integration of the reduced 4Hpad-AE** gives 1.6 $[4Fe\text{-}4S]^{1+}$ cluster per protein (Figure R11b, trace C) that indicates the presence of two possible bound [4Fe-4S] clusters. The spectra of SAM-incubated reduced 4Hpad-AE** has a slightly more pronounced effect (Figure R11b, trace D) when compared to the previously mentioned 4Hpad-AE (Figure R10, trace D).

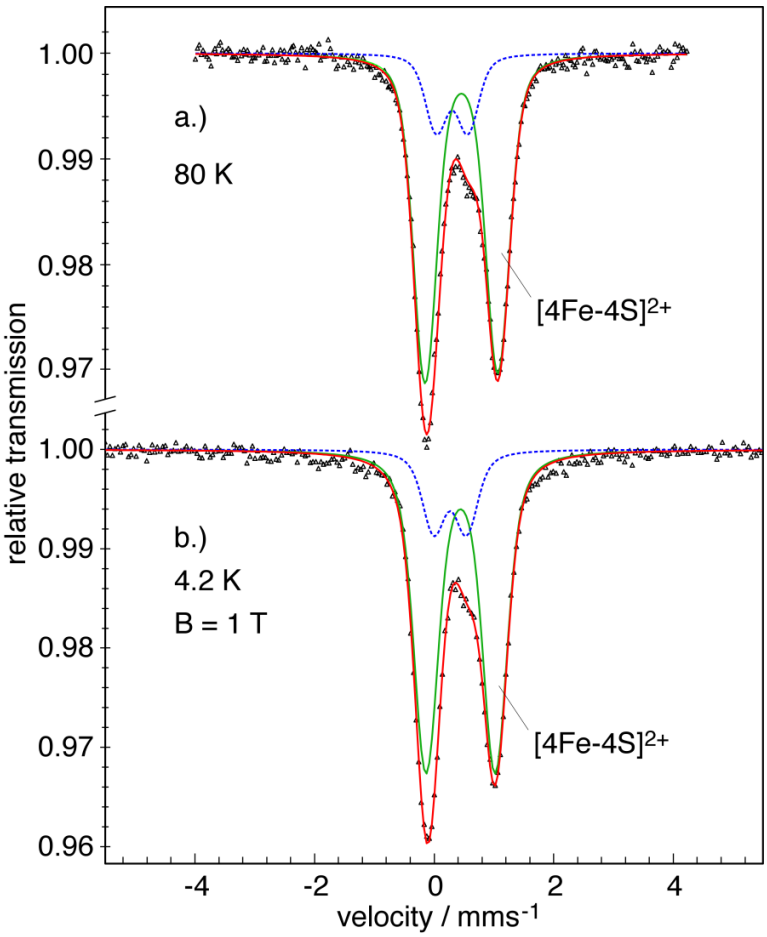


**Figure R12. Mössbauer spectra of 4Hpad-AE*** (4-6 mol $^{57}Fe$ per mol protein, 400 µM in buffer C). (*a.*) Zero-field spectrum recorded at 80 K. Lines represent simulated quadrupole doublets with Voigtian line shapes; Green: $[4Fe\text{-}4S]^{2+}$ clusters (82%, $\delta$ = 0.44 mm/s, $\Delta E_Q$ = 1.22 mm/s, $\Gamma_{Gauß}$ = 0.36 mm/s), Blue: non-cluster $Fe^{III}$ (18%, $\delta$ = 0.3 mm/s, $\Delta E_Q$ = 0.50 mm/s, $\Gamma_{Gauß}$ = 0.32 mm/s). Red line is the superposition of subspectra. (*b.*) Spectrum recorded at 4.2 K with a field of 1 T applied perpendicular to the γ-rays. Simulation with the same subspectra as introduced above; $[4Fe\text{-}4S]^{2+}$

clusters (81%, $\delta$ = 0.44 mm/s, $\Delta E_Q$ = 1.16 mm/s, $\Gamma_{\text{Gauß}}$ = 0.20 mm/s), non-cluster $Fe^{III}$ (19%, $\delta$ = 0.3 mm/s, $\Delta E_Q$ = 0.50 mm/s, $\Gamma_{\text{Gauß}}$ = 0.29 mm/s). The simulations are performed with spin $S$ = 0 for both subspectra (i.e only nuclear Zeeman effect). Figures were prepared by Eckhard Bill at the Max Planck Institute for Chemical Energy Conversion, Mülheim, Germany

The Mössbauer spectrum of as-isolated 4Hpad-AE* (4-6 mol $^{57}$Fe per mol protein) recorded at 80 K shows a slightly asymmetric two-line pattern that could be well simulated with two quadrupole doublets when Voigtian line profiles were applied (Figure R12a). In contrast the alternative fits with Mössbauer-intrinsic Lorentzian line shapes require an ill-defined number of subspectra for technically correct fits. The line shape model represents Gaussian distributions of Lorentzian lines. We assume that the Gaussian part of the line widths reflects slight differences of the iron sites subsumed under the two subspectra. The Mössbauer parameters of the major contribution shown as thin solid line are typical of iron in the mixed valence state (2.5+) as it occurs in reduced $[4Fe\text{-}4S]^{2+}$ clusters (82%, isomer shift $\delta$ = 0.44 mm/s, quadrupole splitting $\Delta E_Q$ = 1.22 mm/s). The second subspectrum (dashed line, 18%, $\delta$ = 0.3 mm/s, $\Delta E_Q$ = 0.50 mm/s) is typical of iron (III), but it cannot be discriminated from the parameters whether it represents oxy-hydride-like contaminations from iron precipitates, not bound clusters or all-ferric $[3Fe\text{-}4S]^{1+}$ clusters, which both have similarly small isomer shift and weak quadrupole splitting.

The Mössbauer subspectra of as-isolated 4Hpad-AE* (4-6 mol $^{57}$Fe per mol protein) at 4.2 K with a field of 1 T show almost the same line pattern found at 80 K (Figure R12b). When paramagnetic species such as oxidized $[3Fe\text{-}4S]^{1+}$ or reduced $[4Fe\text{-}4S]^{1+}$ clusters are polarized by applying magnetic field, they could be easily identified from the large magnetic splitting due to strong internal fields at the iron nuclei, arising from spin $S > 0$. Since the experimental magnetic splitting is marginal, resulting only from direct nuclear Zeeman effect, it can be concluded that the sample is essentially diamagnetic (with ca. 3% uncertainty due to the limited signal to noise ratio). This rules out the interpretation of the minor (18%) species as paramagnetic $[3Fe\text{-}4S]^{1+}$ clusters. Alternatively, it could arise from diamagnetic oxidized $[2Fe\text{-}2S]^{2+}$ clusters, but that is improbable because reduced EPR samples did not show the characteristic signals from reduced $[2Fe\text{-}2S]^{2+}$ clusters with spin S = 1/2. Further experiments are needed to better quantify the contribution of these putative clusters. Thus it is concluded that the ferric subspectrum found in the Mössbauer spectra is attributed to nano-particles of non-cluster bound iron (III), probably oxy-hydroxides, which may originate from partial

cluster degradation (they show effectively diamagnetism because of fast superparamagnetic relaxation (Glaser, 2011). The diamagnetism of the major subspectrum (82%) readily corroborates the assignment to reduced $[4Fe\text{-}4S]^{1+}$ clusters.

To summarize, the Mössbauer and EPR analysis confirmed the presence of at least two $[4Fe\text{-}4S]^{2+/+}$ cluster in 4Hpad-AE.

## 3.3. Spectroscopic analysis of Δ66-AE

Δ66-AE (as-isolated, tag-free) displayed a brown color with an iron content of 3.5 ± 0.2 mol Fe per mol protein, when analyzed by colorimetric method (Table 3.3.1). UV-vis spectroscopy confirmed the presence of a cubane iron-sulfur cluster as seen by a 50% bleaching of the maximum absorbance at 420 nm (Figure R13A) upon reduction by DT (Sweeney & Rabinowitz, 1980).

### 3.3.1. UV-vis & colorimetric analysis

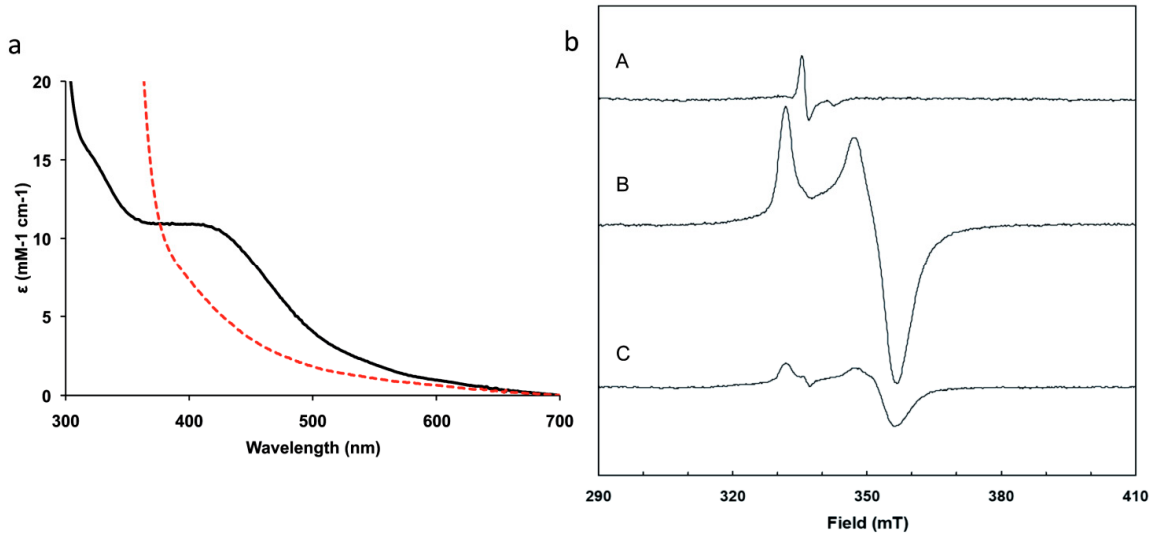


**Figure R13. UV-visible and EPR spectra of Δ66-AE** (a) UV-Vis spectra of purified Δ66-AE (12 µM in buffer C) before (—) and after (---) reduction with a 15-fold molar excess of DT for 5 min. The UV-vis spectrum shows shoulders at 420 nm and reduction with DT causes a 50% bleaching at 400 nm. The iron content calculated from the UV-vis spectra and calorimetric assay are given in the table 3.3.1. (b) EPR spectra of (A) as-isolated Δ66-AE (80 µM in buffer C); (B) as-isolated Δ66-AE (80 µM in buffer C) reduced with a five-fold molar excess of DT; and (C) as in (B) plus incubation with 2 mM SAM for 5 minutes. Spectra were recorded at 10 K with 0.8 mW microwave power, 1.25 mT modulation amplitude and a microwave frequency of 9.459 GHz.

**Table 3.3.1.** Iron content analysis of Δ66-AE

| Δ66-AE | Mol Fe per mol protein | |
|---|---|---|
| | UV-vis | Colorimetric |
| As-isolated $His_6$-tagged | 2.6 ± 0.3 | 2.9 ± 0.2 |
| Non-reconstituted tag free[1] | 2.8 ± 0.2 | 3.5 ± 0.2 |

[1]as-isolated after removal of $His_6$-tag by TEV protease

## 3.3.2. EPR and Mössbauer analysis

EPR spectra of the as-isolated Δ66-AE shows a sharp signal at g=2.02, typical of $[3Fe\text{-}4S]^{1+}$ clusters corresponding to 0.01 $[3Fe\text{-}4S]^{1+}$ cluster per protein (Figure R13b, trace A). Spin integration of the reduced Δ66-AE gives 0.85 $[4Fe\text{-}4S]^{1+}$ cluster per protein (Figure R13b, trace B) that indicates the presence of one bound [4Fe-4S] cluster. The spectra of SAM-incubated reduced Δ66-AE gives 0.20 $[4Fe\text{-}4S]^{1+}$ cluster per protein showing very less extent of cluster reduction.

The liquid-helium Mössbauer spectrum of the as-isolated Δ66-AE with 2.6 ± 0.3 mol $^{57}Fe$ per mol protein (Figure R14A, top) indicates that 94% of the iron is present as oxidized $[4Fe\text{-}4S]^{2+}$ clusters, with 6% of the Mössbauer intensity been attributed to nuisance iron (grey dotted line). The asymmetric contribution from the Fe/S cluster to the spectrum could be fitted with two quadrupole doublets, I and II, with intensity ratio 3:1. This indicates the presence of a slightly distinct iron site in the cubanes. Based on the lower isomer shift and quadrupole splitting the unique site II appears to have slightly more ferric character than the others. The absence of magnetic splitting at the low temperature (3 K, 20 mT applied field) corroborates the assignment of the diamagnetic state for the $[4Fe\text{-}4S]^{2+}$ cluster. Accordingly, the same spectrum was virtually observed at 80 K.

Non-cluster bound iron is absent in Δ66-AE incubated with SAM (Figure R14A, bottom) confirming the stabilizing effect of SAM (Yang *et al.*, 2009). The spectrum is again slightly asymmetric and could be fitted with two subspectra with 3:1 ratio. Apparently, SAM does not change the $[4Fe\text{-}4S]^{2+}$ cluster oxidation state, but affects the electronic structure mostly of site II whereas the other iron sites experience little influence. Hence, similar to what is found in the literature (Kulzer *et al.*, 1998; Yang *et al.*, 2009) we assigned the unique site I to SAM binding.

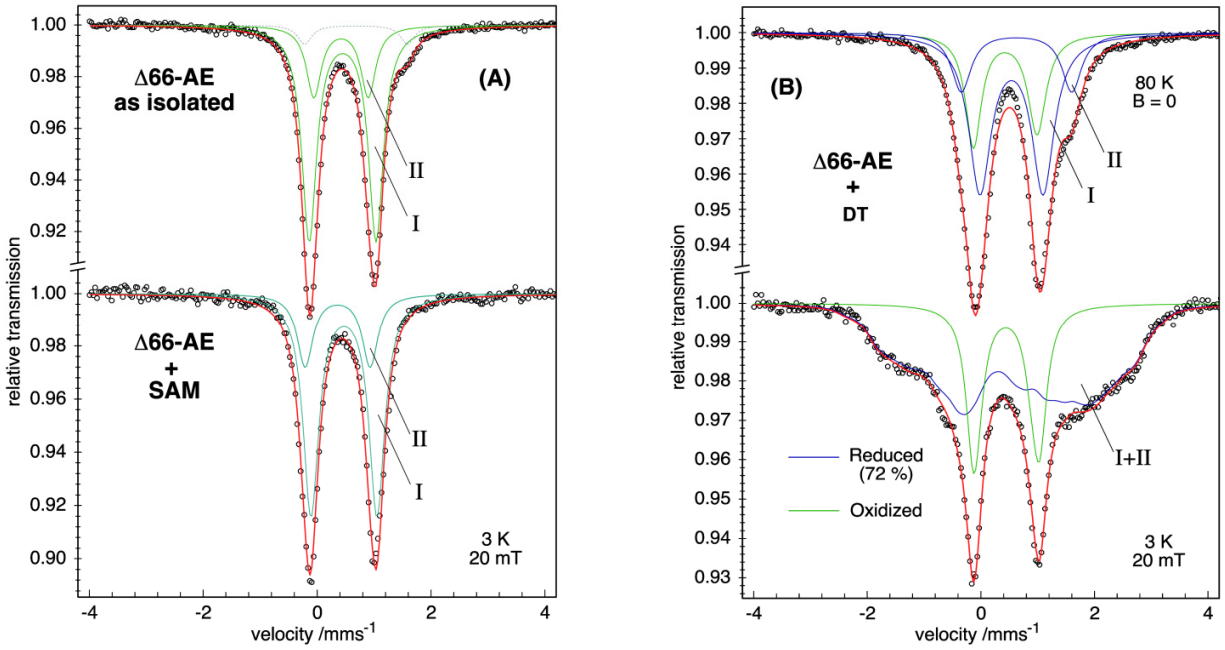


**Figure R14. Mössbauer spectra of Δ66-AE** (A) as-isolated Δ66-AE (0.56 mM in buffer C, top panel) and incubated with 2 mM SAM for 5 min (0.72 mM in buffer C, bottom panel). Both spectra were recorded at 3 K with a field of 20 mT applied perpendicular to the γ-rays. Subspectra I and II are assigned to three similar plus one non-similar iron sites of the $[4Fe\text{-}4S]^{2+}$ cluster, whereas the grey dotted line in the top spectrum marks 6% nuisance iron ($\delta$ = 0.69 mm/s, $\Delta E_Q$ = 1.81 mm/s). (B) Reduced Δ66-AE (0.72 mM in buffer C) reduced with 15 fold molar excess sodium dithionite for 5 min. Top: Zero-field spectrum recorded at 80 K, and bottom: magnetic spectrum recorded at 3 K with 20 mT field applied perpendicular to the γ-ray. The green traces indicate the contributions from remaining oxidized $[4Fe\text{-}4S]^{2+}$ clusters, simulated with parameters taken form Figure R14A top, whereas the subspectra I and II from reduced $[4Fe\text{-}4S]^{1+}$ cluster are shown in blue. Figures were prepared by Eckhard Bill at the Max Planck Institute for Chemical Energy Conversion, Mülheim, Germany

The zero-field Mössbauer spectrum recorded at 80 K from Δ66-AE treated with 15-fold excess of DT (Figure R14B, top) shows a superposition of three subspectra, which can be assigned to I.) 28% remaining oxidized clusters (green, parameters as found for Fig. 14A, top), and ii.) 72% reduced clusters, again showing two subspectra (I and II, in blue). Interestingly, the distinct site I now has acquired the more ferrous character than the others. The paramagnetic nature of the reduced $[4Fe\text{-}4S]^{1+}$ cluster could be demonstrated by an applied-field measurement at 3 K, showing a wide magnetic splitting of subspectra I and II due to the spin S = 1/2 of the reduced cluster (Figure R14B, bottom).

In summary, the Mössbauer and EPR analyses of Δ66-AE with 2.6 Fe ions per polypeptide reveals that Δ66-AE harbors 0.6 [4Fe-4S] clusters [(2.6 Fe) x 0.94/(4 Fe per cluster)] that can occur in ($2^+$) or ($1^+$) state. Taken together, the UV-vis, EPR and Mössbauer results provide clear evidence for the presence of the postulated $[4Fe\text{-}4S]^{2+/+}$ RS cluster in Δ66-AE. Δ66-AE is stable coordinating a Fe/S cluster, being therefore suitable for biochemical and spectroscopic studies.

# 4. Enzymatic assays

## 4.1. Reductive cleavage of SAM (Uncoupled assay)

GRE-AEs catalyze the reductive cleavage of SAM in the absence of its target 4Hpad producing methionine and 5'-deoxyadenosyl radical that further reacts with surrounding protein or solvent molecules generating 5'-deoxyadenosine (Duschene *et al.*, 2009). 4Hpad-AE (7.5 ± 0.2 mol Fe per mol protein) or 4Hpad-AE** (12.0 ± 0.3 mol Fe per mol protein) was pre-reduced with a 15 fold molar excess of DT for 5 min at pH 7.5 at 30 °C. Then, SAM was added to a final concentration of 2 mM and the activation was followed for 2 h. 50 µl samples were withdrawn at fixed time intervals and the product formation was monitored by RP-HPLC after stopping the reaction with 10% trifluoroacetic acid (see materials and methods 9.1.1). The products, 5'-deoxyadenosine and methionine from the reductive cleavage of SAM were quantified by different methods, RP-HPLC, ESI-MS and TLC.

### 4.1.1. 5'-deoxyadenosine detection

SAM cleavage is detected only when the protein is reduced by DT (Figure R15, Trace III). 5'-deoxyadenosine formation is confirmed by comparing its retention time to the 5'-deoxyadenosine standard. 5'-deoxy 5'-(methylthio)adenosine (MTA) and S-adenosyl-L-homocysteine (SAH) are products from the thermal decomposition of SAM (Hoffman, 1986). Adenosine is used as the internal standard. Control reactions were performed in the absence of 4Hpad-AE** (Figure R15, Trace I) and DT (Figure R15, Trace II) where there is no 5'-deoxyadenosine formation.

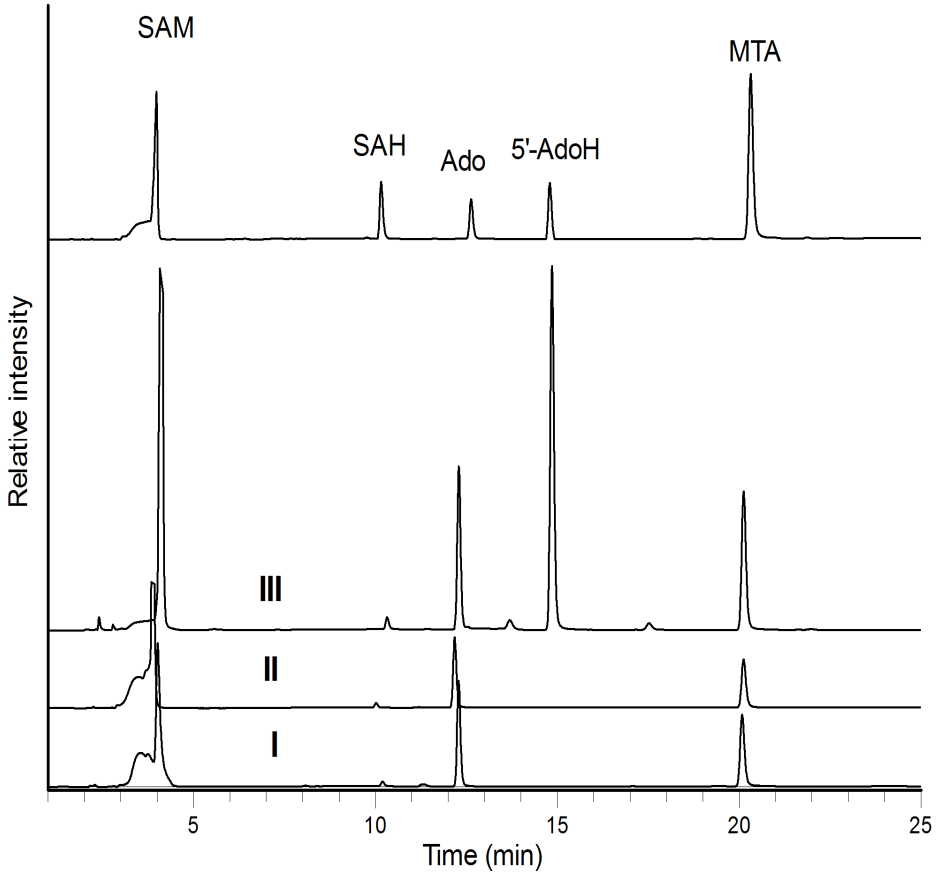


**Figure R15. HPLC analysis of products from the SAM cleavage assay.** Trace I shows the control reaction without 4Hpad-AE**; Trace II shows the assay without DT; Trace III shows the assay in the presence of DT. Adenosine (Ado) was used as internal standard. The upper most trace shows the chromatogram of an equimolar mixture of the standards SAM, SAH, Ado, 5'-AdoH and MTA. The SAH and MTA peaks observed in the assay and control reactions (approx. 10 and 20 min, respectively) are due to thermal decomposition of SAM (Yang *et al.*, 2009). The peaks for SAM in traces I, II and III were truncated for easier visualization. This figure is taken from (Selvaraj *et al.*, 2013).

HPLC elution peaks corresponding to 5'-AdoH and SAM were dried under vacuum and measured for ESI-MS (Figure R16). The identity of this molecule was confirmed by mass spectrometry showing 5'- deoxyadenosine (5'-deoxyadenosyl radical quenched form), generated by the reductive cleavage of SAM.

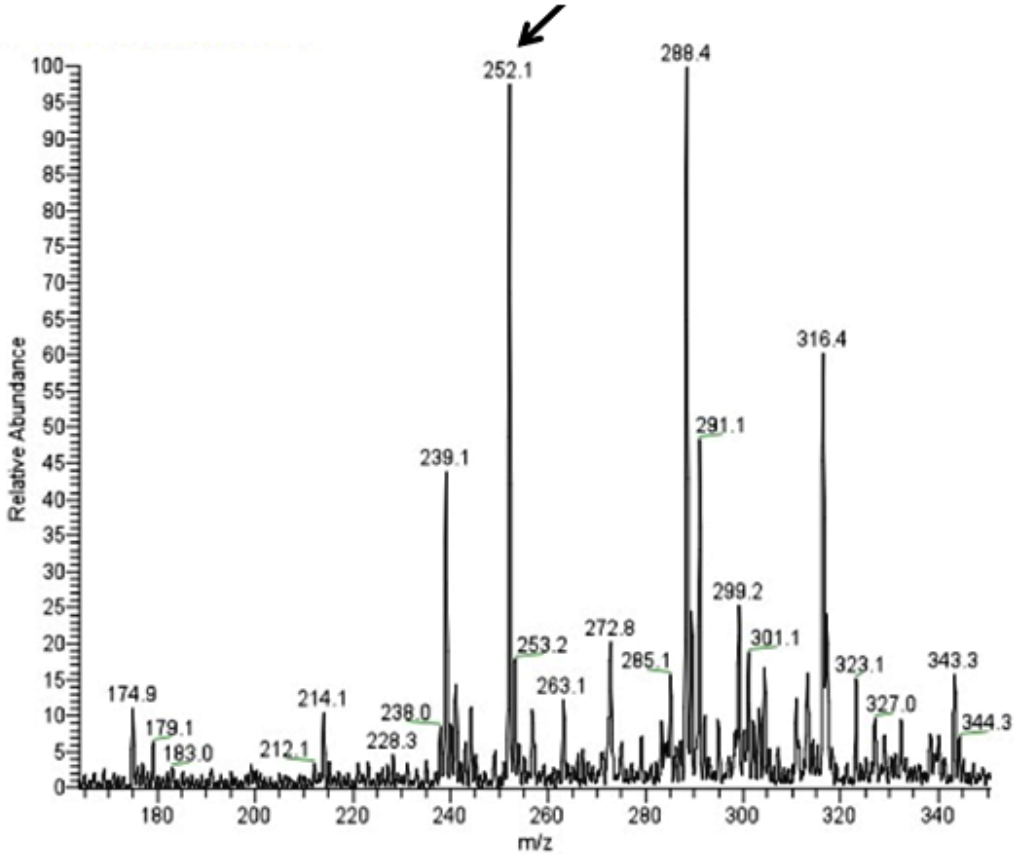


**Figure R16. ESI-MS of 5′-deoxyadenosine.** ESI-MS from the HPLC peak eluted with equal retention time to the 5'AdoH standard. The mass 252.1 indicated by arrow, corresponds to 5'-AdoH plus hydrogen and the mass 288.4 corresponds to the addition of a chloride ion. The flow rate was 8 µl $min^{-1}$ and 100 spectra were collected at 0.8 half width resolution in positive mode (Selvaraj *et al.*, 2013). The figure was provided by Angelika Woyda the Mathematisch-Naturwissenschaftliche Fakultät I, Humboldt University Berlin, Germany.

## 4.1.2. Methionine detection

After stopping the reaction with 10% trifluoroacetic acid, the assay mixture was centrifuged and the supernatant was treated with PITC-reagent to detect the phenylisothiocyanate derivatized methionine (phenylthiohydantoin methionine) by TLC (Dimova, 2003). When visualized by 0.2% ninhydrin in acetone, the TLC showed various chromatographic zones where the purple and red bands represent the derivatized methionine (phenylthiohydantoin methionine) and the non-derivatized methionine, respectively. Background of PITC-reagent is observed in yellow (Figure R17, Spots A & B). Control reactions were performed in the absence of 4Hpad-AE (Figure R17, Spot C).


**Figure R17. TLC of PITC-derivatized methionine.** (A) and (B) 30 and 60 minutes of reaction time, respectively. Stars indicate derivatized methionine (purple bands) (C) No enzyme present (sample taken after 60 min incubation)

These results demonstrate that 4Hpad-AE** was able to reductively cleave SAM to 5'-deoxyadenosyl radical intermediate that was detected as 5'-deoxyadenosine in 4.1.1 and methionine that was detected as in 4.1.2. The specific activity and rate of the reductive cleavage of SAM by 4Hpad-AE and 4Hpad-AE** were tabulated in table 4.1. The unit of activity (U) was defined as one µmol of 5´-AdoH produced per minute.

**Table 4.1.** SAM cleavage activity by 4Hpad-AE and 4Hpad-AE*

| | | As-isolated | Reconstituted | Tag free (non-reconstituted) | Reconstituted Tag free |
|---|---|---|---|---|---|
| 4Hpad-AE | Specific activity (mU/mg) | Not detectable | Not detectable | Not detectable | 6.0 ± 0.5 |
| | Rate ($min^{-1}$) | Not detectable | Not detectable | Not detectable | 0.217 ± 0.018 |
| 4Hpad-AE* | Specific activity (mU/mg) | 1.5 ± 0.2 | 1.9 ± 0.2 | 2.2 ± 0.5 | (4Hpad-AE**) 5.3 ± 1.0 0.40 ± 0.01[a] |
| | Rate ($min^{-1}$) | 0.054 ± 0.005 | 0.069 ± 0.005 | 0.08 ± 0.01 | (4Hpad-AE**) 0.193 ± 0.010 0.014 ± 0.001[a] |
| Δ66-AE | Specific activity (mU/mg) | 2.0 ± 0.1 [a] | Not measured | 2.4 ± 0.2 [a] | 2.2 ± 0.1 [a] |
| | Rate ($min^{-1}$) | 0.058 ± 0.003 [a] | Not measured | 0.070 ± 0.005 [a] | 0.063 ± 0.003 [a] |

[a] The purity of commercial SAM used for the measurements is less than 80%

Although the specific activity of as-isolated 4Hpad-AE was not detected, the rate of 5'-deoxyadenosine production by 4Hpad-AE* (0.054 ± 0.005 $min^{-1}$) was found to be in the range of Pfl-AE (0.03 $min^{-1}$) (Dey *et al.*, 2011). Thus the reconstitution of RS cluster seemed to be more efficient in the presence of ISC proteins. Initially it was thought that the auxiliary clusters most probably have a stabilizing effect on the protein structure, which may influence the kinetics of the RS cluster reduction. But in contrast, the rates for 5'-deoxyadenosine production by Δ66-AE, 0.063 $min^{-1}$ (depending on SAM used) were as efficient as the rates obtained for WT-AE, 0.014 $min^{-1}$ (depending on SAM used). It is concluded the auxiliary clusters do not influence the reductive cleavage of SAM, making the RS cluster solely responsible for this activity. Hence, the RS cluster present in Δ66-AE is fully competent to reductively cleave SAM, which is contradictory to the suggestion that the auxiliary clusters act as conduit for reduction of the RS cluster in 4Hpad-AE (Yu *et al.*, 2006).

## 4.2. Reductive cleavage of SAM in the presence of 4Hpad (Coupled assay)

Influence of 4Hpad on the reductive cleavage of SAM by 4Hpad-AE was inspected as described in 4.1 with addition of 4Hpad in reaction mixture. The reaction was started by the addition of SAM and 5'-AdoH formation was monitored by HPLC. The assay was carried out only for 4Hpad-AE** (12.0 ± 0.3 mol Fe per mol protein) and Δ66-AE (3.5 ± 0.2 mol Fe per mol protein) since they showed the maximum rate of 5'-AdoH formation in their respective uncoupled assays. The increased rate of SAM cleavage by 4Hpad-AE** and Δ66-AE in the presence of 4Hpad (Table 4.2) indicates that complex formation between the two proteins enhances homolytic cleavage of the S-C bond in SAM molecule, (Dey *et al.*, 2011; Jarrett, 2003). Otherwise reduction and homolytic cleavage of SAM is difficult because of the high-energy barrier of reaction (Kampmeier, 2010; Broderick, 2010). The unit of activity (U) was defined as one μmol of 5′-AdoH produced per minute.

**Table 4.2.** SAM cleavage activity

| | | |
|---|---|---|
| 4Hpad-AE** | Specific activity (mU/mg) | 1.10 ± 0.01[a] |
| 12.0 ± 0.3 mol Fe per mol protein | Rate ($min^{-1}$) | 0.04 ± 0.001[a] |
| Δ66-AE | Specific activity (mU/mg) | 4.4 ± 0.2[a] |
| 3.5 ± 0.2 mol Fe per mol protein | Rate ($min^{-1}$) | 0.128 ± 0.005[a] |

[a] The purity of commercial SAM used for the measurements is less than 80%

## 4.3. Correlation between 5'-deoxyadenosine and glycyl radical formation

A time-dependent formation of 5'-deoxyadenosine by HPLC and of the glycyl radical by EPR spectroscopy had been conducted to confirm that 5'-deoxyadenosyl radical was used as activating agent to generate a glycyl radical in 4Hpad. 4Hpad-AE** in buffer C was reduced first and mixed with 4Hpad. The reaction was initiated by adding 2 mM SAM. Samples were taken from the assay mixture at different time intervals and split into two for measuring the amount of 5'-deoxyadenosine by HPLC (Figure R18B) and for measuring the amount of glycyl radical by EPR (Figure R18A).

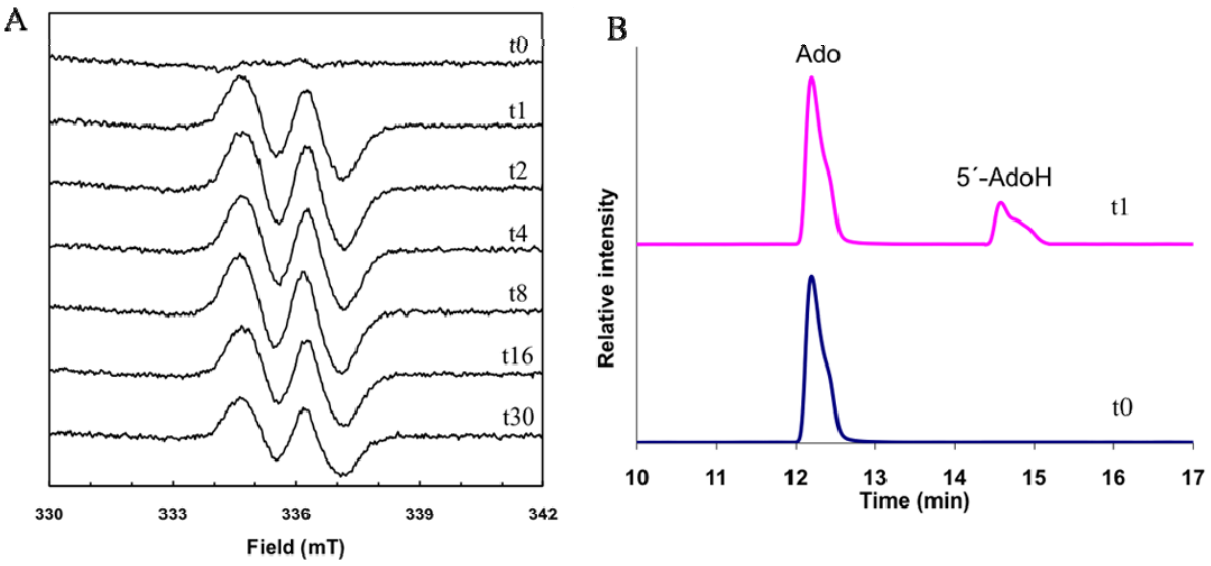


**Figure R18. EPR spectra of glycyl radial formation and HPLC trace of 5'-Deoxyadenosine formation.** (A) Formation of the glycyl radical in 4Hpad (20 µM) was determined by double integration of the EPR spectra. EPR spectra show the time dependent formation of glycyl radical in 4Hpad. Spectra

were recorded at 77 K, with 12.7 µW microwave power, 1.0 mT modulation amplitude, 100 kHz modulation frequency and a microwave frequency of 9.433±0.002 GHz. EPR figures were prepared by Antonio J Pierik at the Core facility for protein spectroscopy, Institute of Cytobiology and Cytopathlogy, Philipps University Marburg, Germany. (B) 5'-Deoxyadenosine production by 4Hpad-AE** was followed by HPLC as described for the SAM cleavage assay. HPLC elution profiles before (trace t0) and after (trace t1) one-minute incubation on 2 mM SAM addition.

The amount of 5'-deoxyadenosine formed in the early phase showed a burst of about 5 µM (dotted line, Figure R19A) that corresponds to the maximum glycyl radical content in 4Hpad as determined by EPR double integration. There is no evidence for the presence of other possible SAM cleavage products such as 5'-deoxy 5'-(methylthio)adenosine (MTA) and *S*-adenosylhomocysteine (SAH) within and after the time required for maximal 4Hpad activation.

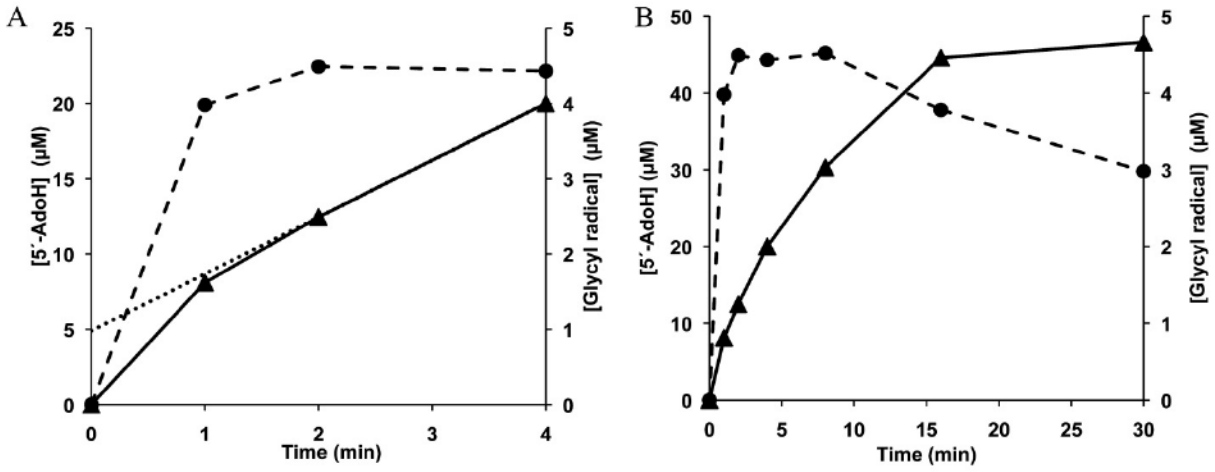


**Figure R19. Cleavage of SAM resulting in the formation of 5'-deoxyadenosine by 4Hpad-AE** and evidence of glycyl radical generation for 4Hpad activation.** Correlation between formation of 5'-deoxyadenosine (—) and generation of glycyl radical in 4Hpad (---). (A) Linear extrapolation of the 5'-deoxyadenosine formation data points at 2 and 4 min to t=0 is shown (----) (B) Correlation between 5'-deoxyadenosine (—) and glycyl radical (---) formations by 4Hpad over 30 minutes.

The correlation between 5'-deoxyadenosine production and glycyl radical generation was also conducted to verify whether Δ66-AE could activate 4Hpad. The time scale for maximum glycyl radical formation was similar for both Δ66-AE and 4Hpad-AE** (within 1-2 min incubation).

However when activated by Δ66-AE, the glycyl radical production was lower and less stable. Approximately 40% less glycyl radical was formed by Δ66-AE with a faster decaying rate ($t_{1/2}$ = 5 min) (Figure R20B) compared to 4Hpad-AE** ($t_{1/2}$ > 30 min) (Figure R19B). As observed in the wild type, the amount of 5'-deoxyadenosine formed in the early phase showed a short burst of about 3 µM (dotted line, Figure R20A) that corresponds to the maximum glycyl radical content in 4Hpad as determined by EPR double integration. Slower glycyl radical formation was also reported for the site-mutagenesis studies covering putative cysteine ligands for strep-tagged 4Hpad-AE (Yu *et al.*, 2006, value not reported).

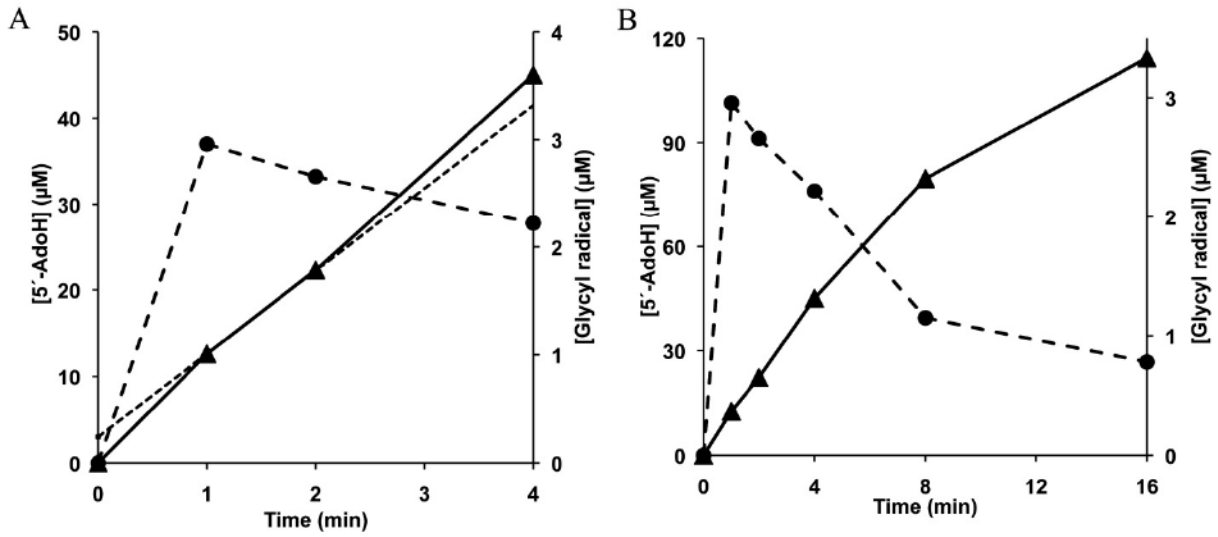


**Figure R20. Correlation between 5'-deoxyadenosine formation and glycyl radical generation in 4Hpad activated by Δ66-AE.** Production of 5′-deoxyadenosine (—) was quantified by HPLC and amount of glycyl radical generation (---) was measured by double integration of EPR spectra. (A) Linear extrapolation of the 5'-deoxyadenosine formation data points at 2 and 4 min to t=0 is shown (‹----) (B) Correlation between 5'-deoxyadenosine (—) and glycyl radical (---) in 4Hpad over 30 minutes.

Δ66-AE is able to activate 4Hpad but with lower glycyl radical yield and a faster decaying time (Figure R20). Thus, Δ66-AE is less efficient to activate 4Hpad than WT-AE. Feasible explanations for this behavior could be drawn from the X-ray crystal structure of PFL-AE with a heptamer peptide substrate bound in the active site (Vey *et al.*, 2008). The crystal structure indicates that Pfl requires a drastic conformational change to bring the Gly-loop that is buried 8 Å below the protein surface, out of the protein core making it more accessible to the active site of Pfl-AE. Recently reported evidences suggest that Pfl can exist in either closed conformation with

the Gly-loop buried in the active site, or in an open conformation with the Gly-loop more solvent exposed and accessible to the Pfl-AE active site (Peng *et al.*, 2010). It is also said that the presence of Pfl-AE favors the open conformation eventually influencing the catalytic activity of its partner enzyme. In case of 4Hpad/4Hpad-AE system, the radical domain of 4Hpad has to get out of the protein core to locate the active Gly-loop that is buried 16 Å below the protein surface. The missing cysteine-rich motif (66 aminoacids) in Δ66-AE is expected to be in close proximity to the Adomet radical core region. Presumably, this close proximity of the putative auxiliary cluster(s) shields the RS cluster in 4Hpad-AE and also the glycyl radical of 4Hpad by relocating the Gly-loop into the active site of 4Hpad (Martins *et al.*, 2011) during complex formation. Thus the lack of the auxiliary cluster(s) could destabilize the glycyl radical in 4Hpad. This study provides insights into the role of auxiliary cluster(s) contributing to the stable complex formation between 4Hpad and its activating enzyme and to shield the RS cluster environment. Once the complex is formed, it is conceivable that the auxiliary cluster(s) involve in mediating the electron transfer to the RS cluster and thereby increasing the rate and stability of glycyl radical formation.

## 4.4. *p*-Cresol production by 4Hpad

4Hpad is activated by 5´-deoxyadenosyl radical produced from the reductive cleavage of SAM by 4Hpad-AE** or Δ66-AE. The resulting product, *p*-cresol was detected by HPLC and quantified using standard calibration curves. The specific activity showed by 4Hpad when activated by either 4Hpad-AE** or Δ66-AE is shown in the table 4.3. Specific activity and turnover were calculated using the molecular mass for a 4Hpad monomer, 110 kDa. The unit of activity (U) was defined as one μmol of *p*-cresol produced per minute.

**Table 4.3.** Specific activity of 4Hpad in *p*-cresol formation.

| | | |
|---|---|---|
| 4Hpad-AE**<br>12.0 ± 0.3 mol Fe per mol protein | Specific activity (mU/mg) | 2.1 ± 0.5<br>1.2 ± 0.2[a] |
| | Rate ($min^{-1}$) | 231 ± 55<br>132 ± 20[a] |
| Δ66-AE<br>3.5 ± 0.2 mol Fe per mol protein | Specific activity (mU/mg) | 0.2 ± 0.08 [a] |
| | Rate ($min^{-1}$) | 22 ± 9 [a] |

[a] The purity of commercial SAM used for the measurements is less than 80%

As Δ66-AE activated 4Hpad with a decreased glycyl radical halftime, the rate for *p*-cresol formation is expected to be low as well. The *p*-cresol formation produced by 4Hpad activated by Δ66-AE is 6-fold lower (22 ± 9 $min^{-1}$, Figure R21B) compared to the activation by 4Hpad-AE** (132 ± 20 $min^{-1}$, Figure R21A and Table 4.3). Thus, Δ66-AE is less efficient than the wild type in activating 4Hpad despite a comparable 5'-deoxyadenosine production. The less stable glycyl radical along with the reduced *p*-cresol by Δ66-AE together indicates that the auxiliary clusters play a significant role in the radical stabilization and thereby favoring the complex formation between 4Hpad-AE and 4Hpad.

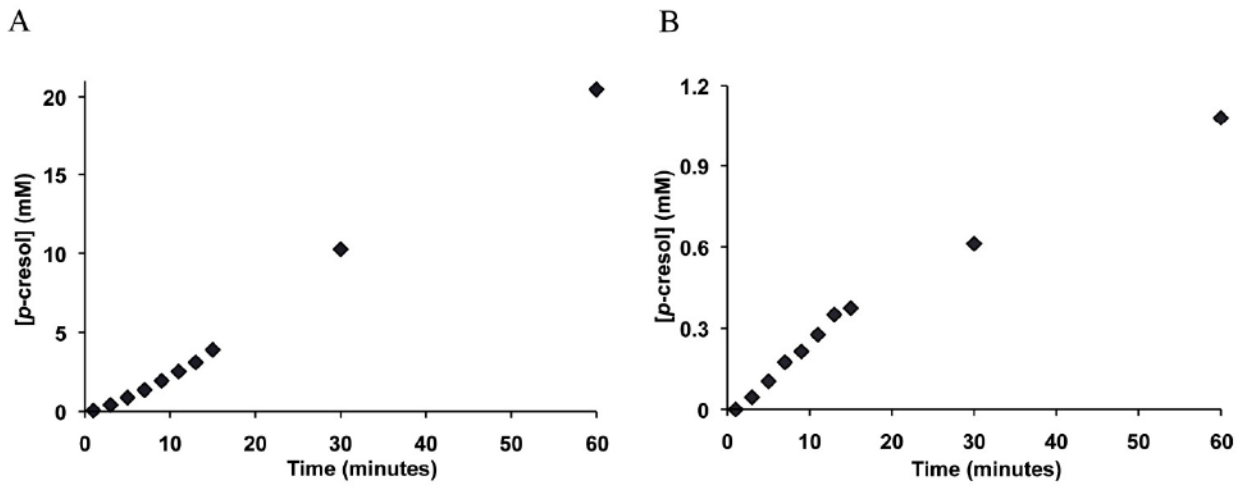


**Figure R21. *p*-Cresol formation by 4Hpad in the presence of 4Hpad-AE** (A) and Δ66-AE (B).** In both cases, there is a lag-phase of about 2 minutes followed by a steady increase in the formation of *p*-cresol for at least sixty minutes. Every measurement was performed twice independently.

None of the 4Hpad variants (E505Q, E637Q, H536Q, HE2Q) showed *p*-cresol production when activated by 4Hpad-AE** (Figure R22). E505 is presumed to be responsible for donating the proton to the thiolate ($S^-$) of Cys503 forming a thiol (SH), which simultaneously loses an electron to the substrate-derived radical, regenerating the thiyl radical ($S^{<}$) in 4Hpad. By changing the E505 to glutamine, the proton donation to the thiolate is blocked thereby hindering the *p*-cresol formation. Similarly the residues E637 and H536Q are involved in anchoring the hydroxyl group of the substrate (4-HPA) by hydrogen interactions. When these residues were mutated to glutamine either independently or together, they failed to produce *p*-cresol. This infers

that both residues play a vital role in holding the substrate in its position thereby contributing their share in the Kolbe-type decarboxylation (Scheme 4, Introduction).

**Table 4.4.** Rate of ***p*-Cresol formation by 4Hpad and its variants when activated by 4Hpad-AE****

| | Rate ($min^{-1}$) |
|---|---|
| Wild type 4Hpad | 231 ± 55 |
| E505Q | Not detectable |
| E637Q | Not detectable |
| H536Q | Not detectable |
| HE2Q | Not detectable |

Every measurement was performed twice independently.

# 5. Kinetics

## 5.1. Michaelis-Menten kinetics

Steady-state kinetic constants for the activating enzyme were determined by measuring the specific activity of DT-reduced 4Hpad-AE** (15 μM) at varying concentration of SAM (0.15 to 4 mM). The product 5'-deoxyadenosine after SAM cleavage was quantified by HPLC (Materials and methods 9.1.1). The initial velocity of 5'-deoxyadenosine production was used to calculate the rate of the reaction. The calculated rate was plotted against SAM concentration. The steady-state constants ($K_m$ and $k_{cat}$) were determined by fitting the plot with a Sigma plot using the Michaelis-Menten equation. $K_m$ for SAM was estimated to be 0.44 ± 0.04 mM with a $k_{cat}$ of 14.9 ± 0.4 $h^{-1}$ (Figure R22). The observed $K_m$ is found to be in the range of physiological concentration of SAM (≈100 μM).

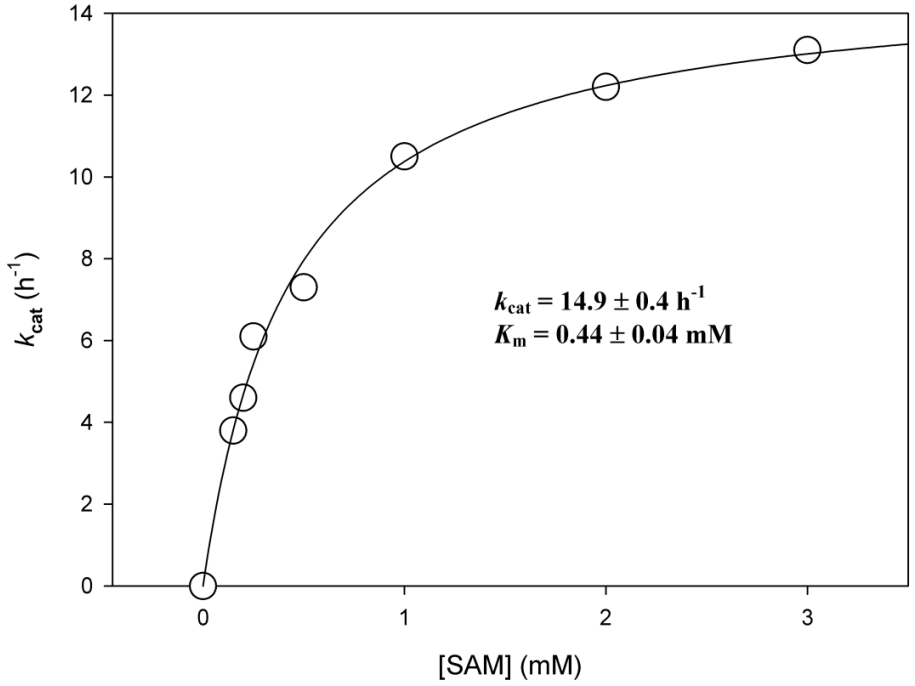


**Figure R22. Steady-state kinetics of uncoupled reductive cleavage of SAM by 4Hpad-AE**** Every measurement was performed twice independently.

## 5.2. Binding affinity of 4Hpad-AE to SAM

The binding of SAM to the oxidized RS cluster was tested by ITC to determine the respective binding affinity for 4Hpad-AE** and Δ66-AE. The protein (50 µM in buffer C) is taken in the reaction cell and titrated against SAM in the injection syringe. Raw data were corrected for heats of dilution and further analyzed by nonlinear fitting using one-site fit model with the software provided by the manufacturer (Origin 7.0). As shown in Figure R23, the binding stoichiometry (N) of 4Hpad-AE** and Δ66-AE for SAM molecule were determined as 0.36 and 0.50, respectively. The binding affinity, $K_d$ calculated for 4Hpad-AE** is 23 ± 7 µM and is in the range reported for Pfl-AE (5.2 µM, aerobic studies, Duschene *et al.*, 2009) and Nrd-AE (10 µM, Bennett *et al.*, 2009) containing only the RS cluster. However, dissociation constants of SAM for activating enzymes containing auxiliary clusters have not yet been reported. Cellular levels of SAM concentration have been estimated to be between 0.18 and 1 mM depending on growth conditions (Dey *et al.*, 2011). The $K_d$ values are found to be at least one-order of magnitude

below the physiological concentration of SAM indicating a high level of active site saturation. Thus, it is feasible that *in vivo* most of the 4Hpad-AE molecules will have SAM bound to the oxidized RS cluster. But the stoichiometry from SAM binding to 4Hpad-AE** as determined by ITC is 0.36, showing that not all molecules are competent for SAM binding (Figure R23A).

Under both aerobic and anaerobic growth, (Sauter & Sawers, 1990) Pfl-AE is heterologously expressed in *E. coli* implying a mechanism to regulate the activity of the enzyme in response to dioxygen levels. It has been shown in (Yang *et al.*, 2009) that Pfl-AE undergoes RS cluster inter-conversions in response to the redox state of the cell. Coordination of small molecules to the unique site of the RS cluster could protect the cluster from oxidative damage by preventing the unique Fe site from cluster dissociation upon air exposure. It is speculated from *in vivo* studies that AMP might protect the labile RS cluster from oxidative damage during aerobic growth, since AMP is considered to be abundant in *E. coli*. This protective effect seems not harmful for activity of Pfl-AE, because SAM displaces the bound AMP (Yang *et al.*, 2009). In this study, ITC is used to test the binding affinity of AMP to the oxidized RS cluster of 4Hpad-AE. No binding is observed and the apparent $K_d$ for SAM did not change in a competitive titration of 4Hpad-AE** with SAM in the presence of AMP. This indicates that AMP does not influence to the activity of 4Hpad-AE for SAM cleavage even though cellular levels of AMP (300 µM) and SAM are similar (Bennett *et al.*, 2009; Thauer *et al.*, 1977). 4Hpad-AE and orthologues are present in strict anaerobes, while Pfl-AE acts in the facultative anaerobe *E. coli*. A protection mechanism as seen for Pfl-AE might not be necessary for the 4Hpad-AE found in strict anaerobes.

The estimated binding affinity for Δ66-AE ($K_d$ = 124 ± 10 µM, Figure R23B) varies only slightly compared with WT-AE and a moderate increase in the stoichiometry for Δ66-AE (N = 0.50) compared with WT-AE (N = 0.36) was measured. The difference in binding energies between the WT-AE and Δ66-AE ($\Delta\Delta G_{bind}$) is ~ 1 kcal mol$^{-1}$. The results show Δ66-AE displays similar SAM binding affinity as WT-AE. The binding affinity of the RS cluster for SAM is unchanged in the absence of the auxiliary clusters. It suggests that the environment of the RS cluster in Δ66-AE is not affected by the absence of the structural part of the auxiliary clusters due to this small difference in SAM binding affinity and reactivity. Thus, under the conditions tested, it is concluded the auxiliary clusters are not necessary for productive cleavage of SAM.

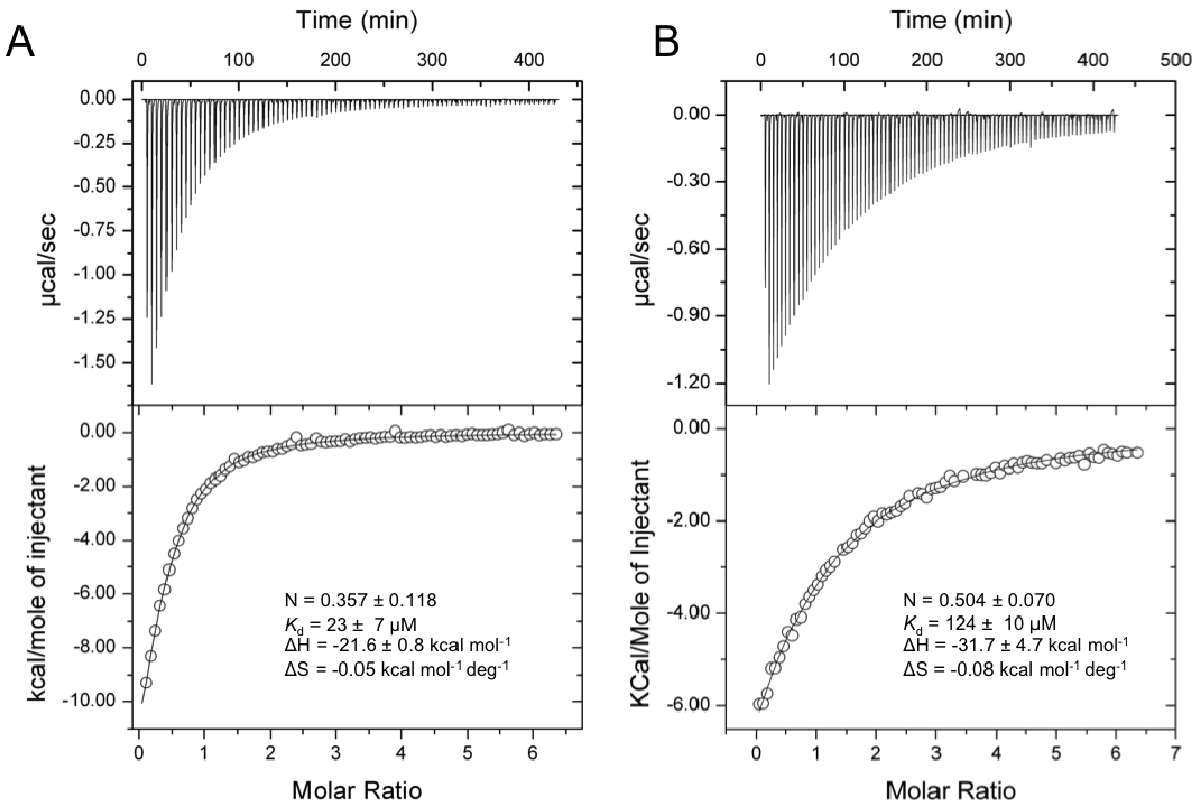


**Figure R23. Isothermal titration calorimetry (ITC) analysis of SAM binding** (A) SAM binding to 4Hpad-AE** (B) SAM binding to Δ66-AE. The top and bottom panels show the raw data of enthalpy change and integrated titration curves corrected for the heat of dilutions, respectively. The line through the data points is the best fit by a one-site binding model yielding the dissociation constants that are shown in the figure. Measurements were performed in duplicate and error estimates represent the standard deviation.

## 5.3. Reduction kinetics

Since the auxiliary cluster(s) in the activating enzymes presumably works as a conduit for reduction of the RS cluster (Yu *et al.*, 2006) reduction kinetics of wild type and Δ66-AE is expected to be distinguishable. To verify this hypothesis, *stopped-flow* technique had been used to follow the reduction of protein by dithionite at 418 nm (Figure R24) as the physiological electron donor of 4Hpad-AE is not known. The reduction kinetics of 4Hpad-AE** (WT-AE) was biphasic with a fast phase ($k_{obs}$ = 0.77 s$^{-1}$; amplitude 0.001) and a slower phase ($k_{obs}$ = 0.077 s$^{-1}$;

amplitude 0.006) (Figure R24). This is first interpreted as a clue to different RS and auxiliary clusters environments with the auxiliary clusters been first reduced (RS cluster is postulated to have a midpoint potential –500 mV; Walsby *et al.*, 2005). Unexpectedly, Δ66-AE shows a similar biphasic behavior with a fast phase ($k_{obs}$ = 0.68 $s^{-1}$; amplitude 0.001) and a slower phase ($k_{obs}$ = 0.068 $s^{-1}$; amplitude 0.008) (Figure R24). Although the protein always eluted as a single peak when analyzed by gel size-exclusion or ion exchange (MonoQ) chromatography, a non-homogeneity of protein sample either by impurity or by Fe/S cluster best explains the biphasic behavior as Δ66-AE only harbors one cluster. The similar biphasic reduction kinetics for both WT-AE and Δ66-AE indicates non-homogeneity is an intrinsic property of 4Hpad-AE produced heterologously, irrespective of numbers and types of the Fe/S clusters present.

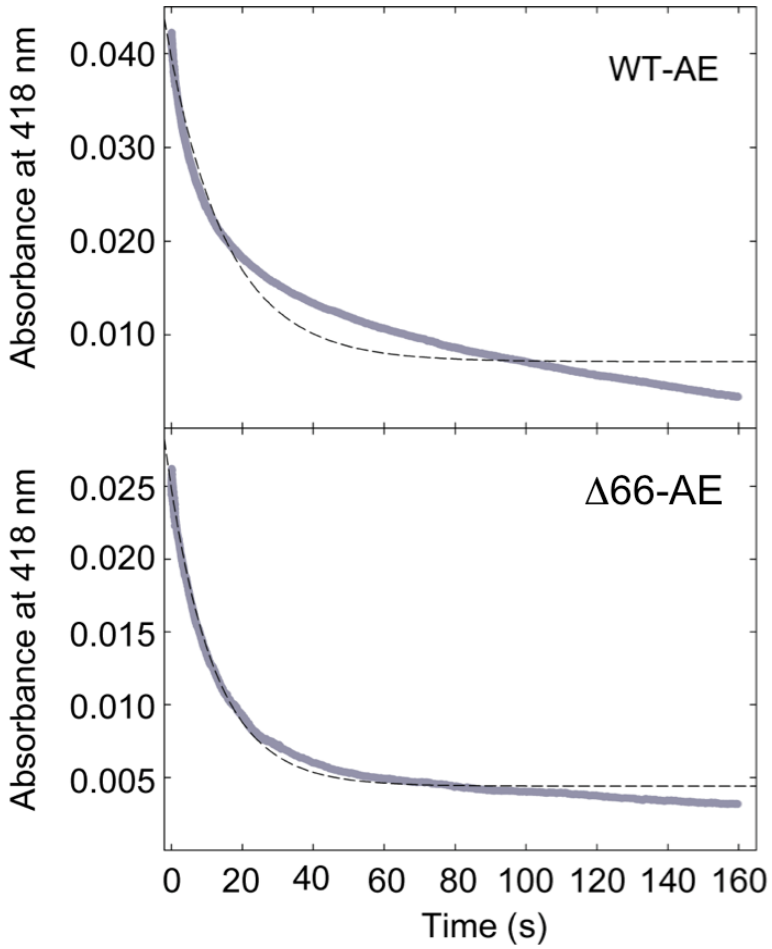


**Figure R24. Reduction kinetics of WT-AE and Δ66-AE**. Reduction of WT-AE (4 μM) and Δ66-AE (8 μM) by 125 μM dithionite followed at 418 nm (solid grey line). For illustration a mono-exponential fit to the data is shown in dashed line.

# 6. Complex formation between 4Hpad and 4Hpad-AE

Complex formation between 4Hpad/4Hpad-AE** and 4Hpad/Δ66-AE were tested under various conditions (see materials and methods 14) by gel size-exclusion chromatography and ITC. No complex formation could be detected so far. This is not surprising since GREs only require stoichiometric amounts of 5'-deoxyadenosine for glycyl radical formation (Eklund & Fontecave, 1999). Since the glycyl radical can be recycled after each turnover, a lasting complex between the GREs and dedicated activating enzymes is not required. The gel filtration chromatograms of the various trials tested in detecting the 4Hpad/4Hpad-AE complex formation are shown in appendix figure A3.

# 7. Crystallization

## 7.1. Co-crystallization of 4Hpad

In this study 4Hpad was co-crystallized with substrates (4-hydroxyphenylacetate, 3,4-dihydroxyphenylacetate) and inhibitor (4-hydroxyphenylacetamide) to verify the catalytic relevance of the substrate bound state. The co-crystals were obtained inside the anoxic glove box in completely different precipitant conditions (Materials and methods 13.1) compared to the substrate bound 4Hpad structure obtained by crystal soaking in the previous work (Martins *et al.*, 2011). Table 7.1 shows the crystals used for the structure determinations of wild type 4Hpad and its mutants. The crystals were grown in 7-8 days, displayed the color of the native protein and diffracted between 2.1 and 1.7 Å. With exception of the HE2Q double mutant, all measured crystals belonged to the $C222_1$ space group with circa 50 % solvent content corresponding to two heterodimers per asymmetric unit (Figure R26, top). The asymmetric unit content was similar as that of the reported 4Hpad structures (substrate-free and substrate-bound), albeit the *b* axis of the new unit cell is around 10-12 Å longer. Table 7.2 shows the data and refinement statistics of all the crystal structures of 4Hpad and its variants reported in this study.

**Table 7.1.** Crystal pictures of 4Hpad and its variants

| Protein | 4Hpad | 4Hpad | 4Hpad | 4Hpad | E505Q | HE2Q |
|---|---|---|---|---|---|---|
| Bound substrate or inhibitor | 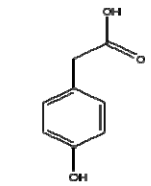 *p*-hydroxyphenylacetate 4-HPA $K_m$ = 2.8mM[a] | 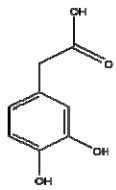 3,4-dihydroxyphenylacetate 3,4-DHPA $K_m$ = 0.5 mM[a] | 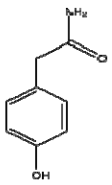 *p*-hydroxyphenylacetamide 4-HPAA $K_i$ = 0.7 mM[a] | 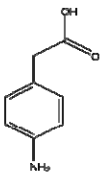 *p*-aminophenylacetate 4-APA | 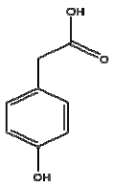 *p*-hydroxyphenylacetate 4-HPA | No substrate bound |
| Crystal |  | 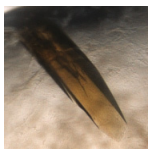 | 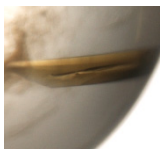 | No crystals obtained |  |  |

[a](Selmer & Andrei, 2001)

Structural analysis of 4Hpad in complex with 4-HPA, 3,4-DHPA and 4-HPAA showed very subtle structural changes in the active site pocket of the protein (Figure R25, bottom) in comparison with the published 4-HPA bound structure of 4Hpad (PDB: 2YAJ). It is proposed in Martins *et al.*, 2011 that the substrate is placed in the active site pocket with the acetyl moiety almost perpendicular to the phenyl moiety, the conformation being essential for decarboxylation. This substrate-binding mode captures a possible catalytic competent complex that presumes to promote the conformational rearrangement of the Gly873/Cys503 loops to generate the thiyl radical and then transfer the radical to the substrate in order to start the reaction. The obtained co-crystal structures of 4HPAD with 4-HPA, 3,4-DHPA and 4-HPAA were in excellent agreement with the observed substrate-binding mode obtained by crystal soaking (Martins *et al.*, 2011). The *meta*-hydroxyl group of 3,4-DHPA interacting with Glu637 displaces a solvent molecule that was present in the cavity in the active site pocket between Glu505 and Glu637 in both substrate free and substrate bound wild type structure (PDB: 2YAJ & 2YAJ) (Figure R25, bottom). 4-HPAA, where the acetate moiety in 4-HPA is replaced by an acetamide moiety cannot be decarboxylated, but seen bound in the active site pocket of the protein in a similar fashion to 4-HPA.

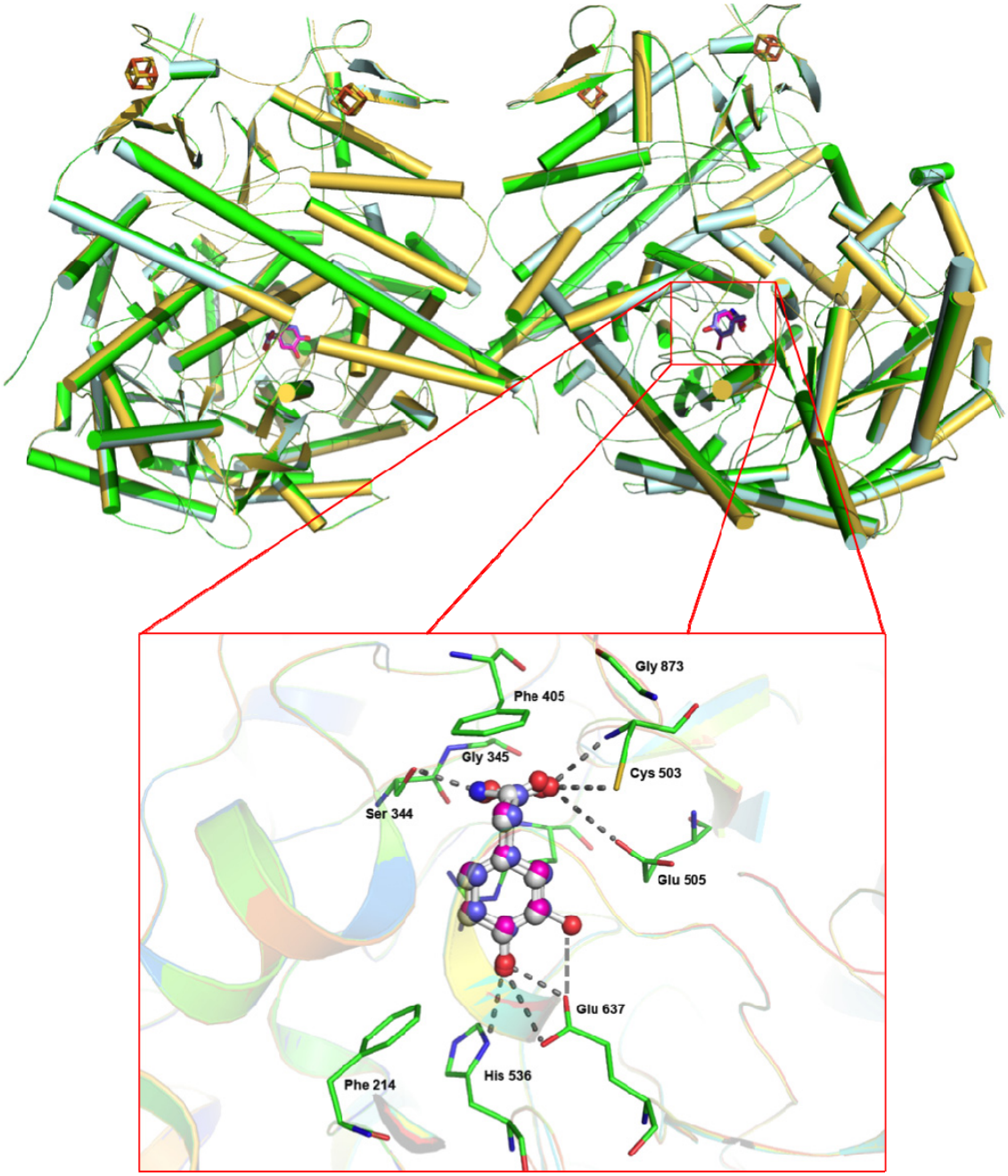


**Figure R25. Overlaid structures of 4Hpad co-crystallized with 4-HPA, 3,4-DHPA, 4-HPAA**. Top: Cylindrical representation of 4Hpad co-crystallized with 4-HPA (green), 3,4-DHPA (yellow), 4-HPAA (cyan). The [4Fe-4S] clusters are shown in yellow and orange sticks. Bottom: Enlarged view of the active site. The substrates, 4-HPA (carbons in grey); 3,4-DHPA (carbons in magenta) and inhibitor 4-HPAA (carbons in blue) are superimposed. Residues that are expected to play a role in substrate binding or decarboxylation mechanism are shown in sticks (carbons in green). Color code for nitrogen atoms is blue, red for oxygen and yellow for sulfur. Dashed lines indicate the interactions by hydrogen-bonding distances (3.4 Å cutoff).

**Table 7.2** Statistics on data collection and structure refinement of 4Hpad and its variants

| Crystal name | 4Hpad + 4-HPA | 4Hpad + 3,4-DHPA | 4Hpad + 4-HPAA | E505Q + 4-HPA | HE2Q* |
|---|---|---|---|---|---|
| Wavelength (Å) | 0.918 | 0.918 | 0.918 | 0.918 | 0.918 |
| Space group | $C222_1$ | $C222_1$ | $C222_1$ | $C222_1$ | $P2_1$ |
| Unit cell constants (a,b,c in Å) | 134.631, 239.048, 150.861 90°, 90°, 90° | 134.761, 239.451, 150.992 90°, 90°, 90° | 134.161, 237.324, 149.970 90°, 90°, 90° | 134.293, 239.255, 150.552 90°, 90°, 90° | 118.221, 175.547, 124.471 90°, 107.8°, 90° |
| Total / unique reflections | 530953 / 140616 | 947169 / 253680 | 2332693 / 452337 | 917323 / 255774 | 407008 / 152128 |
| $R_s$[a] (%) | 9.615 (53.79) | 4.997 (44.73) | 12.92 (55.62) | 6.40 (54.05) | 18.49 (78.35) |
| Resolution (Å) | 34.3 - 2.1 (2.2 – 2.1) | 39.2 - 1.7 (1.8 – 1.7) | 34.1 - 1.8 (1.9 – 1.8) | 46.8 - 1.7 (1.8 – 1.7) | 40.6 - 2.5 (2.7 – 2.5) |
| Completeness (%) | 99.63 (99.56) | 98.66 (96.87) | 97.27 (93.36) | 98.43 (97.10) | 98.85 (96.71) |
| I / σI | 11.72 (2.73) | 17.09 (2.85) | 9.99 (2.21) | 12.86 (2.36) | 8.09 (2.02) |
| R / $R_{free}$-factor (%)[b] | 14.84 / 19.33 | 14.48 / 17.39 | 16.15 / 20.55 | 19.06 / 21.97 | 21.62 / 24.23 |
| Rms deviation from ideal geometry | | | | | |
| Bonds (Å) | 0.012 | 0.011 | 0.019 | 0.014 | 0.010 |
| Angles (°) | 1.37 | 1.50 | 1.96 | 1.41 | 1.30 |

Numbers in brackets denote the values found in the highest resolution shell.
[a] $R_s = \Sigma_h \Sigma_i | I_i(h) - \langle I(h) \rangle | / \Sigma_h \Sigma_i I_i(h)$; where i are the independent observations of reflection h.
[b] The $R_{free}$ factor was calculated from 5% of the data, which were removed randomly and excluded from the refinement.
HE2Q* Preliminary refinement statistics.

It is also stated in Selmer & Andrei, 2001, Martins *et al.*, 2011 that the hydroxyl group at the *para*-position could be significant in anchoring the substrate in the active site pocket by hydrogen bond interactions to His536 and Glu637 and also stabilizes the *p*-benzoquinone methide radical anion intermediate through resonance structures (Figure R26).

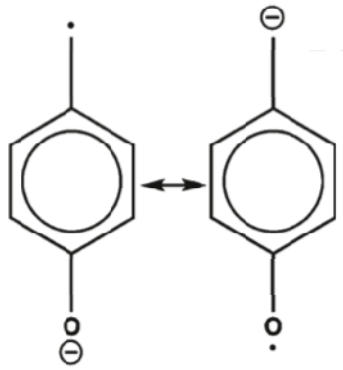

**Figure R26. Resonance stabilized *p*-benzoquinone methide radical anion intermediate**

Several attempts had been made during the course of this study to co-crystallize 4Hpad with 4-aminophenylacetate (4-APA) but in vain indicating the importance of the hydroxyl group in anchoring the substrate in the active site pocket. Efforts to crystallize 4Hpad with 4-nitrophenylacetate were also not successful and this explains the stabilization of the substrate by the vast hydrogen bonding interactions of the His536 and Glu637 with the hydroxyl group of the substrate.

## 7.2. Crystal structure of 4Hpad variants

Glu505 that is presumed to be responsible for donating the proton to the thiolate ($S^-$) of Cys503 and also to form a hydrogen bond with the carboxyl group of the substrate (Martins *et al.*, 2011). By changing the E505 to glutamine (E505Q), the proton donation to the thiolate is blocked thereby hindering the *p*-cresol formation. When the crystal structure of native protein (PDB: 2Y8N) was used as a model for refining the E505Q variant, the negative electron densities observed at one of the oxygen atom of Glu505 residue confirmed the presence of Gln505 and thereby the mutation. Albeit the crystal packing of the E505Q crystal has not been changed compared to the wild type (Table 7.2) as well as the active site pocket (Figure R27), the impaired

production of *p*-cresol by E505Q provide a valid evidence for the proposed role of Glu505 as the proton donor.

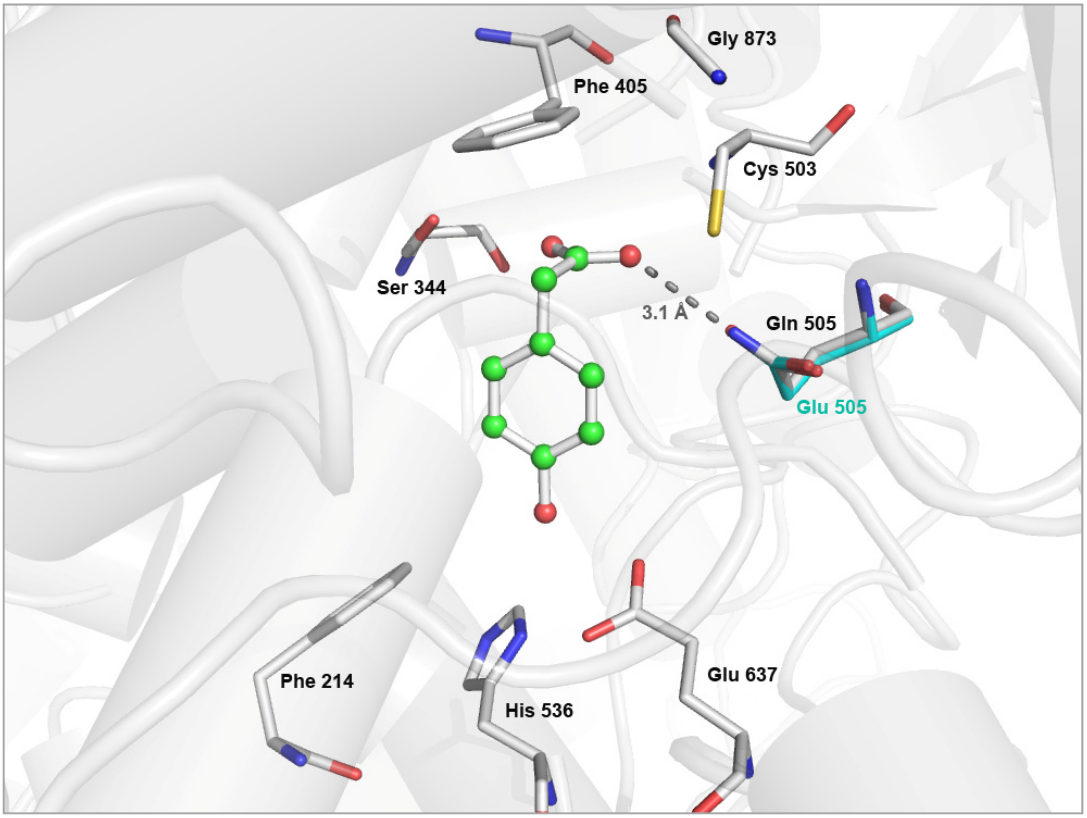


**Figure R27. Active site pocket of E505Q variant with bound 4-hydroxyphenylacetate.** 4-HPA, is shown in ball and stick representation (carbons in green and oxygens in red). Residues that are expected to play a role in substrate binding or decarboxylation mechanism are shown in sticks. The Glu505 in 4Hpad wild type that is mutated to Gln505 in E505Q is superimposed (carbons in cyan). Dotted grey line indicates the interaction of Gln505 with the substrate.

The residues Glu637 and His536 are in hydrogen-bonding distance to the phenolic hydroxyl group of the substrate are expected to involve in anchoring the substrate's hydroxyl group. Glu637 is a proton acceptor/donator involved in substrate activation and decarboxylation (Martins *et al.*, 2011; Feliks *et al.*, 2013). His536 interacts closely with Glu637 and also with the hydroxyl group of the substrate. These residues were mutated to glutamate independently (E637Q, H536Q) and together (HE2Q). The crystal picture of HE2Q is showed in table 7.1. Refinement of this structure is ongoing, but preliminary refinement statistics are provided in table 7.2. HE2Q crystallizes in a different space group ($P2_1$) and has four heterodimers per asymmetric unit. The variant fails to show substrate binding unlike E505Q. During the initial refinement

stage, the active site looks slightly distorted and different from all the above-mentioned structures of 4Hpad. From the preliminary refinement, it can only be stated that the failed substrate binding of HE2Q could be an added evidence for the postulated roles of these two residues and the substrate binding conformation, thereby adding evidences to the proposed Kolbe type decarboxylation.

# Outlook

In this work, the products of the reductive cleavage reaction of SAM during the 4Hpad activation process by 4Hpad-AE have been identified. Available experimental evidences from metal analysis and spectroscopic studies clearly indicate that at least one [4Fe-4S] cluster is bound by the ferredoxin-like insert in addition to the RS cluster of 4Hpad-AE. The role of the auxiliary cluster of 4Hpad-AE seems irrelevant as electron wire to the RS cluster, proposed for other SAM radical enzymes (Yu *et al.*, 2006). Instead this study provides insight into the putative structural role of the auxiliary clusters in activating 4Hpad. However, the information obtained in vitro may not reflect the physiological state of the proteins and associated Fe/S clusters. Further structural information as in anSMEs (Goldman *et al.*, 2013b) and biochemical studies, including *in vivo* (native environmental conditions) characterization and individual mutagenic studies are necessary to pinpoint the stoichiometry and ligand coordination of the auxiliary clusters in 4Hpad-AE, which are essential to assign their function.

Preliminary mutagenesis studies of the 4Hpad residues participating in the proposed Kolbe type decarboxylation have been introduced in this study. Biochemical and structural characterization of these mutants provide valid evidence for the proposed roles for these residues (Martins *et al.*, 2011). EPR spectroscopic trapping of the substrate-based radical intermediate (*p*-benzoquninone methide radical, Martins *et al.*, 2011) by activating the E505Q variant with 4Hpad-AE would be highly informative. It is also necessary to establish the presence of thiyl radical (Cys503) in 4Hpad formed in course of the reaction. Insights into each individual step of the Kolbe type decarboxylation will hopefully lead to a better understanding of the molecular mechanisms of enzymes involving highly reactive intermediates.

The small subunit of 4Hpad is deduced to be responsible for the binding of the [4Fe-4S] clusters and is also predicted to play a role in the regulation of the enzymes' oligomeric state and activity,

which are triggered by reversible serine phosphorylation of the glycyl radical subunits (Yu *et al.*, 2006). The proposed phosphorylation mechanism in 4Hpad could be studied by constructing a N-terminal truncated (deleting first 30 amino acids, harboring the phosphorylation sites) 4Hpad variant. If the variant still forms an active $(\beta\gamma)_4$ complex, the role of phosphorylation in regulating the oligomeric assembly of the protein could be excluded. The residues that coordinate the Fe/S clusters could be mutated to study the role of the clusters in catalysis.

The mechanism of GREs activation is an open question. The crystal structures of 4Hpad-AE and 4Hpad/4Hpad-AE complex which are important milestones for future studies would provide structural insights into the conformational changes that permit the hydrogen abstraction at the glycine Cα *pro-S* of 4Hpad by the transient 5´-deoxyadenosyl radical.

# References

Adams PD, Afonine PV & Bunkóczi G *et al.* (2010) PHENIX: A comprehensive Python-based system for macromolecular structure solution. *Acta Crystallographica Section D Biological Crystallography* **66:** 213–221.

Andrei PI, Pierik AJ, Zauner S, Andrei-Selmer LC & Selmer T (2004) Subunit composition of the glycyl radical enzyme *p*-hydroxyphenylacetate decarboxylase. *European Journal of Biochemistry* **271:** 2225–2230.

Banerjee R (2003) Introduction: Radical Enzymology. *Chemical Reviews* **103:** 2081–2082.

Barker HA (1981) Amino acid degradation by anaerobic bacteria. *Annual review of biochemistry* **50:** 23–40.

Becker A, Fritz-Wolf K, Kabsch W, Knappe J, Schultz S & Volker Wagner AF (1999) Structure and mechanism of the glycyl radical enzyme pyruvate formate-lyase. *Nature structural biology* **6:** 969–975.

Bennett BD, Kimball EH, Gao M, Osterhout R, van Dien SJ & Rabinowitz JD (2009) Absolute metabolite concentrations and implied enzyme active site occupancy in Escherichia coli. *Nature Chemical Biology* **5:** 593–599.

Blaser M (2007) Activaton and regulation of 4-Hydroxyphenylacetate decarboxylase system from Clostridium difficile, Philipps-Univerisität, Marburg.

Boll M & Fuchs G (2005) Unusual reactions involved in anaerobic metabolism of phenolic compounds. *Biological Chemistry* **386**.

Booker SJ (2009) Anaerobic functionalization of unactivated C–H bonds. *Current Opinion in Chemical Biology* **13:** 58–73.

Booker SJ, Cicchillo RM & Grove TL (2007) Self-sacrifice in radical S-adenosylmethionine proteins. *Current Opinion in Chemical Biology* **11:** 543–552.

Borriello SP & Wilcox MH (1998) Clostridium difficile infections of the gut: the unanswered questions. *The Journal of antimicrobial chemotherapy* **41:** 67–69.

Broderick JB (2010) Biochemistry: A radically different enzyme. *Nature* **465:** 877–878.

Buckel W (2009) Radical and Electron Recycling in Catalysis. *Angewandte Chemie International Edition* **48:** 6779–6787.

Buckel W & Golding BT (1998) Radical species in the catalytic pathways of enzymes from anaerobes. *FEMS Microbiology Reviews* **22:** 523–541.

Buckel W & Golding BT (2006) Radical Enzymes in Anaerobes. *Annual Review of Microbiology* **60:** 27–49.

Cabrita LD, Gilis D, Robertson AL, Dehouck Y, Rooman M & Bottomley SP (2007) Enhancing the stability and solubility of TEV protease using in silico design. *Protein Science* **16:** 2360–2367.

Cicchillo RM & Booker SJ (2005) Mechanistic Investigations of Lipoic Acid Biosynthesis in Escherichia coli: Both Sulfur Atoms in Lipoic Acid are contributed by the Same Lipoyl Synthase Polypeptide. *Journal of the American Chemical Society* **127:** 2860–2861.

Cooper DR, Boczek T, Grelewska K, Pinkowska M, Sikorska M, Zawadzki M & Derewenda Z (2007) Protein crystallization by surface entropy reduction: optimization of the SER strategy. *Acta Crystallographica Section D Biological Crystallography* **63:** 636–645.

Craciun S & Balskus EP (2012) Microbial conversion of choline to trimethylamine requires a glycyl radical enzyme. *Proceedings of the National Academy of Sciences* **109:** 21307–21312.

D'Ari L & Barker HA (1985) *p*-Cresol formation by cell-free extracts of Clostridium difficile. *Archives of microbiology* **143:** 311–312.

Demick JM & Lanzilotta WN (2011) Radical SAM Activation of the B 12 -Independent Glycerol Dehydratase Results in Formation of 5′-Deoxy-5′-(methylthio)adenosine and Not 5′-Deoxyadenosine. *Biochemistry* **50:** 440–442.

Dey A, Peng Y, Broderick WE, Hedman B, Hodgson KO, Broderick JB & Solomon EI (2011) S K-edge XAS and DFT Calculations on SAM Dependent Pyruvate Formate-Lyase Activating Enzyme: Nature of Interaction between the $Fe_4S_4$ Cluster and SAM and its Role in Reactivity. *Journal of the American Chemical Society* **133:** 18656–18662.

Dimova N (2003) RP-HPLC Analysis of Amino Acids with UV-Detection. *COMPTES RENDUS- ACADEMIE BULGARE DES SCIENCES; **56**; 75-78:* 75–78.

Duschene KS, Veneziano SE, Silver SC & Broderick JB (2009) Control of radical chemistry in the AdoMet radical enzymes. *Current Opinion in Chemical Biology* **13:** 74–83.

Eklund H & Fontecave M (1999) Glycyl radical enzymes: a conservative structural basis for radicals. *Structure (London, England 1993)* **7:** R257-62.

Emsley P & Cowtan K (2004) Coot: model-building tools for molecular graphics. *Acta crystallographica* **60:** 2126–2132.

Feliks M, Martins BM & Ullmann GM (2013) Catalytic Mechanism of the Glycyl Radical Enzyme 4-Hydroxyphenylacetate Decarboxylase from Continuum Electrostatic and QC/MM Calculations. *Journal of the American Chemical Society* **135:** 14574–14585.

Fish WW (1988) Rapid colorimetric micromethod for the quantitation of complexed iron in biological samples. *Methods in enzymology* **158:** 357–364.

Fontecave M (1998) Ribonucleotide reductases and radical reactions. *Cellular and molecular life sciences CMLS* **54:** 684–695.

Fontecave M (2006) Iron-sulfur clusters: ever-expanding roles. *Nature Chemical Biology* **2:** 171–174.

Fontecave M, Mulliez E & Ollagnier-de-Choudens S (2001) Adenosylmethionine as a source of 5′-deoxyadenosyl radicals. *Current Opinion in Chemical Biology* **5:** 506–512.

Frey M, Rothe M, Wagner AF & Knappe J (1994) Adenosylmethionine-dependent synthesis of the glycyl radical in pyruvate formate-lyase by abstraction of the glycine C-2 pro-S hydrogen

atom. Studies of 2Hglycine-substituted enzyme and peptides homologous to the glycine 734 site. *The Journal of biological chemistry* **269:** 12432–12437.

Frey PA (2001) Radical mechanisms of enzymatic catalysis. *Annual review of biochemistry* **70:** 121–148.

Frey PA, Hegeman AD & Reed GH (2006) Free Radical Mechanisms in Enzymology. *Chemical Reviews* **106:** 3302–3316.

Frey PA, Hegeman AD & Ruzicka FJ (2008) The Radical SAM Superfamily. *Critical reviews in biochemistry and molecular biology* **43:** 63–88.

Friedel MG, Berteau O, Pieck JC, Atta M, Ollagnier-de-Choudens S, Fontecave M & Carell T (2006) The spore photoproduct lyase repairs the 5S- and not the 5R-configured spore photoproduct DNA lesion. *Chemical Communications:* 445.

Gambarelli S, Luttringer F, Padovani D, Mulliez E & Fontecave M (2005) Activation of the Anaerobic Ribonucleotide Reductase by S-Adenosylmethionine. *ChemBioChem* **6:** 1960–1962.

Gill SC & Hippel PH von (1989) Calculation of protein extinction coefficients from amino acid sequence data. *Analytical biochemistry* **182:** 319–326.

Glaser T (2011) Mössbauer Spectroscopy and Transition Metal Chemistry. Fundamentals and Applications. Edited by Philipp Gütlich, Eckhard Bill and Alfred X. Trautwein. *Angewandte Chemie International Edition* **50:** 10019–10020.

Goldman PJ, Grove TL, Booker SJ & Drennan CL (2013a) X-ray analysis of butirosin biosynthetic enzyme BtrN redefines structural motifs for AdoMet radical chemistry. *Proceedings of the National Academy of Sciences* **110:** 15949–15954.

Goldman PJ, Grove TL, Sites LA, McLaughlin MI, Booker SJ & Drennan CL (2013b) X-ray structure of an AdoMet radical activase reveals an anaerobic solution for formylglycine posttranslational modification. *Proceedings of the National Academy of Sciences* **110:** 8519–8524.

Goldschmidt L, Cooper DR, Derewenda ZS & Eisenberg D (2007) Toward rational protein crystallization: A Web server for the design of crystallizable protein variants. *Protein Science* **16:** 1569–1576.

Heider J & Fuchs G (1997) Anaerobic metabolism of aromatic compounds. *European journal of biochemistry / FEBS* **243:** 577–596.

Heider J, Spormann AM, Beller HR & Widdel F (1998) Anaerobic bacterial metabolism of hydrocarbons. *FEMS Microbiology Reviews* **22:** 459–473.

Hoffman JL (1986) Chromatographic analysis of the chiral and covalent instability of S-adenosyl-L-methionine. *Biochemistry* **25:** 4444–4449.

Hui AK, Armstrong BH & Wray AA (1978) Rapid computation of the Voigt and complex error functions. *Journal of Quantitative Spectroscopy and Radiative Transfer* **19:** 509–516.

Jarrett JT (2003) The generation of 5'-deoxyadenosyl radicals by adenosylmethionine-dependent radical enzymes. *Current opinion in chemical biology* **7:** 174–182.

Kabsch W (1993) Automatic processing of rotation diffraction data from crystals of initially unknown symmetry and cell constants **26:** 795–800.

Kampmeier JA (2010) Regioselectivity in the homolytic cleavage of S-adenosylmethionine. *Biochemistry* **49:** 10770–10772.

Klock HE, Koesema EJ, Knuth MW & Lesley SA (2008) Combining the polymerase incomplete primer extension method for cloning and mutagenesis with microscreening to accelerate structural genomics efforts. *Proteins: Structure, Function, and Bioinformatics* **71:** 982–994.

Klock HE & Lesley SA (2009) The Polymerase Incomplete Primer Extension (PIPE) method applied to high-throughput cloning and site-directed mutagenesis. *Methods in molecular biology* **498:** 91–103.

Knappe J, Neugebauer FA, Blaschkowski HP & Ganzler M (1984) Post-translational activation introduces a free radical into pyruvate formate-lyase. *Proceedings of the National Academy of Sciences of the United States of America* **81:** 1332–1335.

Kulzer R, Pils T, Kappl R, Huttermann J & Knappe J (1998) Reconstitution and characterization of the polynuclear iron-sulfur cluster in pyruvate formate-lyase-activating enzyme. Molecular properties of the holoenzyme form. *The Journal of biological chemistry* **273:** 4897–4903.

Lanz ND & Booker SJ (2012) Identification and function of auxiliary iron–sulfur clusters in radical SAM enzymes. *Biochimica et Biophysica Acta (BBA) - Proteins and Proteomics* **1824:** 1196–1212.

Layer G, Heinz DW, Jahn D & Schubert W (2004) Structure and function of radical SAM enzymes. *Current Opinion in Chemical Biology* **8:** 468–476.

Leuthner B, Leutwein C, Schulz H, Horth P, Haehnel W, Schiltz E, Schagger H & Heider J (1998) Biochemical and genetic characterization of benzylsuccinate synthase from Thauera aromatica: a new glycyl radical enzyme catalysing the first step in anaerobic toluene metabolism. *Molecular microbiology* **28:** 615–628.

Li L, Patterson DP, Fox CC, Lin B, Coschigano PW & Marsh ENG (2009) Subunit Structure of Benzylsuccinate Synthase. *Biochemistry* **48:** 1284–1292.

Marsh EG, Patwardhan A & Huhta MS (2004) S-Adenosylmethionine radical enzymes. *Bioorganic Chemistry* **32:** 326–340.

Marsh ENG, Patterson DP & Li L (2010) Adenosyl Radical: Reagent and Catalyst in Enzyme Reactions. *ChemBioChem* **11:** 604–621.

Martins BM, Blaser M, Feliks M, Ullmann GM, Buckel W & Selmer T (2011) Structural Basis for a Kolbe-Type Decarboxylation Catalyzed by a Glycyl Radical Enzyme. *Journal of the American Chemical Society* **133:** 14666–14674.

McCoy AJ, Grosse-Kunstleve RW, Adams PD, Winn MD, Storoni LC & Read RJ (2007) Phaser crystallographic software. *Journal of Applied Crystallography* **40:** 658–674.

Meijers BKI & Evenepoel P (2011) The gut-kidney axis: indoxyl sulfate, *p*-cresyl sulfate and CKD progression. *Nephrology Dialysis Transplantation* **26:** 759–761.

Nakamura M, Saeki K & Takahashi Y (1999) Hyperproduction of recombinant ferredoxins in escherichia coli by coexpression of the ORF1-ORF2-iscS-iscU-iscA-hscB-hs cA-fdx-ORF3 gene cluster. *Journal of biochemistry* **126:** 10–18.

Nicolet Y, Amara P, Mouesca J & Fontecilla-Camps JC (2009) Unexpected electron transfer mechanism upon AdoMet cleavage in radical SAM proteins. *Proceedings of the National Academy of Sciences of the United States of America* **106:** 14867–14871.

Ollagnier S, Mulliez E, Schmidt PP, Eliasson R, Gaillard J, Deronzier C, Bergman T, Graslund A, Reichard P & Fontecave M (1997) Activation of the anaerobic ribonucleotide reductase from Escherichia coli. The essential role of the iron-sulfur center for S-adenosylmethionine reduction. *The Journal of biological chemistry* **272:** 24216–24223.

Peng Y, Veneziano SE, Gillispie GD & Broderick JB (2010) Pyruvate Formate-lyase, Evidence for an Open Conformation Favored in the Presence of Its Activating Enzyme. *Journal of Biological Chemistry* **285:** 27224–27231.

Sambrook J & Fritsch EaMT (1989) *Molecular cloning: a laboratory manual. 2nd ed.* Cold Spring Harbor Laboratory Press.

Sandala GM, Smith DM & Radom L (2010) Modeling the Reactions Catalyzed by Coenzyme B 12 -Dependent Enzymes. *Accounts of Chemical Research* **43:** 642–651.

Sauter M & Sawers RG (1990) Transcriptional analysis of the gene encoding pyruvate formate-lyase-activating enzyme of Escherichia coli. *Molecular microbiology* **4:** 355–363.

Sawers G (1998) Biochemistry, physiology and molecular biology of glycyl radical enzymes. *FEMS Microbiology Reviews* **22:** 543–551.

Schreier F (2011) Optimized implementations of rational approximations for the Voigt and complex error function. *Journal of Quantitative Spectroscopy and Radiative Transfer* **112:** 1010–1025.

Schrödinger LL (2010) *The PyMOL Molecular Graphics System, Version 1.3r1*.

Selmer T & Andrei PI (2001) *p*-Hydroxyphenylacetate decarboxylase from Clostridium difficile. A novel glycyl radical enzyme catalysing the formation of p-cresol. *European journal of biochemistry / FEBS* **268:** 1363–1372.

Selmer T, Pierik AJ & Heider J (2005) New glycyl radical enzymes catalysing key metabolic steps in anaerobic bacteria. *Biological Chemistry* **386**.

Selvaraj B, Pierik AJ, Bill E & Martins BM (2013) 4-Hydroxyphenylacetate decarboxylase activating enzyme catalyses a classical *S*-adenosylmethionine reductive cleavage reaction. *JBIC Journal of Biological Inorganic Chemistry* **18:** 633–643.

Sharp PM & Li WH (1987) The codon Adaptation Index--a measure of directional synonymous codon usage bias, and its potential applications. *Nucleic acids research* **15:** 1281–1295.

Shisler KA & Broderick JB (2012) Emerging themes in radical SAM chemistry. *Current Opinion in Structural Biology* **22:** 701–710.

Smith & Macfarlane (1997) Formation of Phenolic and Indolic Compounds by Anaerobic Bacteria in the Human Large Intestine. *Microbial ecology* **33:** 180–188.

Sofia HJ, Chen G, Hetzler BG, Reyes-Spindola JF & Miller NE (2001) Radical SAM, a novel protein superfamily linking unresolved steps in familiar biosynthetic pathways with radical mechanisms: functional characterization using new analysis and information visualization methods. *Nucleic acids research* **29:** 1097–1106.

Stubbe J & van der Donk WA (1998) Protein Radicals in Enzyme Catalysis. *Chemical reviews* **98:** 705–762.

Sweeney WV & Rabinowitz JC (1980) Proteins containing 4Fe-4S clusters: an overview. *Annual review of biochemistry* **49:** 139–161.

Thauer RK, Jungermann K & Decker K (1977) Energy conservation in chemotrophic anaerobic bacteria. *Bacteriological reviews* **41:** 100–180.

Ugulava NB, Gibney BR & Jarrett JT (2001) Biotin Synthase Contains Two Distinct Iron−Sulfur Cluster Binding Sites: Chemical and Spectroelectrochemical Analysis of Iron−Sulfur Cluster Interconversions. *Biochemistry* **40:** 8343–8351.

Unkrig V, Neugebauer FA & Knappe J (1989) The free radical of pyruvate formate-lyase. Characterization by EPR spectroscopy and involvement in catalysis as studied with the substrate-analogue hypophosphite. *European journal of biochemistry / FEBS* **184:** 723–728.

Vey JL, Yang J, Li M, Broderick WE, Broderick JB & Drennan CL (2008) Structural basis for glycyl radical formation by pyruvate formate-lyase activating enzyme. *Proceedings of the National Academy of Sciences of the United States of America* **105:** 16137–16141.

Viehe HG, Janousek Z, Merenyi R & Stella L (1985) The captodative effect. *Acc. Chem. Res.* **18:** 148–154.

Wagner AF, Frey M, Neugebauer FA, Schafer W & Knappe J (1992) The free radical in pyruvate formate-lyase is located on glycine-734. *Proceedings of the National Academy of Sciences of the United States of America* **89:** 996–1000.

Walsby CJ, Ortillo D, Yang J, Nnyepi MR, Broderick WE, Hoffman BM & Broderick JB (2005) Spectroscopic Approaches to Elucidating Novel Iron−Sulfur Chemistry in the "Radical-SAM" Protein Superfamily. *Inorganic Chemistry* **44:** 727–741.

Walsby CJ, Hong W, Broderick WE, Cheek J, Ortillo D, Broderick JB & Hoffman BM (2002) Electron-Nuclear Double Resonance Spectroscopic evidence that *S*-adenosylmethionine binds in contact with the catalytically active $[4Fe\text{-}4S]^{+}$ cluster of Pyruvate Formate-Lyase Activating enzyme. *Journal of the American Chemical Society* **124:** 3143–3151.

Yang J, Naik SG, Ortillo DO, García-Serres R, Li M, Broderick WE, Huynh BH & Broderick JB (2009) The Iron−Sulfur Cluster of Pyruvate Formate-Lyase Activating Enzyme in Whole Cells: Cluster Interconversion and a Valence-Localized [4Fe-4S] 2+ State. *Biochemistry* **48:** 9234–9241.

Yu L, Blaser M, Andrei PI, Pierik AJ & Selmer T (2006) 4-Hydroxyphenylacetate Decarboxylases: Properties of a Novel Subclass of Glycyl Radical Enzyme Systems. *Biochemistry* **45:** 9584–9592.

# Appendix

## 1. Appendix tables

**Table A1.** Thermocycler conditions for PCR reactions of cloning of Δ66-AE

| | | | |
|---|---|---|---|
| Initial denaturation | 98 °C | 2 min | |
| Denaturation | 98 °C | 15 sec | 30 cycles |
| Annealing | 65 °C | 15 sec | |
| Extension | 72 °C | 4 min | |
| Final extension | 72 °C | 10 min | |

**Table A2.** Thermocycler conditions for PCR reactions of cloning of AE-9M

| | | | |
|---|---|---|---|
| Initial denaturation | 98 °C | 2 min | |
| Denaturation | 98 °C | 10 sec | 35 cycles |
| Annealing | 65 °C | 10 sec | |
| Extension | 72 °C | 25 sec | |

**Table A3.** Thermocycler conditions for PCR reactions of mutagenesis of 4Hpad variants

| | | | |
|---|---|---|---|
| Initial denaturation | 95 °C | 1 min | |
| Denaturation | 95 °C | 30 sec | 18 cycles |
| Annealing | 60 °C[a] | 1 min | |
| Extension | 68 °C | 7 min[b] | |
| Final extension | 68 °C | 1 min | |
| | 4 °C | End | |

[a] best result of 50 – 65 °C gradient thermocycle is taken, [b] 1 minute/kb of plasmid length

**Table A4.** Factors tested to improve the expression of recombinant 4Hpad

- *Escherichia coli* expression strains BL21(DE3), BL21 CodonPlus, Rosetta™(DE3) and Rosetta™(DE3) pLysS.
- Fermentation in LB, mTB, TB and LBG media.
- Fermentation at 20, 25, 28 and 30 °C after induction.
- Fermentation at 4 °C for 16 hours before cell harvest without any orbital agitation.
- Induction with anhydrotetracyclin (ATH, 0.1– 0.2 ng/ml).
- Protein expression for 4, 6 and 24 hours before cell harvest.
- Addition of ethanol (2 %) before or at induction time.
- Addition of iron (0.1 – 0.5 mM) in the form of ferrous ammonium sulfate or ferric citrate, and reduced sulfur (0.1 – 0.5 mM) in the form of cysteine or sodium sulfide before and/or at induction time.
- Aerobic growth with orbital agitation or anaerobic growth under $N_2$ atmosphere.

**Table A5.** Conditions tested to improve the reconstitution of Fe/S clusters

- Incubation with 2 -10 mM β-mercaptoethanol or DTT.
- Various incubation times with β-mercaptoethanol ranging from 30 min to 3 hours.
- Addition of iron (10 to 30 fold) in the form of ferrous ammonium sulfate or ferric ammonium citrate, and sulfur (10 to 30 fold) in the form of lithium sulfide or sodium sulfide.
- Various incubation times of the reconstitution mixture ranging from 2 hours to 24 hours.
- Presence of auxiliary proteins from the ISC assembly machinery (lysates from *E. coli* cells harbouring the pRKISC plasmid) during the cell lysis.

# 2. Appendix figures

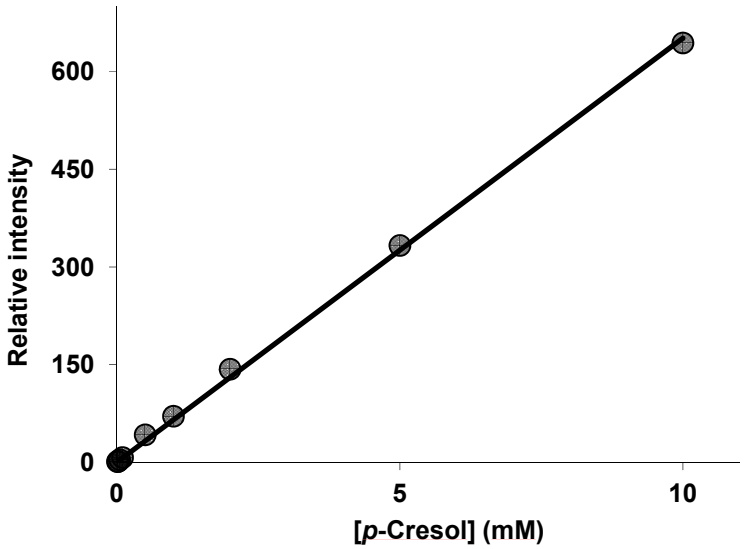


**Figure A1. Standard curve used for the calculation of [*p*-cresol] formed during 4Hpad activation** (Results and discussion, 4.4). Amount of *p*-cresol formed was calculated by using the equation [*p*-cresol] = (Relative intensity + 0.073)/0.7441with a correlation coefficient of $R^2$=0.99933.

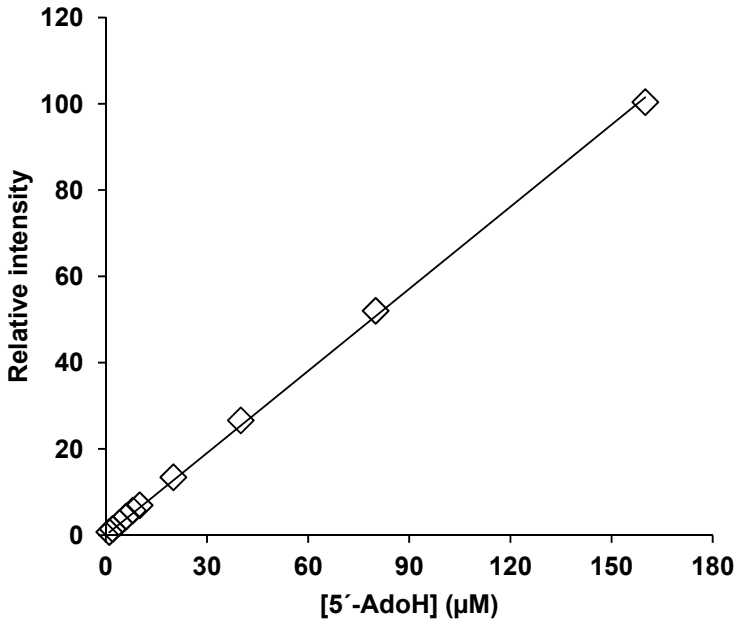

**Figure A2. Standard curve used for the calculation of [5´-AdoH] formed during all enzymatic assays of 4Hpad-AE** (Results and discussion, 4). Amount of 5´-AdoH formed was calculated by using the equation [5´-AdoH] = (Relative intensity - 0.6179)/0.6285 with a correlation coefficient of $R^2$=0.99965.

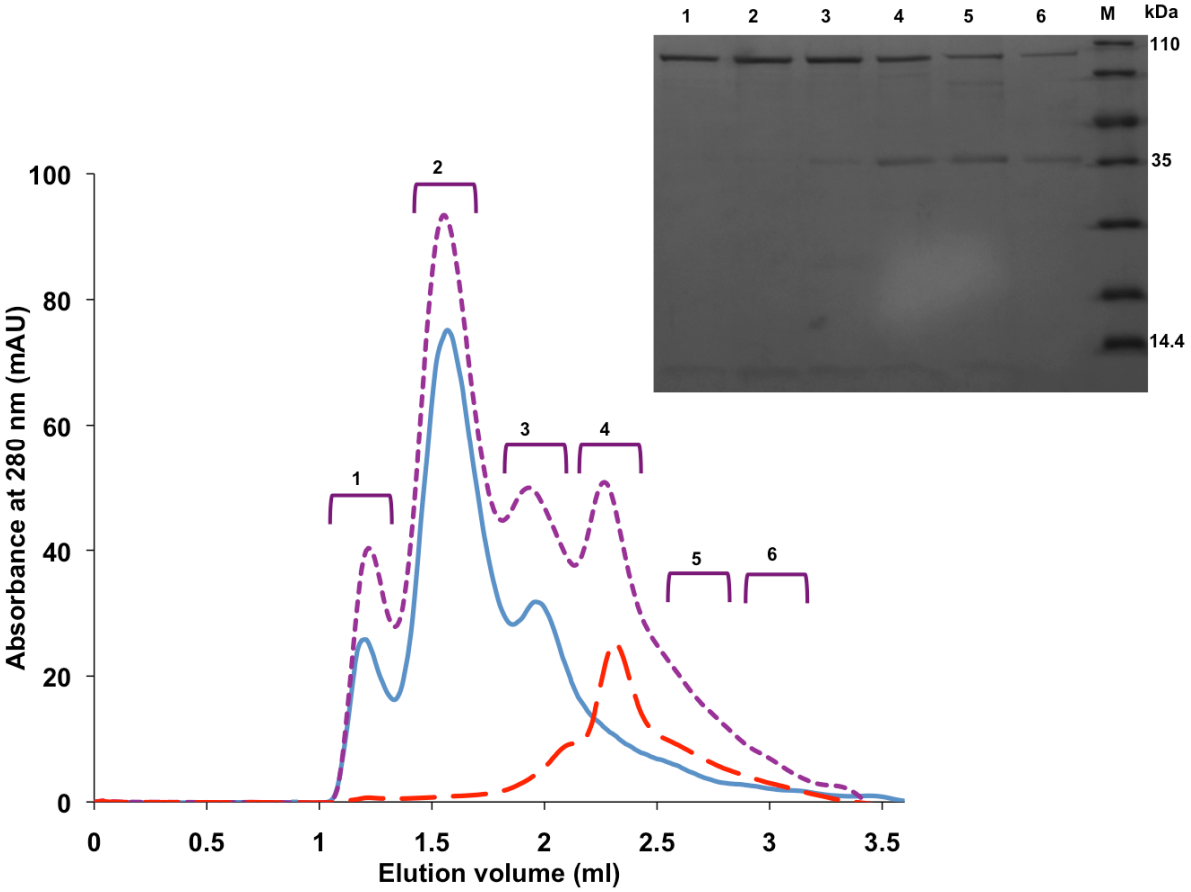


**Figure A3. Complex formation trials between 4Hpad/4Hpad-AE** (Results and discussion, 6). Elution profiles of 4Hpad (blue), 4Hpad-AE** (red) and 4Hpad/4Hpad-AE** incubated mixture (purple) in buffer C. Insert: Coomassie blue-stained 12% (w/v) SDS-PAGE of peak fractions from the 4Hpad/4Hpad-AE** incubated mixture. Lane M; Molecular mass protein markers. Peak fractions in the elution chromatogram and the corresponding lanes in the gel are numbered.

# 3. SDS-PAGE

Running gel: 12 or 16% (w/v) Acrylamide, 375 mM Tris(hydroxymethyl)aminomethane (Tris)/HCl (pH 8.8), 0.1% (w/v) Sodiumdodecylsulfate (SDS), 0.08% (v/v)

N,N,N',N'-Tetramethylethylenediamine (TEMED), 0.05 % (w/v) Ammoniumperoxodisulfate (APS)

Stacking gel: 6% (w/v) Acrylamide, 125 mM Tris/HCl (pH 6,8), 0.1% (w/v) SDS, 0.08% (v/v) TEMED, 0.05% (w/v) APS

Loading buffer (4 x): 200 mM Tris (pH 6,8), 8% (w/v) SDS, 0.4% (w/v) Bromophenolblue, 40 (v/v) Glycerine, 400 mM Dithiothreitol (DTT)

Running buffer (10 x): 1.92 M Glycine, 248 mM Tris, 1% (w/v) SDS

Staining solution: 0.025% (w/v) Coomassie Brillant Blue G250, 10% (v/v) Acetic acid

Destaining solution: 10% (v/v) Acetic acid

SDS-PAGE was prepared according to Laemmli (Laemmli, 1970). The protein molecular weight marker used in this study was from Fermentas (β-Galactosidase, 116 kDa; Bovine serum albumin, 66.2 kDa; Ovalbumin, 45 kDa; Lactate dehydrogenase, 35 kDa; REase Bsp98I, 25 kDa; β-Lactoglobulin, 18.4 kDa; Lysozyme, 14.4 kDa). The samples were mixed with loading buffer and denatured by heating to 95 °C for 5 min prior to loading on the gel. The electrophoresis was performed at a voltage of 80 V for 20 min and 160 V till the tracking dye reached the bottom of the gel. Then the gel were stained with the staining solution for 20 minutes and then incubated in the destaining solution until the background loses its color.

# Selbständigkeitserklärung

Hiermit erkläre ich, dass ich die vorliegende Arbeit selbstständig verfasst und keine weiteren als die angegebenen Hilfsmittel verwendet habe.

Berlin, den 10.12.2013 Brinda Selvaraj